Universität für Bodenkultur Wien

Department of Agrobiotechnology, IFA-Tulln

Institute of Natural Materials Technology

Head of Institute: Ass.Prof.Dr. Norbert Mundigler

Advisor/Advisors: Univ.Prof.Dr. Rupert Wimmer

SEMI-CRYSTALLINE BIOPOLYMERS WITH CARBON-BASED FILLERS:

ELECTRICAL, MECHANICAL AND THERMAL PROPERTIES

Dissertation
for obtaining a doctorate degree
at the University of Natural Resources and Applied Life Sciences Vienna

Submitted by
Pauline Rivière

Paris, January 2017

“Every now and then go away, have a little relaxation, for when you come back to your work your judgment will be surer.”

Leonardo Da Vinci (1452-1519)

Acknowledgements

This thesis was mainly conducted at the Institute of Natural Materials Technology of the Department of Agrobiotechnology (IFA Tulln) of the University of Natural Resources and Life Sciences, Vienna (BOKU). At first, I like to express my thanks to my supervisor Prof. Rupert Wimmer, and to the head of the Institute, Ass. Prof. Norbert Mundigler for their continuous encouragements, support and assistance. I also would like to extent my gratitude to the entire crew of the institute, for their steady technical assistance with conducting all the experiments. I like to acknowledge the Institute of Wood Technology and Renewable Materials of BOKU, for providing me access to special facilities, and assisting me with expertise. I am particularly grateful to the following people: Dr. Henry Bock from the Heriot-Watt University in Edinburgh for hosting me at his institute and helping me with developing a deeper scientific understanding in my subject matter; to Dr. Tiina Nypelö from the Division of Chemistry of Renewable Resources (BOKU) for her close collaboration here at BOKU, but also back at the North Carolina State University (NCSA); to Dr. Ines Fritz from the Institute of Environmental Biotechnology (BOKU) for her help with analytical devices and support in the design of experiments, and last not least to Dr. Michael Obersriebnig formerly from the Institute of Wood Technology and Renewable Materials (BOKU) for his collaboration with atomic force microscopy. Like to thank also Dr. Erik Van Herwijnen from Kompetenzzentrum Holz GmbH-(Wood K plus), and Mr. David Kaserer as well as Mr. Gerhard Emsenhuber, both Institute of Wood Technology and Renewable Materials, BOKU, for repeated help in the realization and interpretation of experiments.

May I also thank deeply Prof. Dr. Dietmar Pum from the Department of Nanobiotechnology, BOKU), for support and advice in electron microscopy. Likewise, to Prof. Alex Berg at the University of Concepción, Prof Radovic from the University of Pennsylvania State for his expertise and the very valuable piece of advice, and the Unit of Technological Development in Coronel, Chile, for the instructive and very welcoming research stay, that included also the use of special equipment.

I am grateful to Mr. Markus Rempfler, Ms. Noémie Prat, Ms. Eva Sykacek, and Ms. Alexandra Simader, Ms. Marine Dupire, Ms. Anita Tran, Ms. Lucy Montgomery, Ms. Cornelia Hass, Ms. Archi Dasgupta and Ms. Catherine Cagniart, for editorial assistance, and for keeping me motivated all along this thesis.

Cost Action FP1105, particularly Dr. Soledad Peresin, is acknowledged for providing funding that allowed the intensive collaboration with Dr. Henry Bock, and Dr. Tiina Nypelö at NCSA (USA). My thanks are also due to the companies Velox, Toho Tenax, Procotex, Apply carbon and former C-polymers for providing required raw materials.

Mr. Frieling from the Technical University of Dortmund, Prof. Dr. Achim Walter Hassel from the Johannes Kepler University in Linz, and Ms. Dorothea Schwarz from DEKRA EXAM GmbH, Dr. Andreas Klug, formerly from the NanoTecCenter Weiz, are all acknowledged for intensive help with the electrical conductivity measurements.

I would also like to thank the following persons that I had the privilege to meet during this four years, discussing various topics in connection with my thesis: Prof. Liska and Prof. Archodoulaki from the Technical University of Vienna, Dr. Juan Matos from the Unit of technological development of Coronel, Chile and Mr. Jonathan Bernardo Usuba Valdebenito from the University of Concepción, Chile.

Last not least, I am grateful to the European and regional financed program EFRE, which supported the first five months of the project, and to the Government of Low-Austria for completing this financial support to three years.

This thesis is dedicated to my family and friends.

Abstract (German, English and French)

Die Modifizierung von natürlichen Polymeren zur Erreichung von z.B. elektrischer Leitfähigkeit kann deren Anwendungsbereiche essentiell erweitern. In dieser Arbeit wurden kohlenstoff-basierte Zusatzstoffe wie Kohlenstofffasern, rezyklierte Kohlenstofffasern und Kohlenstoff-Nanoröhren (MWCNTs) mit unterschiedlichen biobasierten Polymeren: Polymilchsäure (PLA), Poly(β-hydroxybutyrat-co-valerat), Polyethylen (Bio-PE) und Polyamide kombiniert, mit dem Ziel, die elektrische Leitfähigkeit von Spritzgußteilen wesentlich zu erhöhen. Mikroskopische Analysen zeigten, dass durch den Schmelze-Misch-Prozess eine effektive Verteilung und Individualisierung der meisten Füllstoffe in der Polymermatrix erreicht werden konnte. Lediglich in PLA haben die MWCNTs bei niedrigem Gehalt eine bevorzugte Ausrichtung gezeigt, und in Bio-PE konnte die effektive Individualisierung der MWCNTs nicht demonstriert werden. Bei guter Füllstoff-Polymer Wechselwirkung, gezeigt durch verbesserte Zugfestigkeit, hat die Anwendung von leitfähigen Füllstoffen mit höherem Verhältnis von Länge zu Durchmesser zur Verbesserung der elektrischen und mechanischen Eigenschaften des Verbundwerkstoffes bei gleichem Füllstoffgehalt geführt. Die niedrigste elektrische Perkolationsschwelle wurde mit dem Zusatz von MWCNTs in PLA erzielt, was aber gleichzeitig mit der Verringerung von Zugfestigkeit und einer unregelmäßigen Variation der thermischen Stabilität einherging. Die Schnellkühlung des Materials durch das Spritzguss verfahren begrenzte den Effekt von Nanoröhren auf die Polymerkristallisation von PLA und Bio-PE. Schließlich unterschieden sich die thermische Expandierung und Formbeständigkeitstemperaturvariationen durch den Zusatz von MWCNTs bei Messungen auf der Oberfläche von denjenigen im Volumen des Verbundwerkstoffs.

Tailoring the properties of natural polymers is vital to widen the range of future applications. In this thesis, carbon-based fillers (carbon fibres, recycled carbon fibres and carbon nanotubes) are added to various bio-based polymers: poly(lactic acid) (PLA), poly(3-hydroxybutyrate-co-3-hydroxyvalerate), polyethylene (Bio-PE) and polyamide, to improve their electrical conductivity. Microscopic observations indicated that the process of extrusion followed by injection moulding achieved an effective distribution and dispersion of most fillers within the polymer matrix. Solely, in PLA the nanotubes showed a preferential alignment at low loadings, and in Bio-PE the dispersion of the nanotubes could not be demonstrated. In case of good filler-polymer interaction (showed by increased tensile strength), the use of conductive filler with high aspect ratio induced an improvement of composite electrical and mechanical properties at equal filler loading. The lowest electrical percolation threshold was reached with the addition of the nanotubes in PLA, however it was simultaneous to a decrease in tensile strength and to an irregular change in thermal stability. The quick cooling happening during injection moulding limited the effect of nanotubes on crystallisation of PLA and Bio-PE. Finally, the variations in thermal expansion and deflection temperature under load due to the addition of nanotubes and measured at the composite surface differed from the one measured for the bulk.

Keywords: thermoplastics, nanocomposites, carbon, electrical conductivity, nanothermal.

La modification des propriétés des polymères synthétisés à partir de biomasse est cruciale pour diversifier leurs applications. Dans cette thèse, différents matériaux de remplissage à base de carbone (fibres, fibres recyclées et nanotubes) sont ajoutés à des polymères bio-sourcés : acide polylactique (PLA), poly(β-hydroxybutyrate-co-valerate), polyéthylène (Bio-PE) et polyamide, afin d'améliorer leur conductivité électrique. L'analyse de la structure des composites obtenus a montré que le procédé d'extrusion suivi de l'injection par moulage permet une distribution homogène et la dispersion de la plupart des matériaux de remplissage testés. Cependant, dans le PLA, les nanotubes ont montré

à faible concentration un alignement préférentiel et dans le Bio-PE la dispersion des nanotubes n'a pas pu être démontrée. Lorsque le matériau de remplissage conducteur d'électricité et le polymère interagissaient (augmentation de la résistance à la traction), l'utilisation d'un matériau avec un plus grand rapport longueur sur diamètre entrainait une amélioration des propriétés électriques et mécaniques des composites à taux de remplissage égal. La limite de percolation électrique la plus basse a été obtenue par l'ajout de nanotubes dans du PLA, cependant c'était simultané à une diminution de la résistance à la traction ainsi qu'à une variation irrégulière de la résistance à la dégradation thermique du composite. De plus, le rapide refroidissement lié au procédé d'injection par moulage a limité l'effet des nanotubes sur la cristallisation du PLA et du Bio-PE. Enfin, les variations en expansion thermique et en température de fléchissement sous charge liées à l'ajout de nanotubes et mesurées à la surface des composites ont différé de celles mesurées sur le volume.

List of publications

Paper I

Rivière, P., Nypelö, T. E., Obersriebnig, M., Bock, H., Müller, M., Mundigler, N., & Wimmer, R. Unmodified multi-wall carbon nanotubes in polylactic acid for electrically conductive injection-moulded composites. *Journal of Thermoplastic Composite Materials*, 2016, in press

Paper II

Rivière, P., Nypelö, T., Rojas, O. J., Klug, A., Mundigler, N., & Wimmer, R. Space-resolved thermal properties of thermoplastics reinforced with carbon nanotubes. *Journal of Thermal Analysis and Calorimetry*, 2016, in press

Author’s contribution

Microscopic analysis

Ms. Pauline Rivière did the SEM analysis under the supervision of Dr. Pum Dietmar at the Department of Nanobiotechnology of the University of Natural Resources and Life Sciences of Vienna (BOKU) and assisted M. Klug for the measurement at the Institute of Physics of BOKU and M. Ricardo Oliva at the electron microscopy facilities of the University of Concepción, Chile.

Sample production

The masterbatches with MWCNTs were prepared at Cpolymers facility under the supervision of M. Eder. Further preparation of the samples was done by Pauline Rivière with the help of M. Stürmer at the Institute of Natural Materials Technology.

Mechanical characterization

Ms. Pauline Rivière was helped by M. Schlager for the mechanical characterization of the samples at the Institute of Natural Materials Technology.

Electrical measurements

Ms. Pauline Rivière organised the selection and sent the samples to the different scientific partners. Dr. Schwarz, at this time working at Dekra Exam,Germany, did the electrical characterization with two stripes. M. Gerhard Frieling from the Technical University of Dortmund, Germany realized the two-point measurement with the clamped electrodes. Prof. Hassel from the Institute of Physics at Johannes Kepler University of Linz, Austria, did the electrical characterization with the four aligned pin electrodes. M. Paul Patter under the supervision of Dr. Andreas Klug did electrical characterization of the samples at the NanoTecCenter of Weiz, Austria. The rest of the electrical characterization was done by Pauline Rivière at the Institute of Natural Materials Technology.

Nanothermal analysis

Ms. Pauline Rivière did the selection and preparation of the samples before sending them to Dr. Tiina Nypelö, who did all the AFM and nanothermal measurements presented in this thesis at the forest biomaterials Department of North Carolina State University, USA and at the Institute of Wood Technology and Renewable Materials of the BOKU. Ms.Pauline Rivière performed the interpretation and presentation of the results in cooperation with Dr. Nypelö.

Table of contents

1 Introduction

Since the beginning of the 20th century petroleum oil based polymers (synthetic polymers) have been widely used in the production of plastic materials, which are now omnipresent in our everyday life (e.g. phones, bags, toothbrushes...). Polymers are classified in two groups, depending on the link existing between the polymer chains once it is formed. In thermosetting and elastomeric plastics the polymer chains are covalently linked, whereas in thermoplastics the polymer chains are interacting through physical interactions and therefore can be reshaped when heating them to their melting temperature. Different fillers and additives are often added to thermoplastics to adjust the properties and thereby widen their applications. The resulting plastics are also called thermoplastic composites.

1.1 Thermoplastic composites

In industry, many different types of polymers, fillers and additives are available for the production of thermoplastic composites. Common thermoplastic polymers are polyethylene, polyamide and polypropylene. Since resource sustainability concerns have arisen, notable efforts have been made in reducing the ratio of oil-based polymers in the composites. One way to achieve this is replacing them with bio-based polymers obtained from chemical or biological transformation of renewable resources such as plant biomass [1–3].

1.1.1 Bio-based polymers

The demand for bio-based polymers is expected to grow significantly during the next few years. Some of these bio-based polymers can also be biodegradable, i.e., degraded by microorganisms under specific conditions. Plastics mainly made of bio-based polymers or biodegradable polymers are referred to as bioplastics. Based on the year 2012 capacities, the bioplastic production in Europe has been forecasted to increase up to 400 % by 2017 [4].

The two most common types of bio-based and biodegradable polymers introduced to the industry today are poly(lactic-acid) (PLA) and poly(β-hydroxyalkanoate) (PHA) [5–7]. PLA is a semi-crystalline polyester based usually on the polymerization of L-lactic acid as produced through fermentation of corn starch [8,9]. Some D-lactic acid monomers can be introduced in the polymer structure as well [10]. PLA has already been successfully established for applications ranging from textiles, medical appliances to food packaging [11,12]. At low crystallinity, PLA has a glass transition temperature around 60-65°C and becomes sticky at ambient temperature. To ease the extrusion and injection process, the compounds are often thermally annealed, which increases its crystallinity and thereby its glass transition temperature [13]. PHA can be obtained from various gram-positive bacteria of the genus *Bacillus* as intracellular reserve material [7]. One of the most widely used PHA is the poly(β-hydroxybutyrate-co-valerate) (PHBV), a copolymer of poly(β-hydroxybutyrate) PHB and poly(β-hydroxyvalerate). The copolymerization provides lower crystallinity compared to the homopolymer PHB. Compared to neat PHB the PHBV blend is less brittle and has a lower melting temperature without any decrease in the degradation temperature [14,15].

It is also possible to synthesize thermoplastics from biomass, for example: polyethylene and polyamide. One hundred percent bio-based polyethylene (Bio-PE), is produced through the fermentation of sugars into ethanol, followed by polymerization process [3,16]. Completely as well as partially bio-based polyamide (Bio-PA) can be obtained through polycondensation of castor oil derivatives [3,17].

Similar to thermoplastic oil-based polymers, bio-based polymers properties can be modified by the addition of fillers and additives. Some examples are: glass and carbon fibres, natural fibres, clay, montmorillite, pigments, and impact modifiers. These fillers are used to enhance mechanical, thermal, electrical properties of the composites or modify composite weight, price or colour. Thereby new application sectors as technical composites, household items, or packaging materials are accessed. As an example, natural fibres or particles, as obtained from hemp, flax or wood can be used to enhance some of the polymer properties, such as increasing the composite stiffness, reducing the composite weight or change its color [18–20].

Besides filler selection, design of such composites also requires consideration of two important composite characteristics: the composite structure homogeneity and the filler-polymer interaction.

1.1.2 Addition of the fillers

Composite structure homogeneity is dependent on the filler distribution and dispersion in the composite. The distribution of the filler characterizes the homogeneous repartition within a composite, and filler dispersion describes the degree of separation of the filling particles/fibres from each other. If one composite contains filler agglomerates, which are homogeneously present in the whole material, the filler would have a good distribution but a bad dispersion in the composite. If the filler particles/fibres are well separated from each other but are more present in one region of the composite (e. g. in the centre or on one side), the filler would have a good dispersion but a bad distribution. The level of dispersion directly influences the composite properties. Therefore, the production of thermoplastic composite containing fillers is usually done in two steps. The fillers are mixed first in the polymer matrix before being formed in the final product shape. The mixing step is designed to guaranty that the filler is homogeneously distributed and dispersed in the polymer matrix. In the industry of thermoplastic packaging products, a very common process is the melt-mixing on an extrusion line ("compounding") [21,22]. During compounding high shear forces are applied to the material through a co-rotating twin-screw extruder to allow homogeneous distribution and dispersion of short fibres in the polymer matrix [23].

While the structure of the composite is mostly determined during melt-mixing, subsequent mould processes may also have an additional effect on the composite structure [24,25]. Different shaping processes such as injection moulding, compression moulding, extrusion and film blowing can be employed depending on the object to be produced. Injection moulding is known as the most common procedures in thermoplastic industry [26]. It is a discontinuous process allowing the production of finished-3D products by injecting melted material into a mould. It is often used in the production of bottle caps, packaging, automotive parts. In injection moulding, filler can be redistributed and reoriented depending on mould geometry and filler shape. In the case of fibrous or platelet fillers, one expects the formation of two distinct regions: a skin layer and a core region [26–29]. In the skin layer, fillers are aligned in the injection direction due to the higher shear and quick cooling [26]. The production process determines most of the composite structure however the filler type can also induce variations in temperature and melt viscosities affecting the structure of the composite as well. For example, the influence of the addition of wood fibres on the process of thermoplastic biocomposites with extrusion and injection moulding was studied [18,21]. The authors compared melt temperatures, melt pressures and machine load, all determined during extrusion, as well as the injection pressure and dosing time as recorded during injection moulding of different composites to obtain information on the compatibility of the filler with the polymer with respect to melt viscosity. Thus, under constant extrusion parameters increases in melt pressure and machine load were interpreted as increase in melt viscosity. Similarly, an increase in injection pressure, at constant injection moulding production parameters indicated an increase in melt viscosity [18]. However, it was also observed that filler could induce variations in the temperatures applied to the material during the process, due to friction between the filling elements [18]. Additionally, the dosing time, which is the time needed to fill in the mould during injection moulding, can be determined during production to obtain information on the granule geometry and packing.

The second critical issue for composite manufacturing is the interaction between the filler and the polymer [27–31]. It will determine the adhesion between the components and thereby affect its properties. Filler-polymer adhesion can be improved by using polymers with higher affinity to the filler or by surface modifications such as grafting and oxidation [12,25,28,31,32]. It was also suggested that polymers with longer chain are more likely to interact with fillers [27,33]. Filler–polymer affinity can be determined by calculating the wetting or spreading parameter, which is related to surface tensions of the filler, of the matrix and of the filler-matrix interface. Surface tension, also called surface free energy, consists of dispersive and polar surface free energies [34]. They can be calculated from the measured contact angle θ between the surface of drops of liquids with various polarity, and the surface of the solid filler. This contact angle results from the balance between cohesion forces of the liquid and adhesion forces between the liquid and the solid phases [35]. The value of this contact angle is usually directly interpreted in terms of wetting of the solid surface by the liquid. For contact angle inferior to 90° high wetting happens, with 0° meaning a prefect wetting. For higher contact angle the wetting of the surface is unfavourable. When the surface tensions of the solid and liquid phases are known, the wetting can be predicted. Zisman [36] explained that the higher the solid surface tension and the lower the liquid surface tension, the better the wettability. However, if the solid part has a lower surface tension than the polymer matrix, the wetting will be hindered [37,38]. This is further supported by a low polymer-filler surface tension [37].

1.1.3 Main composite properties

The main characteristics for thermoplastic composites are usually those describing the composite mechanical and thermal behaviours. When homogeneous composite structure and good filler-polymer interaction are reached, mechanical and thermal properties of the composite are expected to vary with the filler loading and reach a value between the polymer and the filler properties. The properties investigated to detect mechanical reinforcement are commonly tensile strength, Young's modulus, flexural strength and modulus and impact strength. The improvement of these properties is strongly related to the quality of polymer-filler interaction. Thus, an increase in tensile strength is indicative of a good filler-polymer interaction quality. If the filler is not interacting with the polymer matrix, it can create defects in the composite and mechanical properties of the composite will decrease with the addition of fillers. Thus, the addition of fillers with higher mechanical stiffness can induce an increase in composite stiffness, and new applications as technical plastics can be accessed. Mathematical models have been presented to predict the Young's modulus of reinforced polymers [39–41]. A frequently used one is the Halpin-Tsai equation for short fibres reinforced polymers [39,40]. This model assumes a uniform distribution of fillers, perfect bonding between the fillers and the matrix, and a void-free matrix. It was found to give close results to the experimental data for randomly oriented nanofillers by Mallick et al.[40] and Kanagaraj et al.[42]. This model is a good opportunity to assess the effective use of the short fillers properties in the composite mechanical reinforcement. Thermal stability refers to the description of composite thermal degradation. It is usually described by the degradation start with the onset temperature (temperature at which more than 5 wt% of the composite is degraded) and by the degradation area with the temperature and speed of maximal degradation. If the sample is sensible to oxidation, the results will differ between measurements in air (representing atmospheric condition) and measurements in inert gas (e.g. N_2).

Because of the very low conductivity of many polymer matrices, plastics are generally electrically insulating materials [43]. This is of great interest for the insulation of cables however can be problematic for packaging of electronic items and dangerous goods containers or for automotive components [11,43–47]. Indeed, due to low conductivity, electrical charges may accumulate at plastic product surfaces resulting in detrimental effects that range from the electrostatic attraction of dust to the induction of inconvenient electrical shocks to handlers and electronic systems. To prevent the accumulation of surface charges, it is recommended to use a material classified at least as static dissipative or conductive depending on the application [43]. Such materials are of great interest for the production of electron magnetic interference (EMI) shielding packaging. Commonly, this corresponds to volume conductivity respectively higher than 10^{-9} S m^{-1} or 10^{-3} S m^{-1}, see Figure 1 [11,37,43].

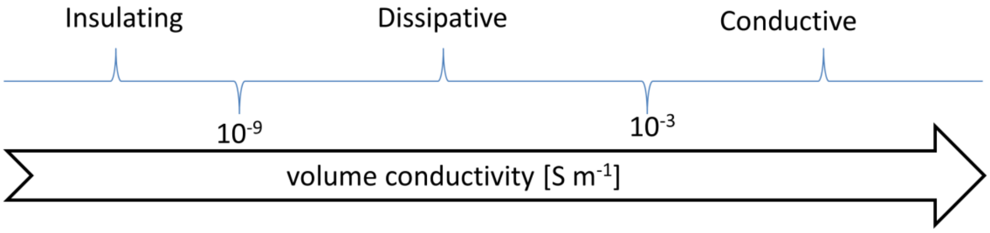

Figure 1: Classification of materials depending on their electrical volume conductivity.

Composite electrical conductivity is expected to increase when adding filler more conductive than the polymer. However, the increase takes place only when a conductive network is formed by the filler through the entire composite. The filler loading corresponding to the conductivity increase, which can also be determined as the peak of the conductivity first derivative regarding filler loading, is called the electrical percolation threshold [43,48,49]. When the filler content is further increased, composite conductivity is expected to increase until it reaches an upper conductivity limit, which can also be determined by level of electrical conductivity.

In some cases, the conductivity will depend on the current applied on the composite. This is usually detected by measuring the voltage potential obtained at different current intensities. If the current-voltage slope is constant, the composite behaves as ohmic resistor (follow Ohm's law, Equation 1). It means that the electrons are directly transferred by the conductive fillers through the composite. Thus, its resistance can be determined directly from measurement with constant current intensity as presented in Equation 1.

$$R = \frac{\Delta U}{I} \quad \text{Equation 1}$$

Where R is the resistance of the sample (Ω), ΔU the potential difference at the terminals of the sample (V) and I the current applied at the terminals of the sample (A).

Non-linear relation between current-voltage potential is indicative of the fact that other conduction mechanisms are happening such as tunnelling and hopping [50]. In tunnelling the electron is transferred through an insulating layer, for example a polymer layer between two semi-conductive/conductive materials, this implies that the voltage potential between the two materials is high enough and the polymer layer thin enough to allow direct transfer. In the hopping mechanism, the electron needs first to hop an energy barrier and then is further transferred by tunnelling [37,50]. Moreover, for thermoplastic composite, the passage of current can induce a heating of the polymer, which reduces the overall composite resistance [51].

Depending on the location of the measurement points, two types of conductivity are usually distinguished: surface and volume conductivities. The conductivity measured is a surface conductivity if all electrodes are in contact with one surface of the sample as in the study of Moon et al.[9], while it is a volume conductivity if the electrodes are applied on opposite surfaces [38,52–54]. The concepts of surface and volume conductivities are commonly used to ease the distinction between the two setups even if the current is always passing through a volume [43]. Volume conductivity is expressed in S m^{-1} while surface conductivity can be expressed in S, in S cm^{-2} or in S sq^{-1}, where sq (square) refers to the "surface" area involved in the measurement [43]. Surface conductivity is widely used to characterize thin layers or films. For homogeneous materials, the surface conductivity can be calculated by dividing the volume conductivity by the thickness of the sample exposed to the current and vice versa [43]. However, due to the skin layer-core region organisation in injection moulding composites, the structure of the composite near its surface can differ from the core and therefore it is expected that the two conductivities are not proportional.

Various methods are presented in the literature to measure volume or surface electrical conductivity of thermoplastic composites [9,28,38,52,53,55–57]. These methods are here classified into three groups: (1) two-point, (2) four-point and (3) ring electrode methods. The two-point method consists in measuring the sample resistance with two electrodes simply applied on two locations on the sample. Sample conductivity is then calculated from the measured resistance as defined by Ohm`s law (Equation 1). However, if the sample is more conductive than the wires or than the contacts between the electrodes and the sample, the measurement with the two-point method does not reflect anymore the sample properties [53,55,56]. To ensure that the resistance measured is really reflecting the sample properties one can decrease the resistance between the electrodes and the sample. This can be done with a conductive paste such as silver paint. Another way is to use four electrodes and measure the voltage potential ΔU with equipment independent from the current source. This method is called the four-point method. This way, the measured voltage corresponds exclusively to the part of the circuit exposed to the current, i.e., the sample. The advantages of this setup are that the contact quality between the source-electrodes and the sample does not influence the voltage potential measured between the sensor electrodes and low resistivity can be quantified [43]. The ring electrode measurement method is a standardized method (IEC 60093-199) widely used for film or sheet characterization. This method clearly distinguishes the determination of the surface conductivity from the volume conductivity [31,55,57]. The volume conductivity is obtained when the current is applied through the electrodes « 1 » and « 3 » as shown in Figure 2, and the electrode « 2 » is insulating (linked to the ground 0V). The surface resistance is obtained when the current is applied through the electrodes « 1 » and « 2 » and the electrode « 3 » is linked to the ground (0V) [31]. In presence of exterior electromagnetic waves, the measurement of low current can present important variation as external electromagnetic waves are added to the signal. To prevent this, shielded cables are used and the system can be placed in a "Faraday cage"[43].

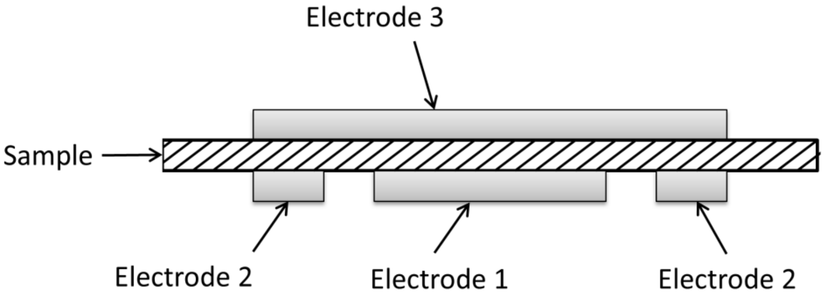

Figure 2: Installation of the ring-electrodes to determine the sample surface or volume conductivity.

To enhance composite electrical conductivity permanently, conductive fillers such as metallic fibres and powders, carbon fibres (CF), carbon black (CB), as well as powders of layered minerals or metal coated polymer, are used [37,43]. Depending on the filler type and loading, the composites can reach volume conductivities above 10^{-3} S m^{-1} and thereby enter the group of electrically conductive materials (Figure 1) [37,43]. Blending with electrically conductive polymers or adding surfactants is also possible, however these blends are less stable than those with rigid fillers and will not be discussed here [43]. Carbon-based fillers are currently preferred over other conductive fillers notably because of their lightness. This work will focus on the effect of different carbon-based fillers on thermoplastic composite properties.

Various theories have been developed to predict the electrical behaviour of two and three dimensional percolation systems [58–62]. Based on the percolation theory of Dubson and Garland and the symmetric and asymmetric theories of Bruggeman on effective media characterization, Mc Lachlan et al.[58] proposed the General Effective Media (GEM) model. They used this model with success to predict electrical percolative conductivity behaviour under direct or alternative current (respectively dc and ac) for various filler types: such as CB or SWCNT [59,63,64]. Celzard et al.[60] compared three models: one mean-field approach considering an homogeneous effective medium, one approach considering the packing of the conductive filler together with empirical filler density and an approach using the excluded volumes due to filler geometry. This last approach was presented as the most adapted model to predict electrical behaviour for polymer carbon fibre composites [60]. Lisunova et al.[65] explained discrepancies between the statistical percolation theory and experimental values in the case of CNT filled polymers by the packing and the agglomeration of the CNT in the composites. This packing was compared to the one observed when considering colloidal systems and they proposed another model for percolation threshold behaviour [65–67]. More recently, Combessis et al.[61] used the Kirkpatrick's model and Nan's Law to approximate the fraction of filler in volume corresponding to the percolation threshold for MWCNT filled epoxy resin. However, they reported that the percolation threshold calculated with Nan's law showed large differences with experimental data for composites containing fibrillar fillers [61]. They suggested that the processing method was strongly affecting the percolation threshold regardless of the chemical nature of the polymer [61].

1.2 Carbon-based fillers in thermoplastic composites

Carbon-based fillers are available in many different shapes: fibre, tube and platelet, and at different dimensions with length varying from some meters (continuous carbon fibres) to some nanometers (fullerene). Carbon fibres and carbon nanotubes will be further considered here.

1.2.1 From carbon fibres (CF) to carbon nanotubes (CNT)

Carbon fibres result from the progressive stabilization of polyacrylonitrile fibres by heating them in air up to 300°C followed by carbonization at high temperature (1000 to 3000°C) in an oxygen-free furnace. Carbon fibres are widely used in combination with thermoplastics and thermosets to reinforce polymer mechanical properties [68]. For injection moulding, the continuous carbon fibres are cut to a length of 6 mm. They are available with various surface modifications (called “sizing”), to enhance filler-polymer interaction and thereby mechanical properties [31,43]. Recycled carbon fibres (RCF) of various origins are also considered for composite reinforcement, and can as well enhance the thermoplastics electrical conductivity [43,68]. Recycled carbon fibres can be obtained from old composite parts containing continuous carbon fibres by melting or degrading the polymer matrix with high temperatures (up to 500°C) and milling or directly by milling unused continuous carbon fibres together.

With the rapid development of nanofiller production, research on conductive composites has been focusing on the utilization of carbon-based nanofillers, especially on carbon nanotubes (CNTs), carbon black and carbon nanofibres [37,69,70]. Carbon nanotubes are particularly attractive as they combine many outstanding properties including mechanical strength and stiffness as well as thermal and electrical conductivities that are superior to those of most other fillers [71–73]. The first production of CNTs was realized using an arc discharge method. It consisted in inducing carbon nanotube growth by applying an electric arc discharge between two graphite electrodes at low pressure and neutral atmosphere. The electrical arc induced the sublimation of carbon from the electrodes, which reassembled in nanotubes. Since then, further methods have been developed that are mostly based on physical processes in which the carbon vaporization can be induced by different energy sources such as electric arc-discharge, laser ablation, or solar energy [46,74]. There are also chemical methods to produce CNTs, such as catalytic decomposition of hydrocarbons by electrolysis, heat treatment, or solid pyrolysis [46]. Depending on the production parameters and methods, CNTs with one, two or more concentric graphitic layers are obtained; they are respectively called single, double and multi-walled carbon nanotube (SWCNT, DWCNT and MWCNT). Among above, MWCNTs are the cheapest to produce and unlike SWCNTs, they also offer opportunities for surface modification without detrimental effects on the inner layers [70]. A more recent method called “catalytic chemical vapour deposition” (CCVD, Figure 2) consists in growing carbon nanotube on catalyst particles by heating up methane in a furnace chamber. This method has been reported as the most common technique to produce multi-walled carbon nanotube (MWCNT) at relatively low temperature and large scale, compared to high temperature processes such as arc discharge and laser furnace processes [46,75,76]. MWCNTs produced by CCVD are found to show more defects than when produced with high temperatures processes, however the MWCNTs can be chemically purified afterwards to remove remaining catalyst, and high temperature-treatments under N_2 can be used to repair possible irregularities in the carbon structure [75].

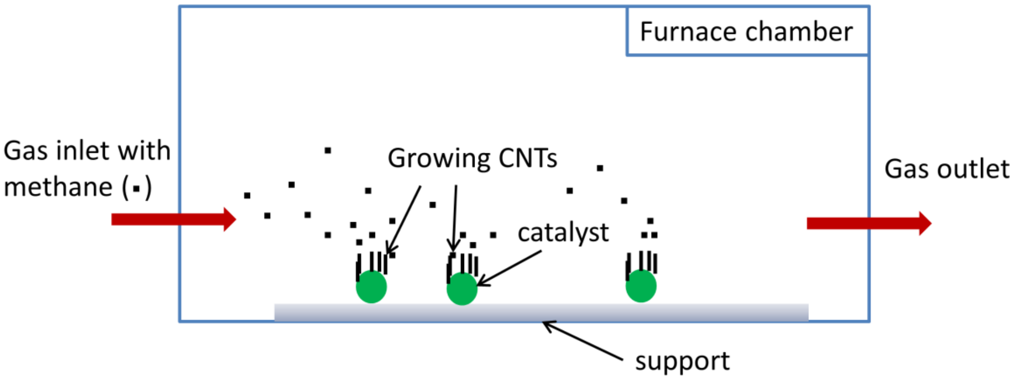

Figure 3 : Description of thermal "catalytic chemical vapour deposition" process (CCVD) to produce multi-walled carbon nanotubes.

1.2.2 Composite structure and CNT entanglement

The carbon fibres distribution and dispersion is generally assessed by scanning electron microscopy on fractured sections of a given composite material, or by optical microscopy using thin films with low filler loading [31,52,57,77]. In the case of MWCNTs, SEM or light microscopy is as well used to observe the macro dispersion of MWCNTs and detect eventual MWCNTs aggregates [23,30]. However, these methods are suboptimal to recognize individual nanometric fillers, which leads to the use of alternative microscopy methods as transmission electronic microscopy on thin films (TEM) or atomic force microscopy (AFM) [23,24,31,78]. AFM consists in scanning sample surface with a tip fixed on a cantilever or probe that can interact with the sample in a continuous way through direct contact called "contact mode", or in a discontinuous way through oscillation called "tapping mode". The movements of the probe are measured by the reflexion of a laser on the back of the probe. This method provides images of the composite surface, however, the topography measurement is also influenced by the variation in material stiffness, whereas with SEM and TEM the observations are influenced by the composite electrical conductivity [31]. These methods are all operating at high spatial resolution.

One of the main issue encountered when using CNT in thermoplastic composites is a poor dispersion in the polymer matrix resulting from bundling and entanglement of the CNTs, leading to unnecessary high percolation thresholds and unnecessary high CNT use [24]. Thus, the effect of processing condition and melt viscosity on CNT distribution and dispersion has been widely described in the literature. Various mixing preparation methods have been tested among which melt-mixing being most suitable for industry [23,25]. With SEM imaging on fractured surfaces, Valentino et al.[30] detected changes in the distribution by melt-mixing of MWCNT in HDPE and in LDPE. They suggested that the presence of aggregates observed for LDPE was due to inappropriate mixing temperatures. In their study, Villmow et al.[26] observed the dispersion of MWCNTs by TEM on cut slides of the original injection moulded plates. Thereby they reported that MWCNTs present in the skin layer were increasingly oriented when higher injection speed and lower melt temperature were selected [26]. Aguilar et al.[52] and Pegel et al.[24] detected that secondary agglomeration of MWCNTs could happen in solution casting, extrusion or pressing and was supported by the use of lower polymer viscosity, shearing stress, pressing speed or high melt temperatures [24,52]. Pegel et al.[24] reported that high shearing forces are needed to disperse CNT. In melt-mixing, shear forces can be increased using high rotation speeds and highly viscous mixtures [23]. The latter was exploited in extrusion by loading the polymer with higher concentrations of CNTs to produce masterbatches, followed by diluting them with neat polymer to achieve the desired concentration [23,25]. Entangled MWCNTs were efficiently dispersed this way, however excessively high shearing forces were suggested to induce CNT degradation [23]. Another way to modify melt viscosity and CNT distribution was presented by Kordkeilli et al.[79]. They reported that when mixing wood flour and SWCNT in maleic anhydride grafted polyethylene, the SWCNT were found to fill the void between the wood flour particles and the polymer matrix. Al-Saleh et al.[37] and Leute et al. [43] also suggested that when volume filler such as wood flour is present in the composite, the filler distribution is limited to the remaining regions of polymer matrix, and the fillers can form a network at lower loading.

1.2.3 Composite properties, filler aspect ratio and filler surface modification

MWCNT were found to induce high improvement in composite mechanical properties at lower loading when compared to carbon fibres [32,74]. As for carbon fibres, the effect of MWCNTs on the properties has been reported to vary with filler-polymer interaction. Nuriel et al.[34] found similar wettability tendencies for unmodified carbon fibres, carbon nanofibres and MWCNTs, by polyethylene glycol (PEG) and by polypropylene (PP). Wetting took place for both polymers with all carbon-based components, but they found lower contact angles with PP, which were interpreted as better wetting [34]. The limit of liquid surface tension able to wet completely or partially MWCNT surfaces was set at 200 mJ m^{-2}, with partial wettability starting at 130 mJ m^{-2} [80,81]. To enable good wettability and thereby CNT-polymer interactions, CNT surface is usually modified in the case a polar polymer such as PLA is used as a matrix [9,52,82]. Moreover, it has been reported that improved filler-matrix adhesion leads to improved filler dispersion [12,25,37,38]. Sathyanarayana et al.[74] suggested that modified CNTs induced strong increase in mechanical properties in the case of polar polymers. They could also induce increases in Young’s modulus for polyolefines such as PE and PP as reported by Kanagaraj et al.[42] and Bao et al.[83].

Similarly, literature on MWCNT-filled composites mostly reports increase in thermal stability from TGA measurements, along with higher loadings [2,84–86]. Ge et al.[2] suggested three mechanisms to explain the improvement observed for polyacrylonitrile filled with oxidized MWCNTs: (1) well dispersed MWCNTs may delay the release of the gas produced during thermal degradation, (2) polymer molecules interacting with MWCNT show reduced degradation, (3) higher thermal conductivity due to the MWCNT network dissipates heat within the composite. In the review by Corcione et al. [84] the authors generalized the plausibility of these mechanisms to explain improvements in thermal stability for CNT-filled polymers. Corcione et al. [84] suggested that energetic stabilization of degradation products by π- π electronic interaction with MWCNTs could happen in ethylene-vinyl acetate copolymer (EVA)-based nanocomposite presented by Beyer et al. [85].

Concerning composite electrical conductivity, some general tendencies are derived from the literature. Conductive fillers with higher aspect ratio always presents lower percolation threshold when polymer type and the production process are not changed [9,28,38,52,53,55–57]. In the case of MWCNT, the reported electrical conductivities and percolation thresholds in thermoplastics are often differing [38,52,53,55–57]. The variations observed were generally related to differences in MWCNTs dispersion, in the polymer matrix conductivity, or in the nanotube surface modification. Thus, Novais et al.[57] obtained higher conductivities on compressed plates by adding unmodified MWCNTs to PLA instead of PLA-grafted MWCNTs. Bauhofer and Kovacs [87] suggested that the presence of a polymer layer at CNT surface limited composite electrical conductivity. As a consequence, percolation threshold increased and the electrical conductivity of the composite decreased [25,53]. These results show that chemical modification of the MWCNT surfaces enabling stronger filler-polymer interaction and supporting filler dispersion can induce degradation of MWCNTs, prevent direct contact between the nanotubes and limit the formation of conductive aggregates profitable to the conductive network [24,38,74]. Additionally, Byrne et al.[25] reported that the addition of electrically inert particulate filler to the composite can support the improvement in MWCNT–filled composite conductivity. This is probably related to a change in filler distribution as reported by Leute et al.[43] and Al-Saleh et al.[37] in presence of wood flour. Tunnelling and hopping effects were also suggested to induce variations in conductivity depending on the current applied for composite filled with CF, CB, carbon nanofibres and CNTs [37,87–90].

Moreover, with the development of the melt-mixing process techniques for CNTs it was reported that efficient nanotube dispersion of unmodified nanotubes could be obtained by extrusion. Surface modification may not be necessary to disperse the tubes in polymer such as PLA or polycarbonate, as shown in the studies by Mack et al.[28], Villmow et al.[23], and Novais et al.[57]. These authors used unmodified MWCNTs in polycarbonate and PLA to produce composites by melt mixing followed by compression moulding or injection moulding, obtaining reasonable dispersion. Besides the secondary agglomeration described by Pegel et al.[24] and Aguilar et al.[52], and happening during composite processing was reported to induce an increase in electrical conductivity. The author explained this by the improved nanotube–nanotube contact.

This raises the question of the interest of MWCNT surface modification in the design of electrically conductive composite. Thus, if enhanced electrical conductivity is a priority, the use of unmodified MWCNTs can be of greater interest, but will possibly be detrimental to mechanical and thermal stability. The few studies found on the effect of unmodified carbon nanotubes on composite mechanical properties reported slightly increasing or decreasing tensile strength [28]. Regarding the effect of unmodified MWCNTs on thermoplastic composite thermal stability, many studies reported an improved thermal stability of the composites using unmodified MWCNTs, compared to the neat polymer [8–10,91]. However, the improvement varied with the amount of added MWCNTs, and with the range of applied temperature. Schartel et al.[92,93] reported for polyamide 6 that the addition of unmodified MWCNTs did not affect the polymer thermal decomposition. In their study Wu et al.[91] added unmodified MWCNTs to PLA and observed no variation in temperature at which 5wt% of the material is degraded (T_d) but an increase of around 10°C of the temperature at which maximum degradation speed is observed (T_{dmax}) when 5 wt% MWCNTs were added. In this study, the unmodified MWCNTs induced even higher T_{dmax}, compared to modified MWCNTs. This result was unexpected as the dispersion of the unmodified MWCNTs was very poor compared to the one of the modified MWCNTs. The authors explained their result by the higher increase in thermal conductivity of unmodified MWCNTs in regards to the effect of MWCNT dispersion at high loadings.

Besides electrical and mechanical behaviours and thermal stability, another important behaviour to control in thermoplastic composite is the thermal behaviour. This is of importance to understand the dependence of composite properties to variations in temperature but also to select composite processing conditions.

1.3 Carbon nanotubes effect on semi-crystalline polymer thermal behaviour

One way to characterize the effect of temperature on composites is to assess the variation in composite properties after exposing the composite to heat for a given time in a furnace. This heat treatment is also called annealing and depends on the temperature selected and the treatment time. It is applied to plastics notably to reduce or remove residual stresses and strains, and improve some physical properties. However it was also reported that thermal annealing of filler-polymer composite could induce a migration of the filler up to a complete separation of the filler from the polymer matrix [62,63,65,66]. This phenomenon was further described through the analysis of variations in composite electrical conductivity due to annealing. The annealing was first reported to increase percolation threshold and decrease conductivity [63,65]. For example, Lisunova et al.[65] observed a decrease in electrical conductivity with annealing temperature, when annealing MWCNT filled ultrahigh molecular weight polyethylene at temperatures higher than the polymer melting point. They related this to an effect of positive temperature coefficient (PTC) on resistivity [65]. The segregation of the filler happening during annealing was then related to various modification of the composite state such as the relaxation of polymer chains, the diffusion of the conductive fillers to melted crystalline areas or polymer thermal expansion [65]. Recently, Combessis et al.[48] described the migration of MWCNT during annealing in ethylene-co-vinyl acetate (EVA). They observed strong increases in electrical conductivity at constant MWCNT low loading (0.1 wt%) over annealing time. This phenomenon is called dynamic percolation. It was attributed to two successive mechanisms: entropic polymer chain relaxation followed by filler auto-assembly. Filler auto-assembly consisted in the diffusion of filler and aggregates through the matrix, which was found to possibly result in phase separation visible to the naked eye. Badard et al.[62] further studied MWCNT migration in silicone oil. They observed that at short time after stopping the stirring, dynamic percolation happened but with further annealing time the percolation network turned into isolated macro-clusters, which settled. They concluded that little aggregation of the fillers obtained through annealing in samples filled with conductive filler fraction near percolation lowered the percolation threshold. However, further segregation resulted in insulating materials, which can explain the results related to the PTC effect on composite resistivity in the literature. Badard et al.[62] also suggested that large scale diffusion of filler aggregates would be prevented by the presence of a percolating path and controlling annealing time in solid compound could allow blocking the migration of MWCNT clusters in an optimal conductive networking.

In the case of thermoplastic composite made with semi-crystalline polymers during melt-processing, the polymers experience an additional thermal transition called crystallisation. During crystallisation, the polymer chains can arrange to form crystals and induce the presence of crystalline and amorphous regions in the polymer matrix resulting in local changes of the composite properties. Therefore, for semi-crystalline polymers, annealing around crystallisation temperatures can also be used to increase the crystallinity of the polymer matrix. Polymer crystallisation process can be nucleated in presence of fillers. It is then called heterogeneous nucleation. Macroscopic fillers were found to nucleate polymer crystallisation as reported by Feller et al.[94] for long stainless-steel fibres in isotactic PP. However, nanofillers (talc, sodium stearate, carbon nanotubes...) were found to emphasize this effect due to their higher aspect ratio [95–97]. Therefore, MWCNTs ability to nucleate semi-crystalline polymer crystallisation has been intensively studied [25,27,70,77,97–100].

1.3.1 Polymer crystallisation and MWCNT

Crystallisation can happen during melt cooling, solid stretching or solution evaporation. If the polymer mobility allows it, the crystalline region will form one big crystal, called spherulite. Under specific shearing forces and elongation stress, polymer chains organized in shish-kebab structures. These structures consist of one linear polymer chain (shish) aligned in the elongation or shearing direction surrounded by folded polymer chains remaining in a plane perpendicular to the shish and thereby forming the kebab [97,101]. This induced great improvement of the mechanical properties of the composite and was even experimented as nanotube surface modification by growing polymer kebab at CNT surface during ultrasonication or dynamic packing injection moulding (DPIM) [99,101]. Through heterogeneous nucleation the formation of numerous and more homogenous repartitions of spherulites are induced within the composite [98]. The spherulites and crystalline regions formed deviate the polarized light differently as the amorphous regions and can therefore be detected by polarized light microscopy [98].

Some studies observed by differential scanning calorimetry (DSC) that MWCNTs can nucleate polymer crystallisation [95,96]. This was usually detected by a start of crystallisation at higher temperature during cooling or an increase in the crystallisation speed [95,96]. It can also be directly deduced from an increase in the polymer matrix crystallinity, calculated from the DSC analysis. However, other studies on MWCNT-filled thermoplastics also reported a decrease in crystallinity when MWCNTs were added. They explained this by the fact that MWCNTs could also limit the polymer chain mobility, which therefore can less freely rearrange in crystals and that the nucleation efficiency depended on the cooling rates and on the used polymer [72,83,93,102–106]. Concerning the localisation of the nanotubes, regarding the crystalline polymer regions, studies explained that when MWCNTs act as a nucleating agent, their surface will be covered by a crystalline polymer layer [23,25,107,108]. However, other studies described that the MWCNTs were more abundant in the amorphous regions after crystallisation as also reported by Leute [43] for carbon black filled PP [82]. Thereby the segregation of the filler already reported due to polymer chain relaxation and entropic filler aggregation by Combessis et al.[48] could be emphasized in the case of semi-crystalline polymer by the auto-assembly of the polymer chains.

1.3.2 Polymer crystallinity and composite properties

Higher crystallinity are generally associated with a higher glass transition temperature, which improves thermal resistance and enhances the barrier properties [97,98]. For example the higher elasticity of PLA at low crystallinity is of great interest for blow-forming and film production processes [97,98]. However, for the production of technical plastics, PLA crystallinity at the highest degree possible is preferred. In general, there is a particular interest to maximize the crystallinity of plastic materials during high-performance production processes, for which the cooling time is minimized, for example in injection moulding [13,97]. Depending on the number, size and repartition of the crystals the thermal transitions of the composite will differ and this can affect the electrical and mechanical properties of the composite. For example, the decrease in spherulite sizes obtained with heterogeneous nucleation was suggested by Zhang et al.[102] to support resistance to crack opening in impact strength test and thereby improved composite impact strength. As explained earlier, increased crystallinity was reported to induce filler migration giving a decrease in electrical conductivity percolation threshold and an increase in electrical conductivity [48,100,108]. This effect of polymer crystallization is comparable to the description of Badard et al.[62] on the positive effect of controlled annealing on filler polymer composite conductivity for filler loadings near percolation. This indicates that during polymer crystallization, MWCNT are more probably aggregated in amorphous regions than covered by a crystalline polymer layer, which would have hindered the transfer of electrons between the MWCNTs [25,26,108]. These theories point out the importance of considering the polymer crystalline state when analysing the electrical conductivity of semi-crystalline thermoplastic composites. To further understand the mechanisms implied in the mechanical and thermal behaviours of unmodified MWCNT-filled composite properties, thermo-mechanical analyses as the characterization of thermal deflection behaviour can be performed.

1.3.3 Deflection behaviour of nanocomposites

Deflection behaviour reflects the relation between composite mechanical and thermal properties. It is usually characterized by observing the bending of a composite bar under a given load when increasing the temperature (HDT A or HDT B methods). To deeper understand the effects of nanofillers on composite properties, techniques for probing composite properties at the micro and nanoscale have been developed, i.e. microthermal analysis and nanothermal analysis (nanoTA) [109]. The benefit of nanothermal analysis regarding microthermal analysis is the ability to probe thermal behaviour of materials at nanoscale. One example of nanothermal analysis set-up is atomic force microscope (AFM) coupled with a heatable tip able to probe the thermal transitions. In short, this nanoTA works by bringing an AFM probe with a tip diameter of about 20 nm in contact with the sample surface. The probe is heated up at constant heating rate. The heating raises the molecular mobility under the tip, as the heat is conducted to the sample. When temperature reaches the softening/melting point of the material under the probe, the tip sinks into the sample. The movement of the probe is monitored through the deflection of its cantilever. The sinking of the probe into the sample will be seen as a change in the deflection and is translated into a "thermal ramp". This is referred to as a transition temperature microscopy (TTM) map that enables probing of the melting point within spatial variations.

Nanothermal analysis has recently been emerging in the field of polymer science. It has been shown to be applicable for exploring polymer blends to identify the polymeric constituents [110]. In a comparison of micro and nanothermal analyses, Gotzen et al.[111] found that nanoTA is able to probe the early stages of the melting process. Such effects might be unrevealed for bulk analysis. Nikiforov et al.[112] used band excitation nanothermal analysis to study polystyrene-polymethyl metacrylate composites. The possibility to identify the different phases of the polymer mixes enabled observations on the phase separation behaviour. In the area of renewable polymers Ago et al.[113] used nanoTA to identify regions of lignin within polyvinyl alcohol nanofibres. This was possible due to their differentiating melting temperatures.

A few reports have compared the nanothermal analysis with DSC. Germinario et al.[114] studied crosslinked polymer coatings with the two techniques. They further confirmed the benefit of nanoTA as a surface sensitivity technique, hence being advantageous for phenomena taking place at the nanoscale, which was in their case crosslinking. Since nanoTA is based on probing the very surface of the substrate in use, it is highly suitable for analysis of coatings as well. As an example, Vähä-Nissi et al.[115] explored atomic layer deposition of an aluminium oxide layer on cellulosic substrate. However, it is not known yet how this method reacts in the presence of an electrically conductive composite.

2 Objective and definition of the research topic

In the present thesis, carbon-based fillers having different aspect ratios were mixed by extrusion with various polymer types. Composites were formed through injection moulding to assess the effect of filler aspect ratio and filler-polymer interaction on injection moulding composite structure and properties. Selected polymer types poly(lactic-acid) (PLA), poly(3-hydroxybutyrate-co-3-hydroxyvalerate) (PHBV), polyethylene (PE) and polyamide (PA) presented different structure and surface polarity, which were expected to induce different levels of filler-polymer interaction with the selected carbon-based fillers. PLA and PHBV are both polyesters and therefore present ester functions at their surface, which are very polar. Polyamide contains amide linkages and methyl groups exposed at their surface, which are mildly apolar. Polyethylene presents alkyl groups on its long regular polymer chain surface, which are less polar than all the previously presented groups and functions. It was suggested that polymers with lower polarity and thereby lower surface tension were more susceptible to develop van der Waals linkages with unmodified carbon fillers than the polymer with polar functions. Moreover, if the carbon fibres contain a sizing, that is, surface modification adapted to the polymer, better filler-polymer interaction and higher improvements of the composite mechanical properties are expected. More particularly if the sizing presents the same chemistry as the used polymer. Carbon fibres with varying surface sizing (polyester, polyamide, polyurethane), recycled carbon fibres with and without polyester surface sizing, and unmodified MWCNTs were used for comparison. Among the CF fibres sizing used, polyurethane sizing contains urethane groups, which are mildly polar and are usually used to chemically react directly with polyurethane during reticulation and not expected to induce strong polar interaction with the polymer. Additionally, few samples filled with CF and RCF were mixed with wood fibres to explore the effect of the addition of volumic non-conductive filler on the electrical conductivity. Melt mixing by extrusion followed by injection moulding was used to process all composites except the samples filled with MWCNTs for which the melt mixing was done in two steps: production of a masterbatch and dilution.

The first hypothesis of this study was that (1) melt mixing by extrusion before injection moulding induces homogeneous composite structure with all types of carbon fillers tested, and that the fillers alter the process. When comparing the effect of the different filler types on mechanical, thermal and electrical properties it was hypothesized that: (2) filler with higher aspect ratio and higher filler-polymer interaction obtained by filler surface sizing gives the best mechanical and thermal properties improvements but not the best electrical properties improvements since filler surface sizing hinders direct contact between the conductive fillers. Further analysis of the effect of MWCNTs on polymer crystallisation, thermal transition and deflection temperature measured from the bulk and at nanoscale is expected to (3) show that unmodified MWCNTs nucleate polymer crystallisation inducing increase in polymer crystallinity, thermal transition temperature and deflection temperature independent from the filler-polymer interaction. It is also hypothesized that (4) the nanothermal analysis will reveal aspects beyond the bulk methods due to being a surface sensitive nanoscale method and being able to access the early stages of the heat induced transformations.

3 Materials and Methods

3.1 Materials

Samples were prepared using six types of thermoplastic polymer filled with carbon-based fillers. Poly(lactic-acid) (PLA) NatureWorks® PLA 3051D and PLA 3251D were purchased from Resinex Group, Austria. According to the provider product data sheets they had relative solution viscosity of 3.30 and 2.50 with a standard deviation of +/-0.10. Relative viscosity reflects in the case of a polymer the resistance of the dissolved polymer to gradual deformation by shear stress or tensile stress in regards to the resistance of the pure used solvent. The solvent type and polymer concentration used for this characterization were not given by the producer. The two types of PLA had D-isomer percentages of 4.15 +/-0.45 and 1.4 +/-0.2, respectively. The poly(3-hydroxybutyrate-co-3-hydroxyvalerate) (PHBV) used in this work was obtained from provider TianAn biopolymer ENMAT^{TM} (China). High density 94.5% bio-based polyethylene SHA 7260 (Bio-PE) was a product of Braskem®. This type is derived from ethanol obtained from biomass fermentation. Two types of polyamide were used: the polyamide Vestamid® DS 18 (PADS 18) and the polyamide Vestamid Terra HS 18 (PAHS 18) by Evonik Industries (Germany). PADS 18 was obtained from the polycondensation of two castor oil derivatives, i.e. 1,10-decamethylene diamine and 1,10-decanedioic acid, the latter also called sebacic acid. This type of polyamide is 100% bio-based. PAHS 18, which is obtained from sebacic acid, combined with synthetic 1,6-hexamethylene diamine, is only partially bio-based: up to 62% of the PAHS 18 is made of derivatives from oil of castor bean. The used polymers are listed in Table 1, along with corresponding information given by the producers.

Table 1: Properties of the used polymers, according to producer's data sheets

Polymer	Density ASTM D792 (or ISO 1183 at 23°C)	Softening temperature [°C] ASTM D1525 (or ISO 306 by method A, 10N)	Tensile strength at yield [MPa] ASTM D638 (or ISO 527-2)	Melting temperature [°C] ASTM D3418 (or ISO 11357)	Melt flow index [g 10min^{-1}] ASTM D1238
PLA 3051D	1.25	-	48	150-1651	10-25 (210 °C 2.16 kg^{-1})
PLA 3251D	1.24	-	48	160-1701	70-85 (210 °C 2.16 kg^{-1})
PHBV (method not specified)	1.25	166	39	170-176	-
Bio-PE	0.955	124	29	-	20 (190 °C 2.16 kg^{-1})
PADS 18 (method ISO)	1.05	196	54	200	-
PAHS 18 (method ISO)	1.07	220	61	222	-

[1] Crystalline melt temperature

In this work the tested electrically conductive fillers were exclusively carbon-based. Carbon fibres from three different producers: Zolltek ^{TM} from Toray Group, USA, Toho Tenax from Teijing Group, Japan and SGL Carbon Group, Germany, were all at a length of 6 mm with diameters varying between 3 µm and 7.2 µm, having also different surface sizing: polyester, polyamide or polyurethane as described in Table 2.

Recycled carbon fibres were obtained from Apply Carbon SA (France), which is specialized in the cutting and recycling of technical and synthetic fibres. During the production of carbon filaments, spools were regularly kept to ensure the process quality. They are milled together giving a mixture of milled carbon fibres (CF MLD), equipped with various polymer surface sizing. Both recycled cqrbon fibre types had a density comprised between 1.7 and 2.0. For a part of the production, sizing was removed by thermal treatment (at 400 °C, under N_2) to produce low sizing CF MLD (CF.LS MLD), that is illustrated in Figure 4.

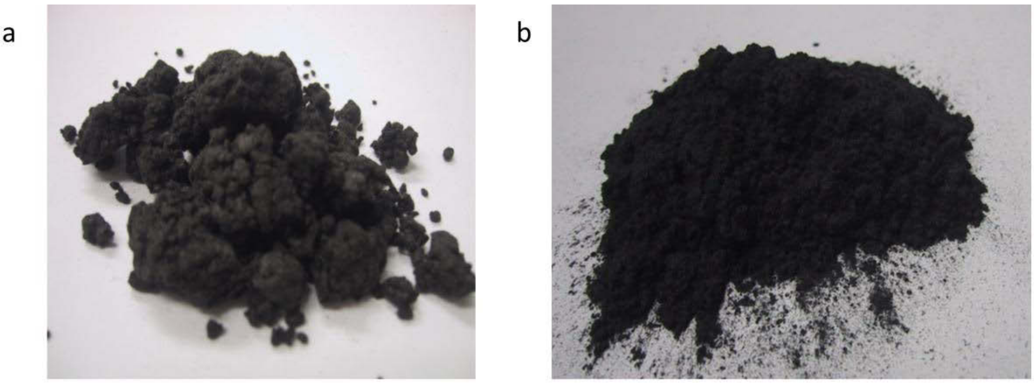

Figure 4: Recycled carbon fibres: (a) milled (CF MLD) and (b) milled with low surface sizing CF.LS MLD.

Wood fibres Lignocel BK 40-90® from J. Rettenmaier & Söhne GmbH+Co KG consisted of cubic softwood (spruce) fibres, with 1 to 2 mm in diameter. Figure 5 presents a scanning electron micrograph of the wood fibre surface.

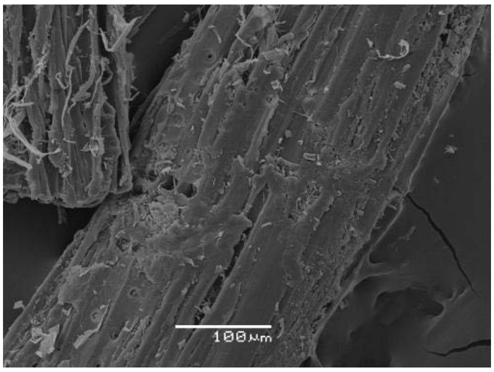

Figure 5: SEM image of the Lignocel® wood fibre surface (scale bar 100 µm).

MWCNTs were provided by C-polymers GmbH. They were produced via catalytic carbon vapour deposition process followed by purification with acid and heat treatment at 600-1000 °C under inert gas atmosphere (N_2). The MWCNTs were reported to have a diameter inferior to 50 nm and an average length between 1 and 20 µm. According to information given by the producer their density was between 1.6 and 1.8 g cm^{-3}, and the specific electrical resistivity from 10^{-3} to 10^{-4} Ω cm. The resulting MWCNTs were entangled (Figure 6). Dimensions of RCF and MWCNT fillers were manually determined from 100 fibres for RCF and from 20 tubes for MWCNTs on SEM images using the publicdomain software ImageJ. In addition, for the MWCNTs, the amount of catalyst remaining with the MWCNTs was determined by TGA: five samples of MWCNTs were heated up from 25 to 700 °C under air (60 mL min^{-1}) at 10 K min^{-1}.

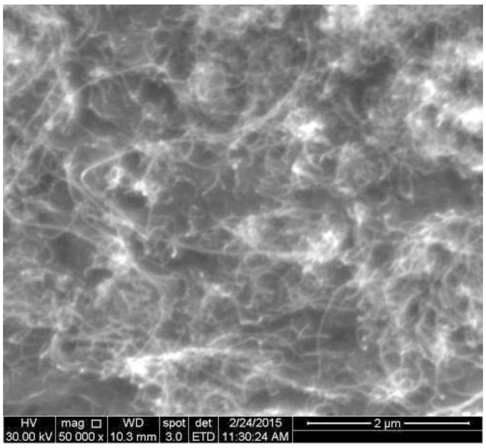

Figure 6: Pristine MWCNTs observed by SEM (scale bar length is 2 µm).

Table 2: Properties of the used fillers, according to producer's data sheets

Label	Description	Product name	Provider	Length [mm]	Diameter [µm]	Surface sizing
CFA1	Carbon chopped fibres	PANEX 35/48	ZoltekTM	6	7.2	6-9 wt% polyester
CFA2	Carbon chopped fibres	PANEX 35/65	ZoltekTM	6	7.2	2.75 wt% polyurethane
CFB1	Carbon fibres	HT C493	Toho Tenax Europe GmbH	6	3	Polyurethane
CFB2	Carbon fibres	HT C604	Toho Tenax Europe GmbH	6	3	Polyamide
CFC1	Carbon fibres	C30 carbon 5006 PUT[1]	SGL Group	6	7	2.7 wt% polyurethane
CF MLD	Milled carbon fibres	T700-MLD	Apply Carbon	-	-	2 wt% of various sizing
CF.LS MLD	Milled and heat treated carbon fibres	T700 MLD LS	Apply Carbon	100 ± 20 µm	7	No sizing
Wood fibres	Wood fibres	Lignocel BK 40-90	J. Rettenmaier und Söhne	-	-	No sizing
MWCNT	Multi-walled carbon nanotube	CNT0 w46/12	C-polymers GmbH	1-20 µm	< 50 nm	No sizing

[1] New trade name = Sigrafil® C C6-4.0/240-T130

3.2 Composite preparation

3.2.1 Recipes

The filler types were mixed with the biopolymers at various loadings, as presented in Table 3. Carbon fibre loading varied between 0 and 15 wt%, recycled carbon fibres were added up to 20 wt%, and MWCNT up to 15 wt%. Wood fibres were added to composites containing carbon fibres or recycled carbon fibres at 10 or 20 wt% loadings to observe the effect of adding non-conductive filler on the composite electrical conductivity. The sample preparation steps are presented in Figure 7.

Table 3: Composition of the produced composites.

Production set	Polymer	Filler type	Filler loading [wt%]	Wood fibre loading [wt%]	Extrusion label = BFX	Injection label = BFS
1	PLA 3051D	CFB2	10	0	1	2
	PLA 3051D	CFB1	10	0	2	3
	PLA 3051D	CFA2	10	0	3	4
	PLA 3051D	CFC1	10	0	4	5
	PHBV	CFB2	10	0	5	1
	PHBV	CFB1	10	0	6	6
	PHBV	CFA2	10	0	7	8
	PHBV	CFC1	10	0	8	7
2	PLA 3051D	CFB1	5	0	9	10
	PLA 3051D	CFB1	15	0	10	12
	PLA 3051D	CFB1	10	0	11	11
	PLA 3051D	CFB1	1	0	12	9
	PLA 3051D	CFA1	5	0	13	14
3	PLA 3051D	CFA1	10	0	14	15
	PLA 3051D	CFB1	10	0	15	13
4	PLA 3251D	-	0	0	16	16
	PLA 3251D	MWCNT	0.5	0	17	17

	PLA 3251D	MWCNT	1	0	18	18
	PLA 3251D	MWCNT	2.5	0	19	19
	PLA 3251D	MWCNT	5	0	20	20
	PLA 3251D	MWCNT	7.5	0	28	21
	PLA 3251D	MWCNT	10	0	29	22
	Bio-PE	-	0	0	21	23
	Bio-PE	MWCNT	0.5	0	22	24
	Bio-PE	MWCNT	1	0	23	25
	Bio-PE	MWCNT	2.5	0	24	26
	Bio-PE	MWCNT	5	0	25	27
	Bio-PE	MWCNT	7.5	0	26	28
	Bio-PE	MWCNT	10	0	27	29
5	PLA 3251D	-	-	0	30	30
	PLA 3251D	CFB1	5	0	31	31
	PLA 3251D	CFB1	10	0	32	32
	PLA 3251D	CF MLD	10	0	33	33
	PLA 3251D	CF.LS MLD	10	0	34	34
6	PADS 18	-	-	0	35	37
	PADS 18	CFB2	5	0	36	35
	PADS 18	CFB2	10	0	37	36
	PAHS 18	-	-	0	38	38
	PAHS 18	CFB2	5	0	39	39
	PAHS 18	CFB2	10	0	40	40
7	PLA 3251D	CFB1	10	0	41	41
8	PLA 3251D	CF.LS MLD	10	0	42	42
	PLA 3251D	CF.LS MLD	20	0	43	43
	PLA 3251D	CF MLD	10	0	44	44
	PLA 3251D	CFMLD	20	0	45	45
	PLA 3251D	CFB1	10	10	46	46
	PLA 3251D	CFB1	10	20	47	47
	PLA 3251D	CF.LS MLD	20	10	48	48
	PLA 3251D	CF.LS MLD	20	20	49	49
	Bio-PE	-	0	0	50	50
9	PLA 3251D	MWCNT	15	0	-	51

	Bio-PE	MWCNT	15	0	-	52
	PLA 3251D	MWCNT	2.5	0	-	53
	PLA 3251D	MWCNT	5	0	-	54
	PLA 3251D	MWCNT	10	0	-	55
	Bio-PE	MWCNT	5	0	-	56
	Bio-PE	MWCNT	7.5	0	-	57
	Bio-PE	MWCNT	10	0	-	58
10	PLA 3251D	MWCNT	10	0	51	59
	Bio-PE	-	0	0	52	60
	Bio-PE	MWCNT	5	0	53	61
	PLA 3251D	MWCNT	5	0	54	62
	Bio-PE	MWCNT	10	0	55	63
	PLA 3251D	-	0	0	56	64
	PLA 3251D	CF MLD	20	0	57	65
	PLA 3251D	CF.LS MLD	20	0	58	66
	PLA 3251D	CFB1	10	0	59	67
	PLA 3251D	CF MLD	20	20	60	68
	PLA 3251D	CFB1	20	0	61	69

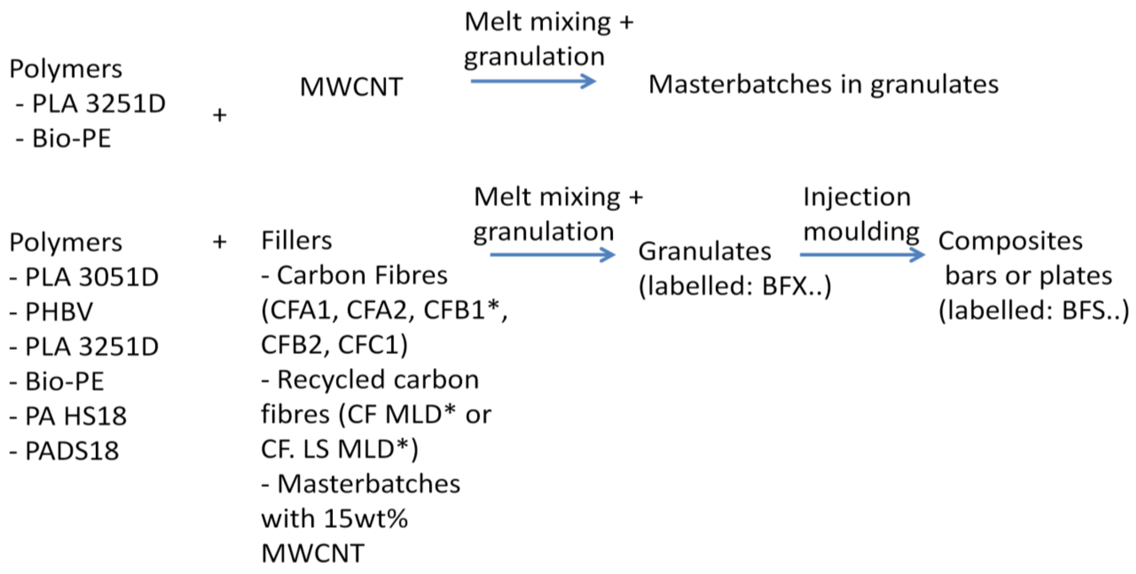

Figure 7: Overview of sample preparation steps. The * indicates that some composites with CFB1, CF MLD or CF.LS MLD were prepared with a wood fibre loading of 10 or 20 wt%

Production parameters were selected to limit variations between the productions based on the same polymer type. However, they had to be modified slightly for some productions (mainly for neat polymers and highly loaded materials) to insure continuous extrusion and

	Bio-PE	MWCNT	15	0	-	52
	PLA 3251D	MWCNT	2.5	0	-	53
	PLA 3251D	MWCNT	5	0	-	54
	PLA 3251D	MWCNT	10	0	-	55
	Bio-PE	MWCNT	5	0	-	56
	Bio-PE	MWCNT	7.5	0	-	57
	Bio-PE	MWCNT	10	0	-	58
10	PLA 3251D	MWCNT	10	0	51	59
	Bio-PE	-	0	0	52	60
	Bio-PE	MWCNT	5	0	53	61
	PLA 3251D	MWCNT	5	0	54	62
	Bio-PE	MWCNT	10	0	55	63
	PLA 3251D	-	0	0	56	64
	PLA 3251D	CF MLD	20	0	57	65
	PLA 3251D	CF.LS MLD	20	0	58	66
	PLA 3251D	CFB1	10	0	59	67
	PLA 3251D	CF MLD	20	20	60	68
	PLA 3251D	CFB1	20	0	61	69

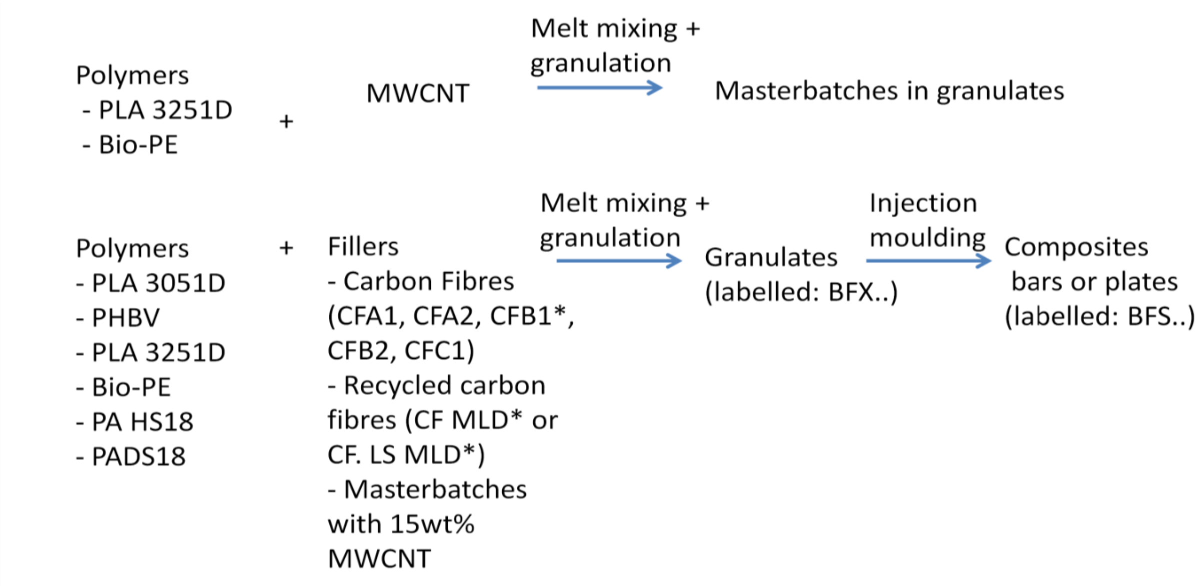

Figure 7: Overview of sample preparation steps. The * indicates that some composites with CFB1, CF MLD or CF.LS MLD were prepared with a wood fibre loading of 10 or 20 wt%

Production parameters were selected to limit variations between the productions based on the same polymer type. However, they had to be modified slightly for some productions (mainly for neat polymers and highly loaded materials) to insure continuous extrusion and keep sample dimensions in conformity with the standardized testing methods. The corresponding variations between the productions parameters are detailed hereafter.

3.2.2 Compounding

The processing parameters were adapted between the productions to obtain a production of continuous string. Parameter variations in composite extrusion are presented in Table 3 and described in the following paragraphs to cluster the productions produced under constant parameters.

The carbon fibre and recycled carbon fibre types, with or without wood fibres were mixed on a Collin® ZK25 extruder (Dr. Collin GmbH, Germany) using the co-rotating twin-screws MAXX 40 D with PLA 3051D, PLA 3251D, PHBV, PAHS 18 and PADS 18. The screws consisted of eight elements organized in six zones as presented in Figure 8: conveying, pre-compression, shearing, relaxation, compression and high compression zones. Neat polymer samples for PLA 3251D, PLA 3051D, PHBV, PAHS 18 and PADS 18 were also processed on the Collin ZK25, using the same parameters to ensure similar thermal history across the samples. Temperature profiles, screw rotation speed and feeding rotation speed used for the compounding are listed in Table 4.

In the productions with PLA 3051D (BFX1-4; 9-15) and PHBV (BFX5-8) extrusion temperature was kept between 150 and 185 °C. Temperatures in zone 4 were constant at 160 °C for PLA 3051D and 170 °C for PHBV. In the production of polyamide-based composites, neat PADS 18 was processed at a temperature between 190 °C and 261 °C. Lower temperatures were used for the other PADS 18-based composites, such as 255 °C. For PAHS 18, the production with neat polymer was done at temperatures between 210 °C and 237 °C, and for the two composites containing carbon fibres between 190 °C and 250 °C. The temperature set for zone 4 was slightly changed between the productions as well as the feeding rotation speeds.

In the case of PLA 3251D, in combination with CFB1 (BFX30-32; 41; 59; 61) or with recycled carbon fibres (BFX33-34; 42; 43-45; 57-58) and with wood fibres (BFX46-49; 60) all productions were prepared at temperatures between 150 °C and 177 °C, an exception was neat PLA 3251D, for which the temperature of zone 3 was lowered to 127 °C, anticipating a cooling of the polymer to produce a continuous string. The composite filled with 20 wt% CFB1 (BFX61) was produced with the narrow temperature range of 160 °C-165 °C. Temperature of zone 4 varied between the productions. The rotation speed of the screw was higher for the production of the original composites with 10 wt% RCF (BFX33-34) than for all other productions (53 rpm and 44 rpm vs. 36-39 rpm). Increasing feeding rotation speeds were used when increasing wood fibre loading. An exception was done for the production with 20 wt% CFB1 and 20 wt% wood fibres (BFX60), which were processed at a lower feeding rotation speed (220 vs. 290-350 rpm).

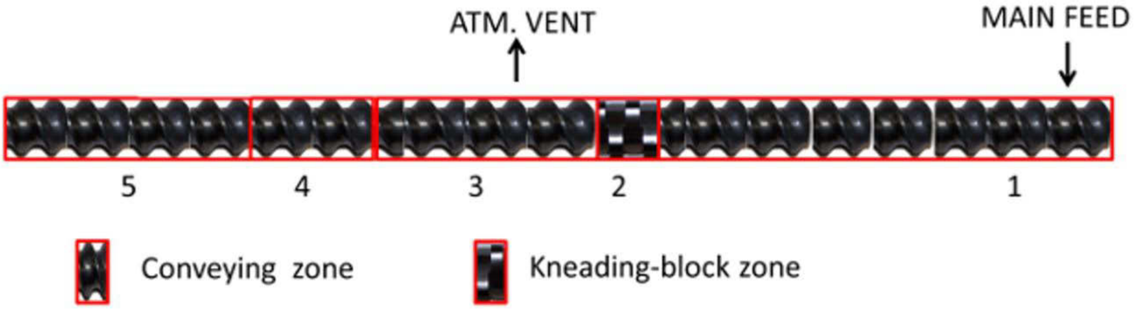

Figure 8: Screw configuration of the Collin® ZK25 extruder used for the production of the composites. The arrows indicate the entry of filler and polymer granulates manually mixed with the polymer granulates (main feed) and the exit of air (atm. vent).

Table 4: Selected process parameters for the extrusion of each composite type and replicate on the Collin® ZK25. The composite productions are gathered in one group if the temperatures varied of less than 2 °C, the screw rotation speed of less than 2 rpm and the feeding rotation speed of less than 105 rpm.

Polymer	BFX (extrusion number)	Temperature [°C]				Screw rotation speed [rpm]	Feeding rotation speed [rpm]
		Zone 1	Zone 2	Zone 3	Zone 4		
PLA 3051D	1-2	156-158	179	160-161	160	45-46	315
	3-4	154-155	180	156	160	46	315
	9	157	180	151	160	45	225
	10;12	150-151	180	155-156	160-161	45	240-345
	11	160	180	160	160	45	335
	13-15	159-160	180	158-160	160	40-42	235-300
PHBV	5-6	155-156	185	175	171-172	45	295
	7-8	158-160	182-183	175-176	170	45-46	280-295
PADS 18	35	190	249	261	251	40	280
	36	190	250	251	250	40	300
	37	200	255	251	244	42	340
PAHS 18	38	210	232	237	218	37	240
	39-40	190	237-240	250	220-221	35-37	270
Bio-PE	21-23	134-136	158-160	160	150	30	175-180
	24-25	140	158-160	160	150	30-35	180-190
	26	130	164	161	155	36	190
	27	132	170	158	155	36	180
	50	160	158	160	151	37	150
	52;53;55	148-150	160-161	158-160	133-135	36-38	140-170
PLA 3251D	16	150	175	160	150	26	220

	17-18	155	175	160	150	30	140-175
	19-20	140-141	175	160	150	30	175-180
	28	120	175	159	155	35	190
	29	105	175	158	160	35	180
	30	160	175	127	150	41	Manually
	31-32;41	160	173-175	157-160	150-152	36-39	220-290
	33	160	175	160	151	53	150
	34	160	175	159	150	44	237
	42	160	175	165	146	38	230
	43-44	160	175	165-166	150-153	37	220
	45	160	175	165	162	36	230
	46	160	171	165	151	37	290
	47	160	175	158	155	37	290
	48	160	175	165	150	37	312
	49	160	175	165	160	37	350
	51	150	161	160	144	38	180
	54	145	160	160	140	37	140
	56	150	153	152	142	35	140
	57	155	170	160	159	36	110
	58	155	165	165	151	37	130
	59	155	170	160	151	36	200
	60	155	170	160	160	37	220
	61	160	165	160	160	36	290

Concerning the MWCNTs, they were first mixed with the thermoplastics PLA 3251D and Bio-PE at 15 wt% loading, using a Leistritz ZSE 27 extruder (co-rotating screws MAXX 40 D) from Leistritz GmbH, Germany; at Cpolymer GmbH, Austria. Screws and temperature profiles were selected in accordance with the recommendations of Leistritz AG for nanomaterials compounding as presented in Figure 9 and Table 5. The masterbatches extrusion was directly followed by granulation.

Table 5: Extrusion parameters for the production of masterbatches ran at 5 kg h^{-1} without vacuum.

Polymer	Temperature	Temperatures of the heating zones (Z) [°C]										
		Z1	Z2	Z3	Z4	Z5	Z6	Z7	Z8	Z9	Z10	Z11
PLA 3251D	Selected	200	200	200	200	200	200	200	200	210	220	220
	Measured	200	203	**205**	**205**	**205**	**205**	**205**	**210**	**220**	**222**	**230**
Bio-PE	Selected	200	200	200	200	200	200	200	200	200	200	220
	measured	200	200	**217**	**233**	**242**	**242**	**247**	**248**	**248**	**249**	**249**

Polymer	Melt temperature	Melt pressure	Motor rotation per minute

	[°C]	[bar]	[rpm]
PLA 3251D	230	40	449
Bio-PE	249	43	449

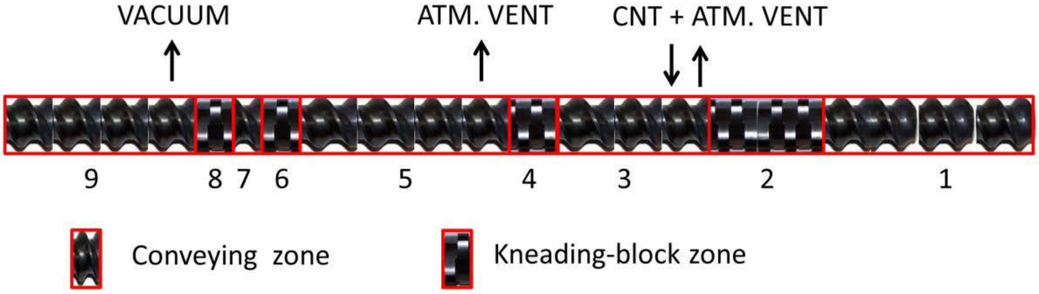

Figure 9: Screw configuration of the Leistritz extruder used for the production of MWCNT-filled masterbatches. Entry of polymer and MWCNTs (in the figure CNT) is on the right (CNT+ATM. VENT), and air outlets (atm. vent or vacuum) are indicated by arrows.

The masterbatches were diluted by melt mixing on a Collin® ZK25 extruder, obtaining strands with 0, 0.5, 1, 2.5, 5, 7.5 and 10 wt% MWCNT loadings. For these extrusions the same screw configuration as described for the extrusions with carbon fibre and recycled carbon fibre filled composites were used. The compounding was always done in closed conditions except for the PLA 3251D-based composite filled with 10 wt% MWCNTs, for which the gas evacuation was opened to release moisture and keep the machine load low. The extrusion parameters are shown in Table 4.

The production of composites containing MWCNTs in PLA 3251D was done in two sets. For the first production set with PLA 3251D (BFX16-20; 28-29), temperatures were kept between 140 and 175 °C. For the productions with 7.5 and 10 wt% loadings the process temperatures for zone 1 were between 120 and 105 °C and higher temperatures were selected for zone 4 (155 and 160 °C), along with higher rotation speeds to obtain a better melt flow of the polymer and lower residence time. For the second production set with PLA 3251D and MWCNTs (BFX51; 54; 56), the processing temperatures were kept between 140 °C and 160 °C. Slightly higher screw and feeding rotation speeds were used for the production with 10 wt% MWCNTs (BFX51), i.e. 38 rpm and 180 rpm, respectively vs. 35-37 rpm and 140 rpm for the two others productions. Similarly, the production of composites containing MWCNTs in Bio-PE was done in two sets. For the two sets of production (BFX21-27; BFX 52; 53; 55) all samples were produced at temperatures between 130 and 170 °C. During the second production set, only the first neat Bio-PE (BFX50) production was done at higher screw rotation speed (37 vs. 30 rpm). Temperature at zone 4 varied between the productions. Extrusion melt temperature, melt pressure and machine load were measured for all composites processed on the Collin® ZK25 to follow their melt behaviour

The extruded strands were further cut to granules on the strand pelletizing system Primo 100 from Rieter GmbH at a length of 4 ± 2 mm.

3.2.3 Annealing and storage

All the compounds were thermally annealed for 4 h at 120 °C and further stored at 80 °C prior to injection moulding.

3.2.4 Injection moulding

Injection moulding was done on a Battenfeld HM 60/210 injection unit using a short nozzle head. The composites were injected into a standardized mould to obtain “bone bars” of 150 mm length, a thickness of 4 mm and with a middle width of 10 mm and a width of 20 mm at the extremities for tensile strength test. For flexural and impact strength tests, bars of dimension 80x10x4 mm were made. Plates with dimensions of 140x140x2 mm were produced as well, using another mould for the characterization of electrical conductivity with ring electrodes on selected samples (BFS41-49 and BFS53-58).

Some production parameters were modified between the productions to limit the variation in sample dimensions and insure an acceptable ejection of the sample. The values selected for the main parameters, i.e. temperature profile, injection speed, back pressure parameters (pressure and time) and cooling time are gathered in Tables 6 to 8. Parameter variations in composite productions are further described for each polymer type used to cluster the productions obtained under constant parameters. For PLA 3051D and PHBV-based composites, the mould temperature, back pressure, back pressure time or cooling time differed slightly between the productions as shown in Table 6. For the first production set with Bio-PE filled with MWCNTs, production parameters changed between the productions with 0-2.5 wt% MWCNTs loading (BFS23-26) and the production with 5-10 wt% MWCNT loading (BFS27-29). During the second production set (BFS50; 60-61; 63) production parameters varied.

The two first production sets with PLA 3251D and MWCNTs (BFS16-22; 59;62; 64) were prepared under constant injection moulding parameters except the 10 wt% MWCNT loading, which was done at higher injection speed (70 against 20 mm s^{-1}) as shown in Table 7. PLA 3251D samples filled with CF (BFS30-32; 41; 46-47; 67; 69) or with RCF (BFS33-34; 42-45; 65-66) and with wood fibres (BFS46-49; 68) were produced at constant temperature profile between 175 °C and 190 °C but injection speed, back pressure parameters and cooling time varied.

A third set of PLA 3251D filled with MWCNTs (Table 8) was prepared without previous dilution of the masterbatches by extrusion (BFS51; 53-55). For this last set, injection speed and back pressure time varied between the productions. For the third production set of Bio-PE filled with MWCNTs and produced without dilution step by extrusion (Table 8), the production with 15 wt% MWCNTs (BFS52) was done at higher temperature than the other composites containing 5; 7.5 and 10 wt% MWCNTs (BFS56-58) (at 195-210 °C vs.175-185 °C). In these three last productions only the mould temperature varied between 20 and 30 °C.

Table 6: Injection parameters used for the production of PLA 3051D, PHBV, PA and Bio-PE-based bars for traction and impact testing.

Polymer	Injection number BFS	Temperatures [°C]				Injection speed [mm s^{-1}]	Back Pressure		Cooling time [s]
		Zones 1-3	Zone 4	Mass	Mould		Pressure [MPa]	Time [s]	
PLA 3051D	2-5	170	180	180	20	20	700	9	25
	9-15	170	180	180	20	20	750	9	20
PHBV	7	185	190	185	60	20	300	5	20
	8	185	190	185	20	20	300	9	25
	1;6	185	190	185	60	20	300	9	25
PADS 18	35-37	230	240	220	60	30	800	9	28
PAHS 18	38-40	260	270	260	60	30	800	9	28

Bio-PE	23-26	175	180	180	20	30	900	8	15
	27	175	185	185	30	60	900	9	15
	28-29	175	185	185	20	60	900	9	15
	50	175	180	180	20	30	900	11	15
	56	175	185	185	30	60	400	9	25
	60	175	180	185	30	60	1000	9	20
	61	175	185	185	30	60	1000	10	20
	63	175	185	185	30	60	1000	13	20

Table 7: Injection moulding parameters used for the production of PLA 3251D-based bars for traction and impact testing

Injection number BFS	Temperatures [°C]				Injection speed [mm s^{-1}]	Back Pressure		Cooling time [s]
	Zones 1-3	Zone 4	Mass	Mould		Pressure [MPa]	Time [s]	
16-21	175	180	180	20	20	800	9	15
22	175	180	180	20	70	800	9	15
30-33	175	180	180	20	20	800	9	18
34	180	190	180	20	20	800	8.5	18
41-44	185	190	180	20	70	700	10	25
45;47	185	190	180	20	70	600	8	20
46	185	190	180	20	70	600	10	20
48	185	190	180	20	70	600	7.5	15
49	185	190	180	20	70	600	9	25
59;62;64	175	180	180	20	20	1250	4	20
65;66	185	190	180	20	70	1200	4	25
67	185	190	180	20	70	1200	5	25
68	185	190	180	20	70	950	4	25
69	185	190	180	20	70	780	4	25

Table 8: Injection moulding parameters used for the production of PLA 3251D-based plates for electrical conductivity measurement with ring electrodes. The three temperatures indicated for the injection number 52 correspond to the respective temperature of zone 1, zone 2 and zone 3.

Polymer	Injection number BFS	Temperatures [°C]				Injection speed [mm s^{-1}]	Back Pressure		Cooling time [s]
		Zones		Mass	Mould		Pressure [MPa]	Time [s]	
		1-3	4						
PLA 3251D	51	175	180	180	20	20	1250	4	20

	53-54	175	180	180	20	20	500	9	20
	55	175	180	180	20	70	500	9	20
Bio-PE	52	195;200; 200	210	200	20	60	900	10	15
	56	175	185	185	30	60	400	9	25
	57-58	175	185	185	20	60	400	9	25

After injection moulding all samples were stored at least two weeks in a climatic room (23 °C and 50% relative air humidity). Samples produced for electrical characterization were manipulated with gloves to avoid deposition of fat.

3.3 Microscopic characterization

3.3.1 Scanning Electron Microscopy (SEM)

Scanning electron microscopy was used to characterize the dimensions of MWCNT, CF MLD and CF.LS MLD and the wood fibres. SEM was also conducted on the fractured surfaces of the different composites with three microscopes.

– FEI Inspect S50 SEM

This equipment was used under low vacuum on the fractured surface of CF and MWCNT-filled polymers with and without a gold coating applied by sputtering.

– A SEM JSM 6380LV

This SEM from JEOL with a tungsten filament was used on pristine CF MLD and CF.LS MLD and wood fibres.

– A Quanta™ 250 FEG-ESEM (environmental scanning electron microscope)

This ESEM was equipped with a Shottky field emission source from FEI. This equipment was used on MWCNT-filled composites with lower beam voltage when compared to the two other SEM.

3.3.2 Atomic Force Microscopy (AFM)

Atomic force microscopy was used to scan the cross section of the test bars prepared for impact strength test of MWCNT-filled composites. AFM imaging was done on the centre of the cross section of PLA 3251D and Bio-PE-based composites containing 0, 1, 5 and 10 wt% MWCNTs. Plane surfaces were prepared by microtoming on a Leica Ultracut R microtome from Leica Microsystem, GmbH with a diamond knife. Two AFMs were used:

– Veeco® Dimension Icon scanning probe microscope with ScanAsyst™

This equipment was used to do AFM imaging in tapping mode with aluminium coated probes and tip radius lower than 10 nm (Budgetsensors).

– Anasys Instruments' AFM+

This equipment was used in contact mode, and is further described in the part 3.8.2. Nanothermal analysis (nanoTA) by AFM" of the chapter materials and methods.

3.3.3 Polarized Light Microscopy (PLM)

Polarized light microscopy was used to determine the position and amount of crystalline regions in the composites depending on the cooling speed. Thin sections were cut from the centre of the injection-moulded bars through microtoming on a manual microtome Jung AG Heidelberg with a width of cut of 50 µm for MWCNT loadings of 0 and 1 wt%. The sections were placed between two glass slides and kept in an oven at 175 °C for 20 min to obtain a film of the material between two glass lamella. To assess the effect of cooling speed on the crystallisation process of semi-crystalline polymers, the melted samples were cooled down at two different cooling speeds. A first set of six sections was taken out from the oven and stored in a cooled room at 15 °C for 2h. The second set of samples was kept in the oven when cooling the oven temperature down to ambient temperature at a slow cooling rate of around 1°C min^{-1}. Images from the films were obtained with an Axio Scope A1 (Zeiss), equipped with polarized light module.

3.4 Electrical characterization

To select an adequate measurement method for the electrical conductivity, methods were tested in cooperation with other research institutes and companies involved in the studies relevant to this thesis. Selected composites were characterized by two-point, four-point and with ring electrode methods. Methods consisting in a direct contact between the electrode and the sample surface were compared to methods implying sample surface preparation such as the application of conductive tape or silver paint. For each method, the calculation of the corresponding conductivity was made with a specific equation.

3.4.1 Two-point methods

Characterization of electrical conductivity with a two-point method was first tried on the CF-filled composite. The resistance was directly obtained from various ohmmeter devices.

A method using two metallic bars was tested with an Amprobe® multimeter. It consisted of a two-point method measuring surface conductivity and was employed on MWCNT-filled composites (BFS16-29) and on PLA 3051D-based composite filled with one type of polyurethane sized CF (CFB1) at 5 to 10 wt% loading (BFS3; 9-12). Two measuring systems, with different distances between the electrodes (4.1 ± 0.1 cm for system A and 10.9 ± 0.1 cm for system B) and different electrodes width (1 and 1.25 ± 0.1 cm respectively) were tested (Figure 10). All samples had a middle width of 0.10 ± 0.05 cm. To assess the reproducibility and time dependence of this method, composites were characterized after 10, 20 s and 1 min measurement with the two measurement systems. Conductivity was calculated with the Equation 2.

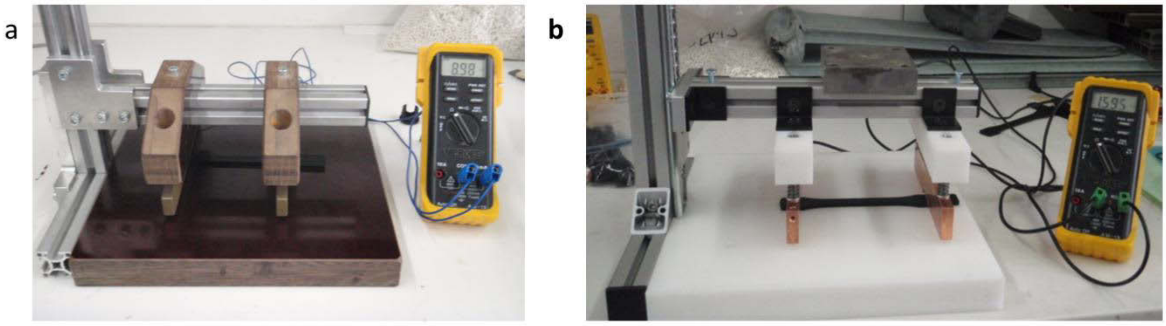

Figure 10: Two-point method with metallic bar electrodes: (a) system A, (b) system B.

$$\sigma = \frac{d}{R \times p} \qquad \text{Equation 2}$$

Where σ is the “surface” conductivity in S, d is the distance between the electrodes in m, R the resistance measured with the Ohmmeter and p characterises the minimum width in m through which the current can pass. In the present case the width of the contact between the electrodes and the sample was bigger than the sample middle width; therefore, p is equal to the middle width of the sample (10 mm).

Electrical surface conductivity was also measured using two parallel tape stripes according to IEC 60079-32-1. This method determines the surface resistance of the composite by placing two electrically conductive tape stripes (length 70 mm, width 1 mm) parallel one to another at the surface of the sample, and at a distant of 7.5-8 mm. According to IEC 60079-32-1, the distance between the electrodes should be larger than the electrode’s length divided by ten as presented in Figure 11. The device used was a Megohmmeter M1501P from Sefelec (voltage, i.e. electric potential difference, up to 1500V), which can characterize materials with surface resistance up to 10^{15} Ω. Therefore, samples that could not be characterized with the DC power supply D3022 (CYE) or the Keithley 2601 A, which had respective voltage limit of 60 and 40V, were characterized with this method. Before the measurement, the samples were stored for more than 24 h at 23 °C, and 33% relative humidity. This measurement method was associated with Equation 2.

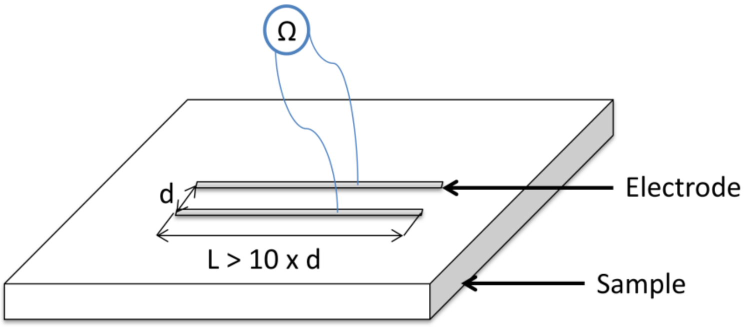

Figure 11: Illustration of two-point set-up using parallel conductive stripes, where Ω indicates the Megohmmeter used for the resistance measurement.

Two-point volume electrical conductivity measurements were done on MWCNT-filled PLA 3251D by fixing two metallic clamps at the extremities of test bars as shown in Figure 12. During the measurement, the electrical values varied with the pressure applied to fix the electrodes. Therefore, measurements were taken when applying the maximum pressure reachable by hand during the fixation of the clamps. The voltage was applied from a laboratory tension source, which could deliver up to 30 V and the current intensity was measured with an ammeter with microampere level of precision. Therefore, resistances up to 30 MΩ could be measured. This measurement method was associated with Equation 3. The effective contact surface *A* for one electrode was of 4.5 10^{-4} m^2. The distance *h* between the two electrodes was 9.0 cm.

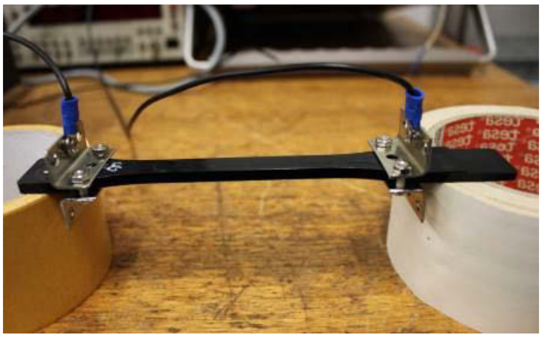

Figure 12: Illustration of the two-point method with clamped electrodes.

A Keithley 2601 A was used to measure the volume electrical resistance with two alligator clips with distance of 5 cm from one to another. It supplied a current of 1.0 mA with a limited voltage at 40V. Measurement was done ten times for one sample with 5 wt% MWCNTs in PLA 3251D (BFS20 type). Further measurements were done for the composite filled with CF and MWCNTs (BFS1-29). Resistance values were recorded 1 min after the current source was switched on for ten different samples for each composite type. It was considered that this system measured the electrical volume conductivity as two different surfaces of the composites are in contact with the electrodes. Volume conductivity was quantified with Equation 3.

$$\sigma = \frac{d}{R \times A} \qquad \text{Equation 3}$$

Where σ is the “volume” conductivity in S m^{-1}, *d* is the distance between the electrodes, *R* the resistance measured with the Ohmmeter and *A* is the limiting section of electron transport through the sample in m². Since no silver paint was applied on the sample surface, the effective contact surface between one alligator clip and the sample surface was approximated at 4.10^{-6} m^2. As it was smaller than the cross section surface of the sample, it was used as limiting section *A* for electron transport.

3.4.2 Four-point methods

Four-point method was used to measure surface conductivity by applying four identical electrodes on one surface of the sample. To insure a good contact between the electrodes and the sample, four points were drawn with silver paint or with gold pads on the sample surface. The connections were done as presented in Figure 14.

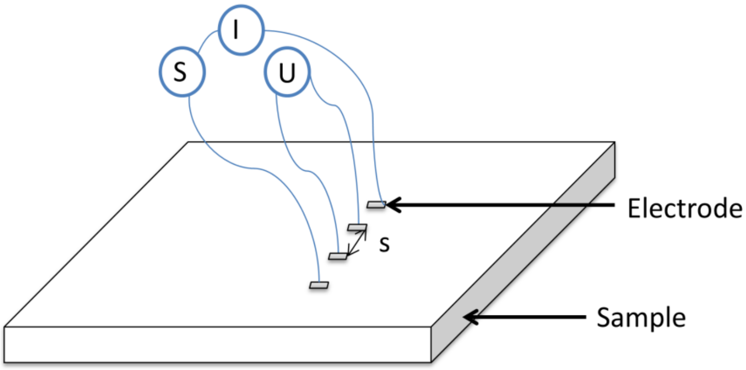

Figure 13: Illustration of the four-point method in surface configuration where S represents the current source equipment, I the ammeter, U the voltmeter and *s* the distance between two electrodes.

The four electrodes are positioned in a row parallel to injection direction and equidistant (with *s*=1 cm). The specific surface electrical conductivity was calculated using Equation 4.

$$\sigma = \frac{I}{\Delta U \times 2\pi \times s} \qquad \text{Equation 4}$$

Where σ is the “surface” conductivity in S, *s* is the distance between two neighbouring electrodes in m, *I* is the current passing through the most external electrodes in A and ΔU is the potential difference measured at the most internal electrodes in V.

The specific volume electrical conductivity was determined by four-point method following European standard EN ISO 3915. The test was performed on rectangular samples sized 70x10x4 mm. In this four-point measurement setup the electrodes are fixed on the cut surfaces and the sensor electrodes measuring the actual voltage potential are positioned on an unmodified surface as shown in Figure 15. Two sensor electrodes were fixed at a constant distance (*d*) of 10 mm. The four electrodes are positioned in a row parallel to injection direction.

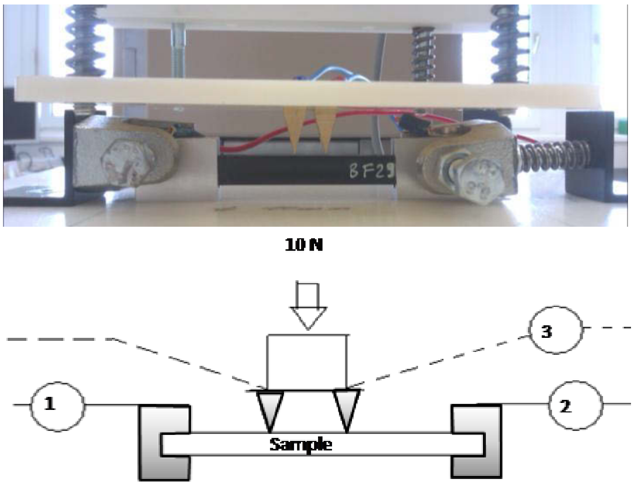

Figure 14: Description of the four-point volume conductivity measurement after EN ISO 3915, 1 is the tension source, 2 the ammeter and 3 corresponds to the multimeter in the voltmeter mode. The electrodes are represented in grey colour.

Three samples were measured for each MWCNT loading. The mean value of the conductivity for each composite was obtained by averaging over all measurements. This measurement method was associated with Equation 5.

$$\sigma = \frac{d \times I}{\Delta U \times A} \qquad \text{Equation 5}$$

Where σ is the "volume" conductivity in S m^{-1}, d is the distance between the electrodes, I is the current passing through the most external electrodes in A, ΔU is the potential difference measured at the most internal electrodes in V and A is cross section surface of the sample in m².

The complete installation is presented in Figure 16 with the voltage source and an ammeter on the left side connected to the shell electrodes. The voltage ΔU was measured between the two sensor electrodes of a Solartron Schlumberger 7150 Digital multimeter. Voltage up to 60 V was generated by the digital DC power supply D3022 (CYE) and applied on shell-electrodes. The current value as provided by the power supply on the circuit, was measured by an Amprobe® multimeter or a Beha Amprobe 37XR-A. This configuration measured the resistivity in the flow direction. Readings were taken after 1 min of stable current (set to values between 0.3 and 25 mA depending on sample conductivity) and stable mechanical loading was applied on the sensor electrodes of 10 N with a Zwick/Roell ZmartPro. The measurement was repeated four times with reversing three times the sample position. The system "electrodes-sample" was isolated from eventual low frequency electromagnetic waves by a grounded Faraday cage as seen in Figure 17.

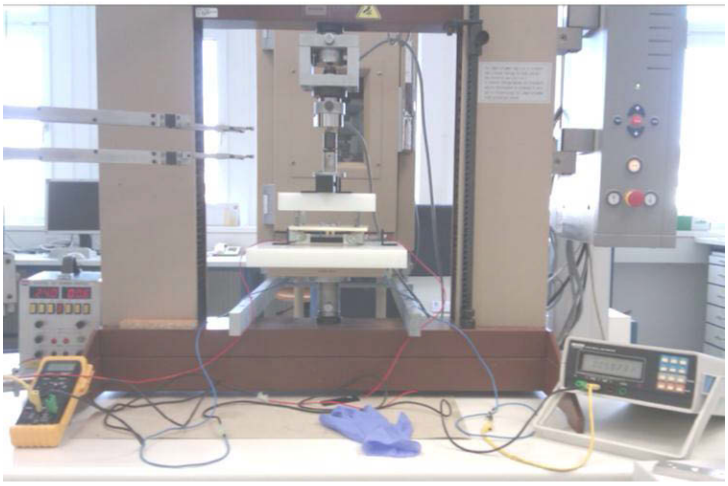

Figure 15: The electrical resistance measurement installation according to EN ISO 3915.

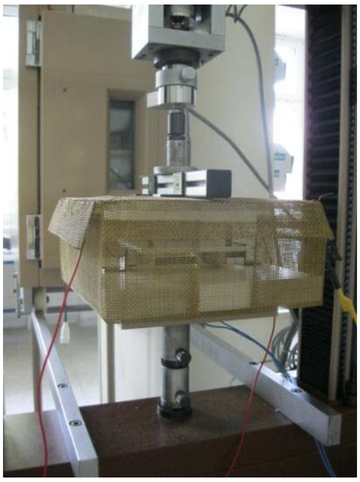

Figure 16: Electrical conductivity measurement system according to EN ISO 3915 placed in a Faraday cage.

In addition, four-point measurements were performed to determine the bulk conductivity of the MWCNT-filled bio-based polymers. Gold pads with a thickness of 100 nm were thermally evaporated onto the samples ($p < 10^{-6}$ mbar), while conductive silver paste was applied on the sample edges (Figure 18). For the electrical characterization a SÜSS PM5 probe station with manipulator needles and a Keithley SourceMeter 2400 (maximal voltage of 200V) were used. Upon application of a constant current I of $5\ 10^{-3}$ A to the conductive silver paste contacts at the sample edges, the potential difference ΔU was measured between two adjacent gold pads with distance d (here equal to 2.6 mm). With a cross section A of 40 mm^2 (sample width: 10 mm, sample thickness: 4 mm) the electrical volume conductivity σ (in S m^{-1}) was determined using Equation 5. This method was used on the set PLA 3251D and Bio-PE-based samples filled with 0, 5 and 10 wt% of MWCNTs directly on the injection moulded bars but also on annealed injected moulded bars, e.g. placed in an oven at 110 °C for minimum four hours.

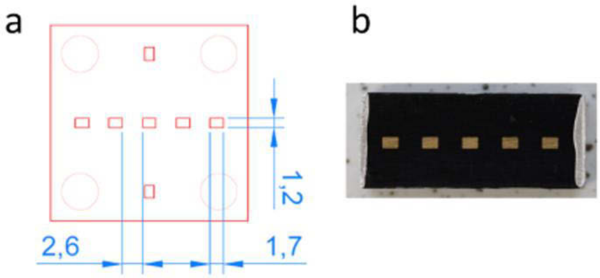

Figure 17: Shadow mask with dimensions of contact pads for determination of the electrical conductivity (a) and typical sample (b).

3.4.3 Ring electrode method

The ring electrode method was used to compare volume and surface conductivities. The two setups measuring either the volume resistance or the surface resistance are presented in the introduction (Figure 3). The calculation of the surface conductivity was done with Equation 2 with *p* as defined in Equation 6 and *d* equal to *g* the distance in m (here 5 10^{-3} m) between the two measuring electrodes and *d1* is the diameter of the intern electrode in m (here 5 10^{-2} m). For the calculation of the electrical conductivity in the volume configuration Equation 3 was used with *d* equal to the thickness of the sample (2 10^{-3} m) and *A* as defined in Equation 7. The resistance was measured with a Solartron Schlumberger 7150 Digital multimeter or with a teraohmmeter TO-3 produced by Fisher elektronik as shown in Figure 19. The teraohmmeter is able to measure resistance from 0.9 10^3 Ω till 1.6 10^{15} Ω. Adequate equipment was selected depending on the level of conductivity of the sample.

$$p = \pi \times (d1 + g) \qquad \text{Equation 6}$$

$$A = \frac{\pi \times (d1 + g)^2}{4} \qquad \text{Equation 7}$$

Figure 18: Method of electrical conductivity measurement with ring electrodes with the Digital multimeter (on the left) or the teraohmmeter (on the right).

Nan’s law as defined in Equation 8 was considered for two-component blends to approximate the critical fraction of filler (V_c in vol%) with *f* the aspect ratio of the fibrillar conductive filler considered.

$$Vc \propto \frac{0.7}{f} \qquad \text{Equation 8}$$

3.5 Mechanical characterization and model

Tensile behaviours were characterized directly on ten injection moulded samples for each composite type to assess the effect of the fillers on composite rigidity and the adhesion between the filler and the polymer matrix. Tensile tests were carried out using a Zwick-RoellZmartPro®, following ISO 527-2. The samples were clamped with 115 mm clamping length and the testing speed was 50 mm min $^{-1}$ for all measurements. Composite toughnesses were assessed through Charpy unnotched impact tests on ten samples for each composite type and conducted with a Frank® Pendelschlagwerk 53303 device following ISO 179/1eU. The hammer delivered an impact energy of 7.5 J and the length of the pendulum was of 390 mm. Each test was repeated ten times. The tensile strength, tensile elongation and Young's modulus were deduced from the stress/strain curves using the Young's modulus equation (Equation 9).

$$E = \frac{\sigma}{\varepsilon} = \frac{F/A_0}{\Delta L/L_0} \quad \text{Equation 9}$$

Where E is the Young's modulus in Pa, σ the tensile stress (in N m^{-2}), which corresponds to the ratio of the force applied F in N on the surface of contact A_o in m² and ε is the extensional strain and corresponds to the sample elongation ΔL regarding its original length L_o.

The Halpin-Tsai model to predict the Young's modulus of short fibres randomly dispersed in polymers was applied in this study for Bio-PE-based composites using the following series of Equations (10 to 13).

$$Ec = \left[\frac{3}{8} \times \frac{1 + 2 \times (L/d) \times \eta l \times Vf}{1 - \eta l \times Vf} + \frac{5}{8} \times \frac{1 + 2 \times \eta t \times Vf}{1 - \eta t \times Vf}\right] \times Ep \quad \text{Equation 10}$$

$$\eta t = \frac{Ef/Ep - 1}{Ef/Ep + 2} \quad \text{Equation 11}$$

$$\eta l = \frac{Ef/Ep - 1}{Ef/Ep + 2\,L/d} \quad \text{Equation 12}$$

$$Vf = \frac{wt}{wt(1 - df/dp) + df/dp} \quad \text{Equation 13}$$

Ec is the approximated Young's modulus of the composite in MPa. *L* the length of the fibres and *d* their diameter, both in m, η_l is the length efficiency factor and η_t the transversal efficiency factor. *Ef* is the modulus of the fibres, *Ep* the modulus of elasticity of neat polymer both in MPa, *wt* the percentage of reinforcing fibres in the composite in weight with *df* and *dp* (in g m^{-3}) the respective densities of the neat fibres and neat polymer. *Vf* is the volume fraction of fibres in the composite without unit.

Ep for the neat HDPE was calculated at 839 MPa from experimental results. *Ef* corresponds to the mean value of tensile modulus of the MWCNTs given by the producer, which was 1.25 10^6 MPa. For the model, the length *L* of MWCNTs was selected between 0.5 and 10 µm, and the diameter *d* selected at 50 nm. Equivalent volume fractions of 0, 0.28, 0.56, 1.41, 2.85, 4.32 and 5.83 vol% were calculated from the mass fraction of the tested loadings, with HDPE density of 0.96 and MWCNT density of 1.7.

3.6 Thermal stability characterization by Thermogravimetric Analysis (TGA)

For each sample, Thermogravimetric Analysis (TGA) measurements using a Iris 209 Netzsch® equipment were done on three replicates (8-12 mg) obtained from the injection-moulding test bars. Samples were heated from 20 to 800 °C at a heating rate of 10 °C min^{-1} with an acquisition rate of 85.71 points min^{-1} under a mix of synthetic air (flowrate of 20 ml min^{-1}) and nitrogen (flowrate of 20 ml min^{-1}).

3.7 Thermal transitions characterization by Differential Scanning Calorimetry (DSC)

The effect of conductive fillers and wood fibres on polymer crystallisation was assessed by a DSC 200 F3 Maia® (Netzsch). Measurements were done on three samples for each compound containing 0, 1, 2.5, 5 and 10 wt% MWCNTs. The samples for crystallinity determination were cut from the tensile test bars, with masses between 5 mg and 15 mg, and were then placed into aluminium DSC pans. The DSC equipment was calibrated with Indium and the measurements were done on three granules sampled from different test bars for each tested composite type. Samples were heated and cooled twice under N_2 atmosphere, between 25 °C and 200 °C, at a heating rate of 10 °C min^{-1}. Two crystallinity ratios were measured: the crystallinity ratio of the sample directly after injection moulding and the crystallinity ratio after one heating step up to 200 °C and one cooling step to 25 °C with a cooling speed of 10 °C min^{-1}. Crystallinities were calculated following Equation 14 and indicated by *Xc1* and *Xc2* for the first and second heating step, respectively. Melting enthalpy of 100% crystallized polymer enthalpy was fixed at 93 J g^{-1} [97] for PLA and at 293 J g^{-1} for HDPE [116]).

$$Xc = \frac{\Delta Hm - \Delta Hc}{\Delta H_m^0 \times wt_p} \qquad \text{Equation 14}$$

Here, Xc is the crystallinity of the polymer in %, ΔHm is the melting enthalpy measured for the sample in J g^{-1}, ΔH^0_m is the melting enthalpy of 100% crystalline polymer in J g^{-1}, ΔHc is the post-crystallisation enthalpy also in J g^{-1} and wt_p is the percentage in weight of polymer in the composite in %.

3.8 Heat deflection behaviour characterization

3.8.1 Heat Deflection Temperature (HDT) measurement according to ISO 75

The heat deflection temperature (HDT) was measured according to ISO 75 to characterize the temperature at which the bulk composite bar fold under a pressure of 0.45 MPa (test HDT B). This was performed on a CEAST HDT VICAT from INSTRON® on three bars for the different MWCNT loadings in PLA 3251D and Bio-PE.

3.8.2 Nanothermal analyses (nanoTA) by AFM

Anasys Instruments' AFM+ was used for thermal probing of the microtomed cross section surfaces of PLA 3251D and Bio-PE composites containing MWCNTs. The measurement was performed by first recording topography images with a surface area of 5x5 μm using a ThermaLever™ silicon probe AN2-200 with tip radius minimum of 30 nm, and then performing a thermal ramp on selected points as illustrated in Figure 20. Prior to measurements the nanoTA probe was calibrated using polycaprolactone, polyethylene and polyethylene terephthalate standards provided by the manufacturer with melting temperatures of 55, 116 and 235 °C, respectively. This was done by matching the melting voltage of the standard material to their known melting temperature.

Various heating rates were tested (10, 25 and 35 °C s^{-1}) and the heating rate of 25 °C s^{-1} was selected for further characterization as it offered an intermediate indentation size. A typical nanoTA measurement was performed by first scanning a 5x5 μm topography and a phase image. Then the nanoTA tip was used to probe the surface with 16 measuring locations for each image forming a Transition Temperature Microscopy (TTM) map. When applicable, the 16 thermal ramps were used for calculating the average thermal ramp. At least two locations on each sample were recorded. After the TTM mapping a topography image with the probe indentations was recorded.

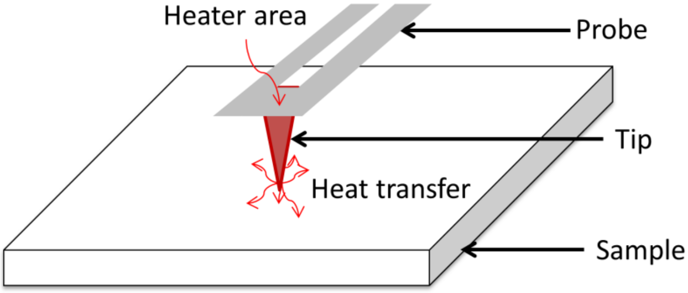

Figure 19: Schematic view of AFM nanothermal measurement principle (Adapted from [117]**).**

3.9 Statistical analyses

For measurement with two or more replicates, the mean value of a set of measurement was presented in the results part with the corresponding standard deviation calculated from the Equations 15 to 17.

For statistical analyses of the data, the software IBM SPSS Statistics 21 was used. Non parametric Kruskal-Wallis test was done to determine significant differences between the data groups with a significance level of 0.05.

$$\bar{x} = \frac{1}{n} \times \sum_{i=1}^{n} x_i \qquad \text{Equation 15}$$

$$s^2 = \frac{1}{n-1} \times \sum_{i=1}^{n} \left(x_i - \bar{x}\right) \qquad \text{Equation 16}$$

$$s = \sqrt{\frac{1}{n-1} \times \sum_{i=1}^{n} \left(x_i - \bar{x}\right)} \qquad \text{Equation 17}$$

Where $\bar{x}$ is called the sample mean and is computed as the sum of all the data x_i measured for the sample i divided by n the total number of measurements done. s^2 is called the variance and is used to assess the spreading of the data around the mean. Finally, s is the standard deviation and is also used to assess the dispersion of the data around the mean. s has the same dimension as the data.

4 Results

Properties of the composite materials are directly dependent on the selected components and their interactions, as well as the processing, the latter determining the distribution and dispersion of the fillers in the polymer matrix. In this chapter, the fillers are described as well as their distribution and dispersion in the composites, the variations in melt temperature, melt pressure and machine load, injection pressure, and in dosing time measured during processing. Then main properties of the composites are analyzed; i.e. electrical conductivity, tensile and impact resistance behaviour, thermal stability. Finally, polymer crystallisation process and crystallinity, glass and melting transitions as well as deflection behaviour of MWCNT-filled composites are presented.

4.1 Analysis of fillers, their distribution and dispersion in the composite

4.1.1 Filler description

Filler dimensions were investigated by microscopy for the RCF, the MWCNTs and wood fibres. Unimodal distribution of the dimensions was observed for MWCNT diameter and wood fibres dimensions. However, for the recycled carbon fibres, i.e. milled carbon fibres (CF MLD) or milled carbon fibres with low sizing (CF.LS MLD), the length distributions were found to be bimodal (Figure 21, Table 9). This indicated that after milling, the recycled carbon fibres were composed of two-size-groups of fibres. The first group was represented by fibres cut to 100 µm for the CF MLD, and to 50-60 µm for CF.LS MLD. The second group corresponded to much longer fibres, having lengths of 600 µm for CF MLD, and 375 µm for CF.LS MLD. For the MWCNTs, a mean diameter of 34 ± 7 nm was determined. The lengths could not be measured because of the MWCNTs entanglement, as visible in Figure 6. This indicated that the milling process used for RCF preparation led to the production of two distinct groups of fibres.

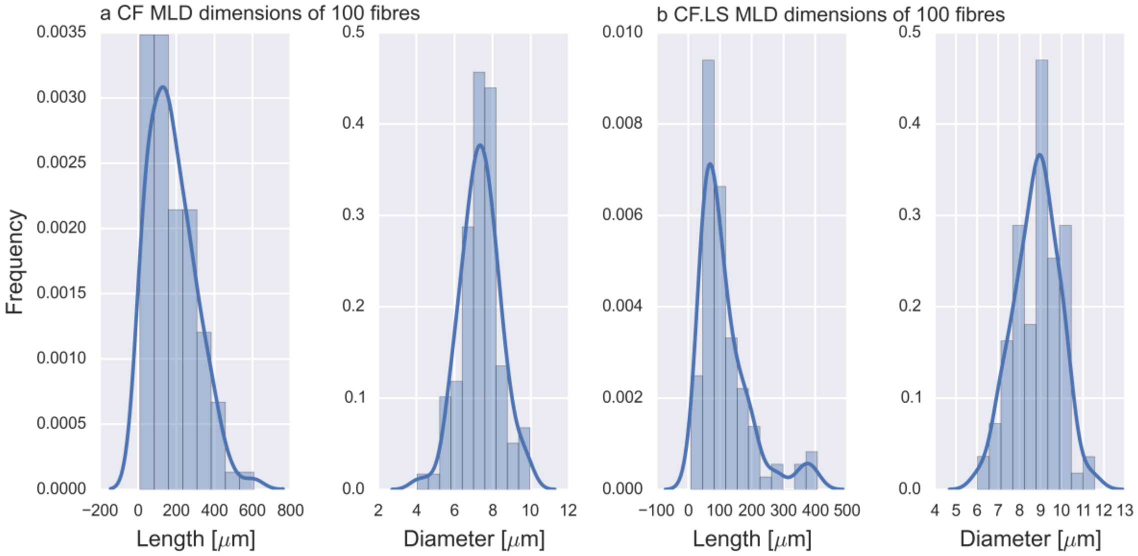

Figure 20: Length and diameter distribution of 100 fibres of CF MLD (a) and CF.LS MLD (b).

Table 9: Dimensions of MWCNT, CF MLD, CF.LS MLD, and wood fibres measured on SEM images.

Filler	Length [µm]	Diameter [µm]	Number of fibres measured
CF MLD	178 ± 122	7 ± 1	100
CF.LS MLD	114 ± 83	9 ± 1	100
Wood fibres	906 ± 325	264 ± 107	35
MWCNT	n.m.	34 ± 7nm	20

n.m.: not measured

Microscopic observation of RCF fibre surfaces showed that the recycled carbon fibres, which had not been exposed to the thermal treatment (CF MLD), were often glued to residues of other fibres and formed packages of 2-3 fibres (Figure 22a). In contrast, the CF.LS MLDs were always found isolated (Figure 22b). The surface of the CF MLD appeared globally smooth with some deformations (Figure 22). Deformations were also observed on the surface of CF.LS MLD at similar frequency but they were almost completely disconnected from the fibre surface (Figure 22d).

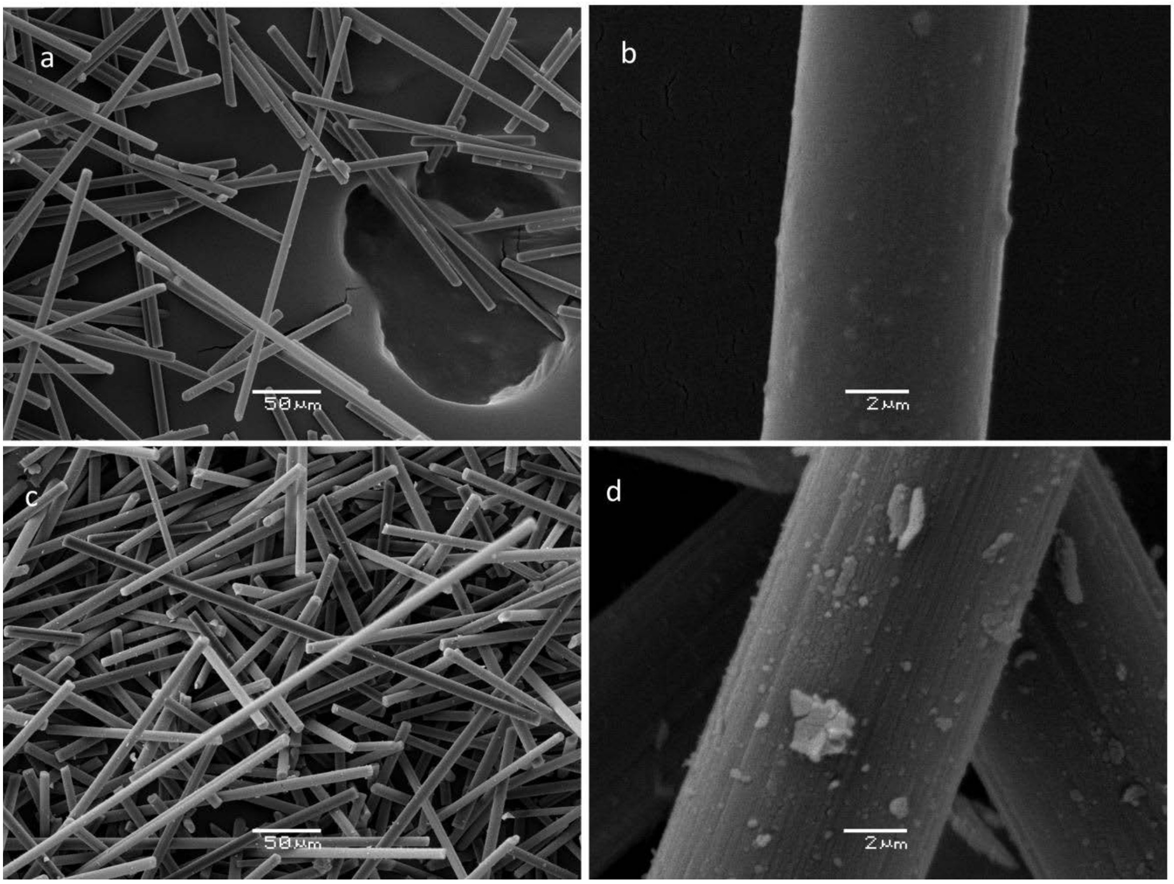

Figure 21: SEM imaging of the milled carbon fibres, CF MLD (a, b) and of milled carbon fibres exposed to thermal treatment, CF.LS MLD (c,d). Scale bar was 50 µm for a and c, and 2 µm for b and d.

4.1.2 Composite structure and filler-polymer interaction

The thermoplastic composites were produced through a pilot process using first compounding by extrusion followed by injection moulding. As it was reported that filler dispersion is mainly depending on the compounding step but can also change during injection moulding [26,28], observation of the filler dispersion was done directly on injection moulded samples. SEM observations showed that the qualitative distribution and dispersion of the different carbon fibre types obtained in PLA 3051D and in PHBV after injection moulding were similar (Figures 23 and 24). No difference in pullout levels was detected across the tested carbon fibre types.

For the recycled carbon fibres-filled PLA 3251D samples, the cross sectional images are presented in Figure 25. The distribution and dispersion of the two RCF types were equivalent. It was observed that the composites filled with recycled carbon fibres (CF MLD) showed fewer pullouts than the composites filled with carbon fibres exposed to thermal treatment (CF.LS MLD). The length of fibre parts that were protruding out of the broken surface was as well shorter for the CF.LS MLD.

When looking at the distribution of the MWCNTs in PLA 3251D or Bio-PE by SEM, it was observed that for both polymer types, the cross section surface was homogeneous. The addition of 0.5 wt% of MWCNTs (Figure 26a) did not affect the surface appearance and the fillers could not be located. However, increasing the loading to 1 wt% rendered the sample fracture surface homogeneously flaky (Figure 26b). The surface texture became even rougher at 5 and 10 wt% (Figure 26c and d).

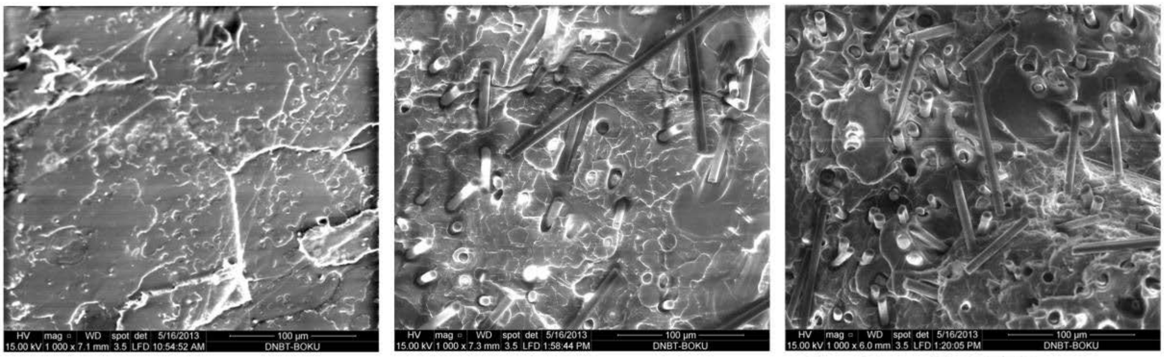

a) Neat PLA 3051D b) + 5 wt % CFA1 c) + 10 wt % CFA2

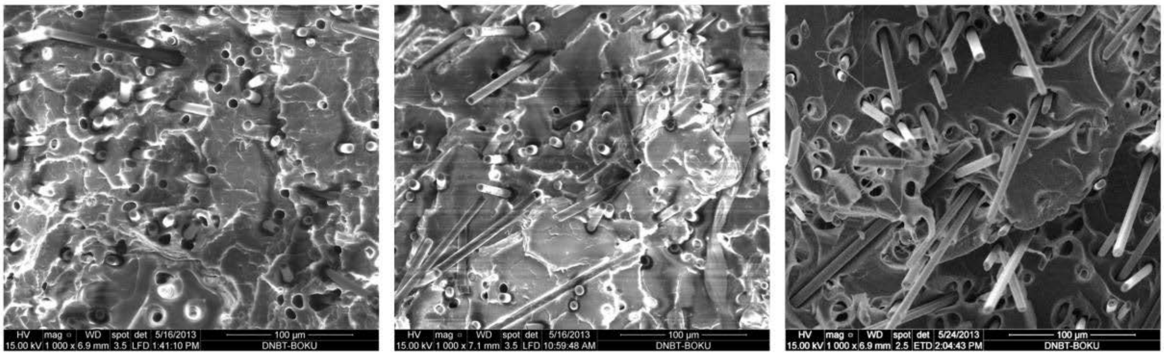

d) + 10 wt% CFB1 e) + 10 wt % CFB2 f) + 10 wt % CFC1

Figure 22: SEM imaging of the cross section of PLA 3051D-based samples (a–e: 4 nm gold coating and f: 10 nm).

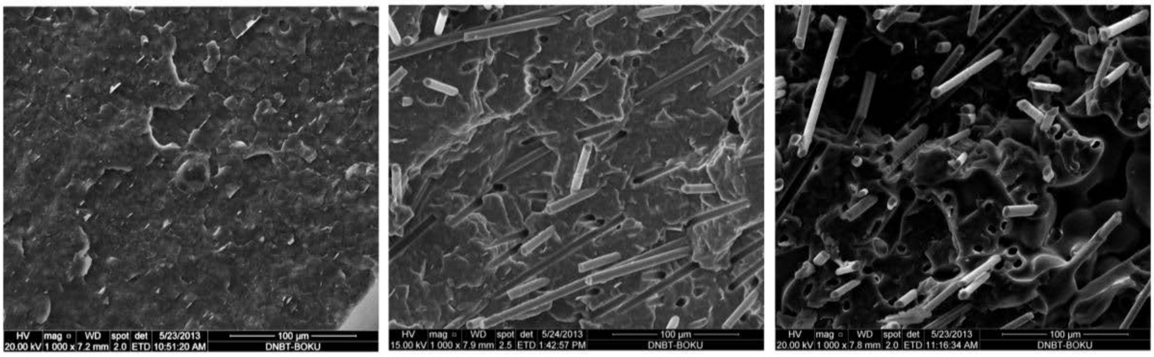

a) Neat PHBV b) + 10 wt% CFB2 c) + 10 wt% CFC1

Figure 23: SEM imaging on the cross section of PHBV-based composites with 10 nm gold coating.

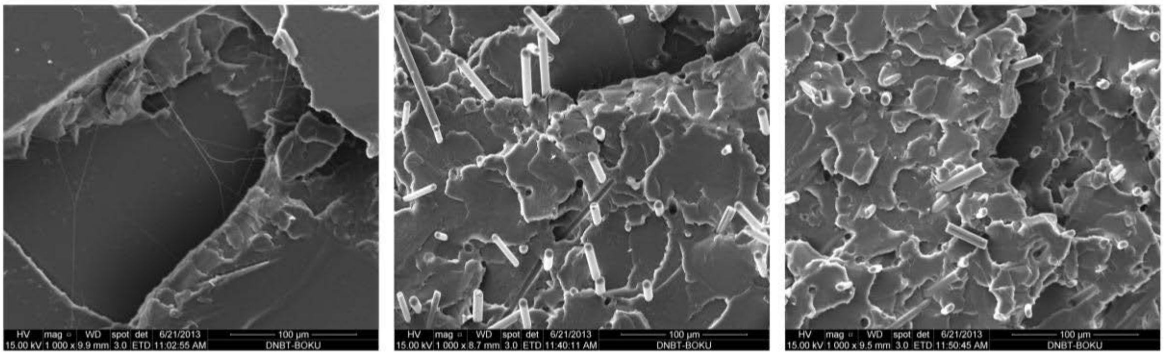

a) Neat PLA 3251D b) + 10 wt% CFMLD c) + 10 wt% CF.LS MLD

Figure 24: SEM imaging on the cross section of PLA 3251D filled with RCF with 8 nm gold coating.

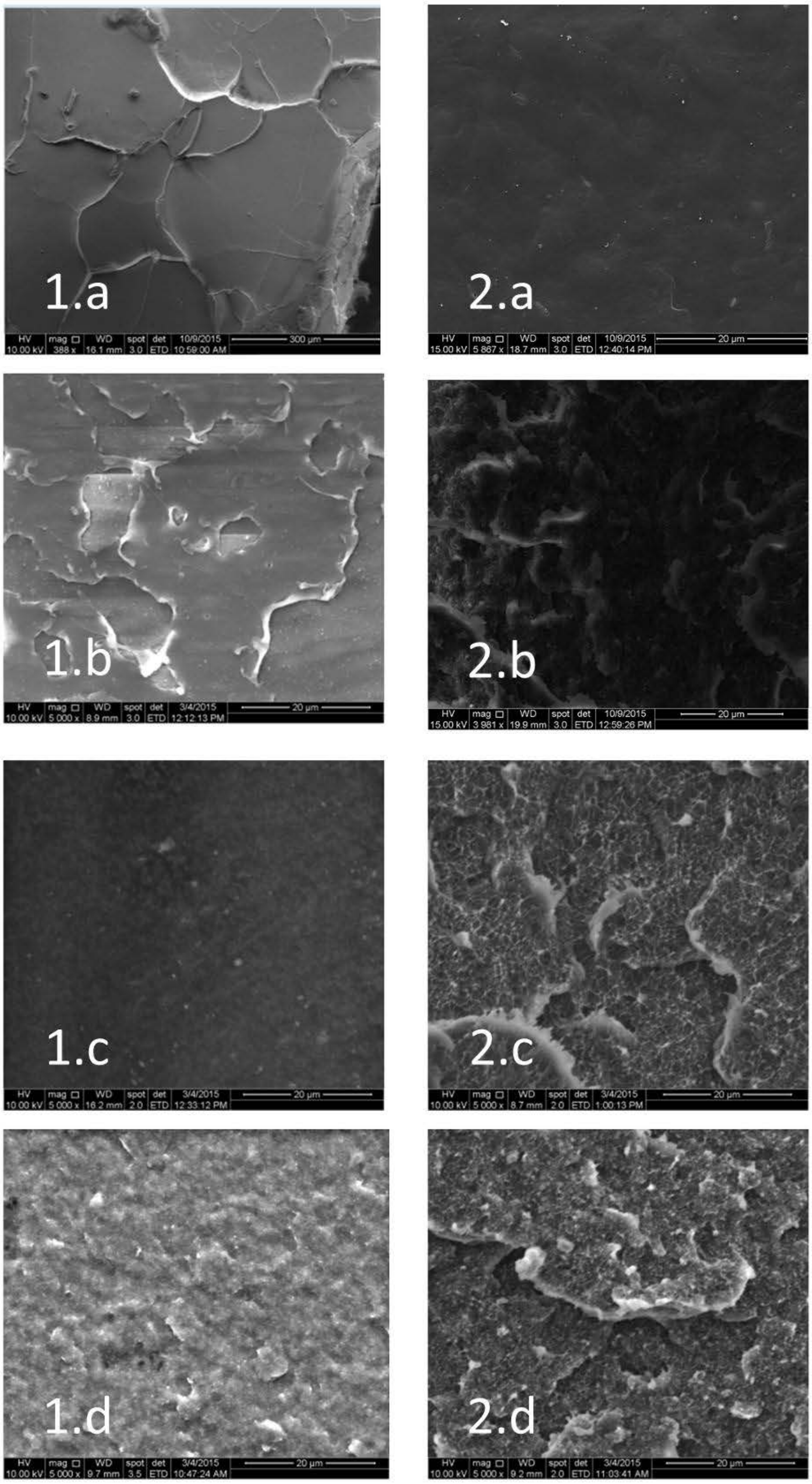

Figure 25: SEM images of the fractured surface obtained after tensile strength test of the PLA 3251D (1) and Bio-PE (2) based composites with 0 (a), 1 (1b), 2.5 (2b), 5 (c) and 10 wt% (d) MWCNT loading. Neat Bio-PE (2a) was prepared via microtoming and all images are taken at magnifications between 4000x and 6000x, with exception of neat PLA 3251D (388x).

To elucidate how the MWCNTs were dispersed into the polymer matrix, high-resolution AFM imaging was performed in tapping mode. Topography profiles and phase images are presented in Figures 27 and 28. Tubular structures having a diameter of around 20 nm are visible in PLA 3251D-based nanocomposites (Figure 27 b-d). Diameters were within the range of those measured for raw MWCNTs, which suggests that the visible fibrous structures are in fact MWCNTs. AFM images indicated that the tubes are quite evenly distributed in the polymer matrix. Thus, it appears that for all the investigated MWCNT loadings the melt processing was effective with separating the nanotubes from each other homogeneously within the PLA 3251D matrix. MWCNTs appeared aligned in the PLA 3251D-based samples filled with 1 wt% loading but not at higher loading. No clear tubular structure was visible in the Bio-PE matrices. Some circular sections were seen at 1 and 10 wt% loading (Figure 28 b-d).

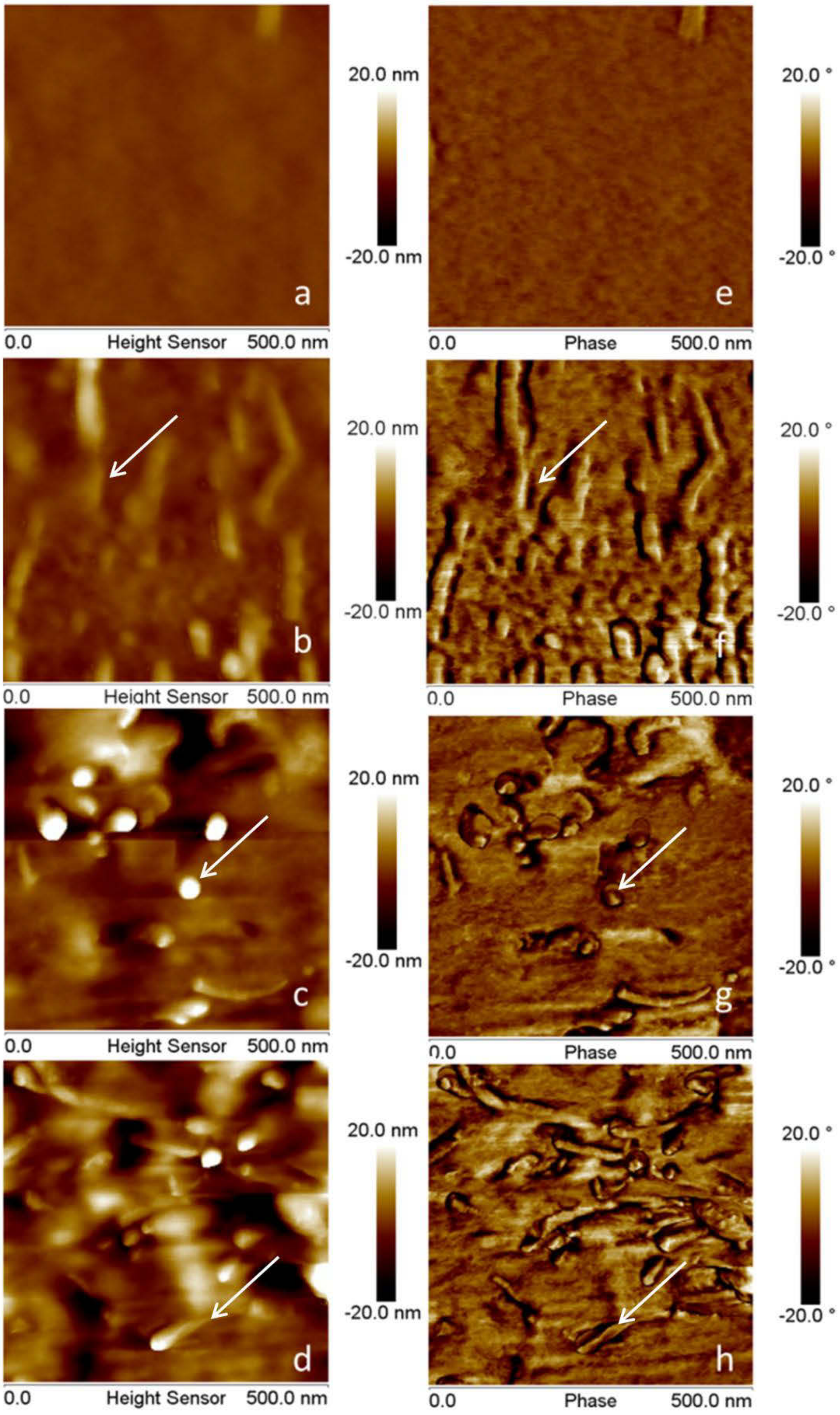

Figure 26: AFM topography (a-d) and corresponding phase images (e-h), recorded in tapping mode showing a section of 0.25 µm^2 of the PLA 3251D composite with 0 (a, e), 1 (b, f), 5 (c, g) and 10 (d, h) wt% MWCNT. The arrows indicate MWCNT location. The cutting direction of the microtome was from the right to the left.

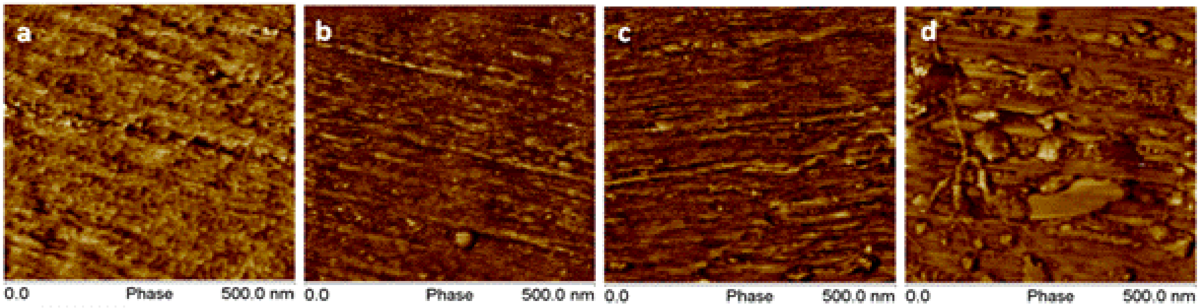

Figure 27: AFM phase images of the Bio-PE composites with (a) 0, (b) 1, (c) 5 and (d) 10 wt% of MWCNT.

From microscopic analyses it became clear that melt mixing by co-extrusion followed by injection moulding allowed a homogenous distribution of all filler types in thermoplastic polymers as expected. In the case of carbon fibre and recycled carbon fibre-filled samples, no difference in filler distribution and dispersion was detected from SEM imaging between the different used types of CF and RCF. Fillers appeared to be well-dispersed and randomly oriented at every loading except for MWCNT-filled composites as concluded from the AFM observations. Microscopic analyses were supplemented by the measurement of output data available from the extrusion and injection moulding processes to observe the effect of filler types on the process.

4.1.3 Melt behaviour during extrusion and injection moulding

The extrusion and injection output data are presented in Figures 29 to 32. The data of production set done at equal or close processing parameters are connected with segments on the Figures. For most of the productions, the melt temperature measured at the die of the extruder corresponded to the programmed temperature for zone 4. When the temperature programmed for zone 4 was increased, the melt temperature was also increased and polymer viscosity decreased at the die resulting in lower melt pressure. This was particularly detected when comparing the productions with 10 and 20 wt% of wood fibres in 20 wt% CF.LS MLD filled PLA 3251D (BFX48-49) and also for the first production set of MWCNT-filled PLA 3251D with 7.5 and 10 wt% loading (BFX28-29) when compared to PLA 3251D filled with 0 to 5 wt% MWCNTs (Figure 32a).

Melt pressure and machine load generally increased with the amount of carbon fibres added to PLA 3051D or PA, but decreased when the production was done at lower screw rotation speed; i.e. for PLA 3051D with 10 wt% CFB1 (BFX15, annotated with a * in Figure 29) and with CFA1 (BFX13-14). The injection pressures always increased with the carbon fibre loading, with exception of PLA 3251D and PAHS 18-based samples, for which the injection pressure reached the maximum at a loading of 5 wt%. This was not related to variation in the production parameters and could therefore not be explained here. The dosing time generally increased with the amount of filler.

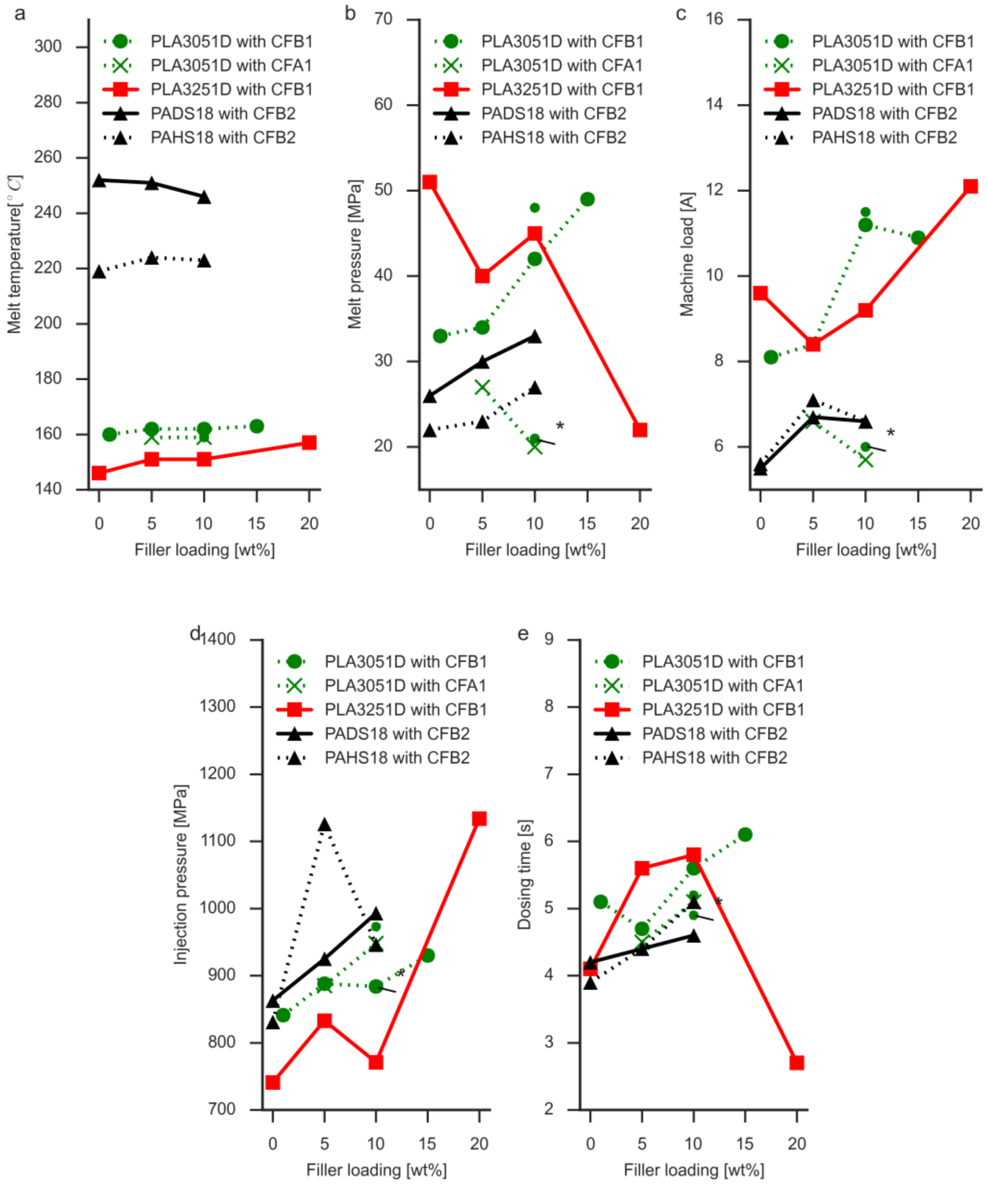

Figure 28: Melt temperature (a), melt pressure (b) and machine load (c) during extrusion and injection pressure (d) and dosing time (e) in injection moulding of the composite filled with increasing carbon fibre loading for PLA 3051D (BFX2;9-15), PLA 3251D (BFX30-32;61), PADS 18 (BFX35-37) and PAHS 18 (BFX38-40). Data corresponding to PLA 3051D filled with 10 wt% CFB1 (BFX15) are annotated with *.

During extrusion of the different types of carbon fibre and recycled carbon fibre at 10 wt% (Figure 30a-c), the production with CFC1 in PHBV (BFX8) presented a melt temperature 8 °C higher than the temperature chosen for zone 4. In PLA 3051D, all carbon fibres gave equivalent melt pressure and machine load, except for two polyurethane sized CF: for CFB2 (BFX1), which delivered lower melt pressure and machine load, and for CFC1 (BFX4) delivering also a lower machine load compared to the other tested carbon fibre types. This suggested a better compatibility between the polyamide sized CF and the PLA 3051D than the other CF types. In PHBV the addition of CFC1 (BFX8), having a polyurethane sizing, gave a higher melt temperature than the temperature selected for zone 4 and lower melt pressure than with all the other carbon fibre types tested: CFB2, CFB1, CFA2 (BFX5-7). This temperature increase was surprising as no increase was detected in another CF type (CFA2), having similar dimension and surface sizing than CFC1. The lower melt pressure obtained for CF MLD when compared to CF.LS MLD is explained by a better compatibility between the CF MLD and the PLA 3251D inducing better flow ability of the material. Melt pressures obtained with the recycled carbon fibres were always lower than those obtained with 10 wt% CFB1 in PLA 3251D (BFX32; 41), and more particularly with 10 wt% CF MLD (BFX33; 44). The machine load obtained at 10 wt% of CFB1 (BFX32; 41) was higher than the one obtained with 10 wt% CF MLD (BFX33; 44), whereas it was lower than the one obtained with CF.LS MLD (BFX34; 42).

The injection moulding of the samples with CFB2 and PLA 3051D gave the highest dosing time (6.1 s) and CFA2 gave the lowest (4.8 s) of the four carbon fibre types tested (BFS2-5). In PHBV, dosing time was found lower for CFB2 (BFS1), and higher for CFC1 (BFS7) than for the two other tested carbon fibre types: CFB1 (BFS6) and CFA2 (BFS8). When comparing productions processed under constant injection parameters, the dosing time was lower for polyurethane sized CF in PLA 3051D than with polyamide sized CF. In the case of PHBV-based composite filled with polyamide sized CF, lower dosing time were found than with polyurethane sized carbon fibres. This was interpreted as relative better packing of polyurethane sized CF in PLA 3051D and of polyamide sized CF in PHBV.

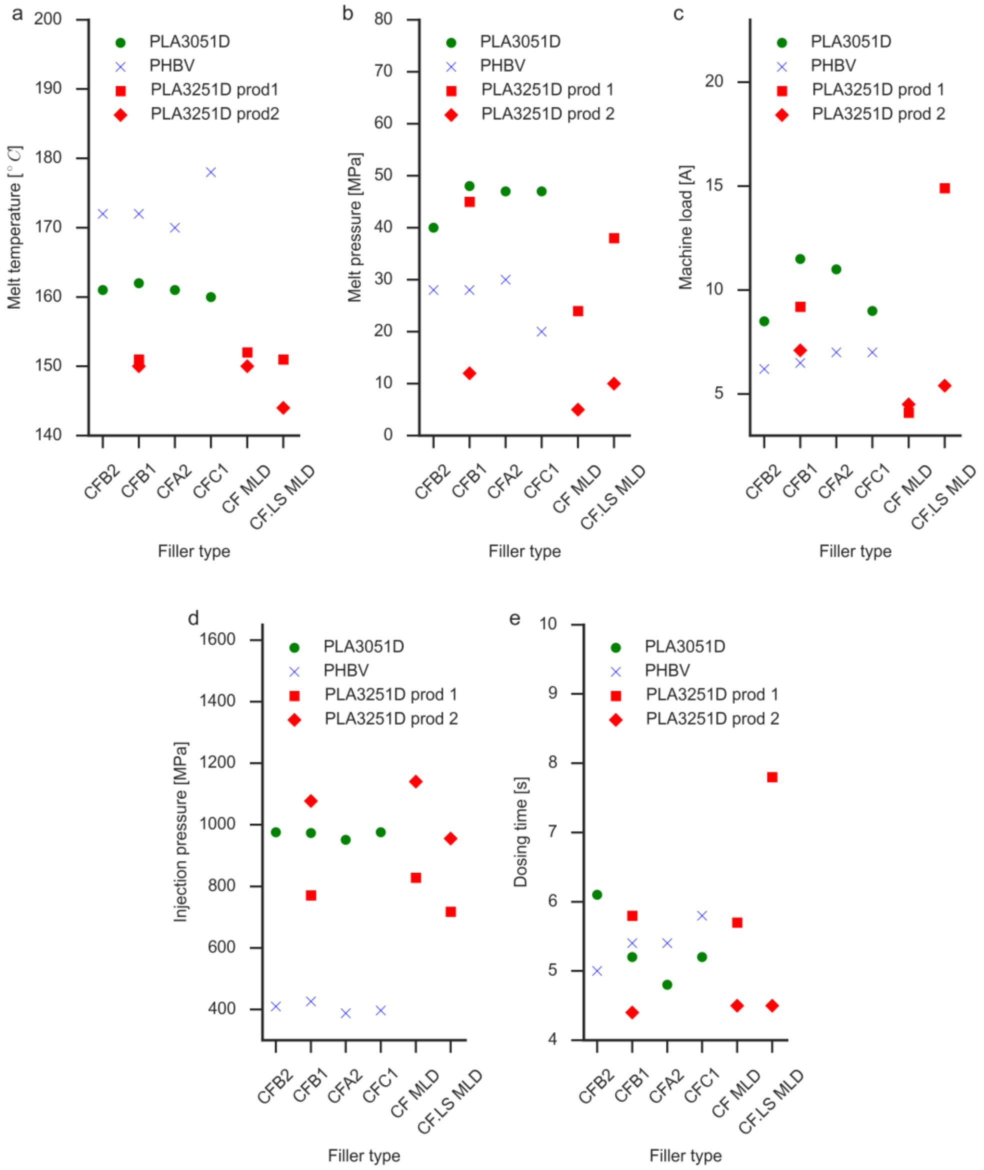

Figure 29: Melt pressure (a), melt temperature (b) and machine load (c) values during extrusion, injection pressure (d) and dosing time (e) of the injection moulding step for the composites filled with 10 wt% of different filler types in PLA 3051D (BFX1-4), PLA 3251D (BFX32-34; 41-42; 44) and PHBV (BFX5-8).

Wood fibres were added to PLA 3251D in addition to CFB1 or RCF. A particular high melt pressure was recorded for one production with CFB1 at 10 wt% (BFX32), which was not related to variations in the production process parameters. Melt temperatures measured during extrusion were lower than the temperature selected for zone 4 for the productions with 20 wt% wood fibres and 20 wt% CF.LS MLD (BFX49) and with 20 wt% of wood fibres and 20 wt% of CF MLD (BFX60) in PLA 3251D respectively of 4°C and 9°C. The melt pressure increased for every composite type with the amount of wood fibres, with the exception of wood fibres combined with CF.LS MLD in PLA 3251D for which the melt pressure decreased by 15 MPa from 10 wt% to 20 wt% wood fibre loading. Machine load was also higher when wood fibres were added, with exception at loads between 0 to 10 wt% wood fibres added to 10 wt% CFB1 in PLA 3251D, for which the machine load did not vary.

Concerning the injection moulding of the composites filled with wood fibres, injection speed, back pressure and cooling time settings were modified across productions. However, temperature settings were kept constant for each polymer type except for PLA 3251D, for which the first production with 10 wt% CFB1 and without wood fibres (BFS32) was exposed to a maximum temperature 10 °C lower than for the other composites. This first production with 10 wt% CFB1 (BFS32) was not considered in the following comparisons and was annotated with a * in Figure 31. Injection pressure was found to increase with raising wood fibre loading. No clear tendency was detected for the dosing time.

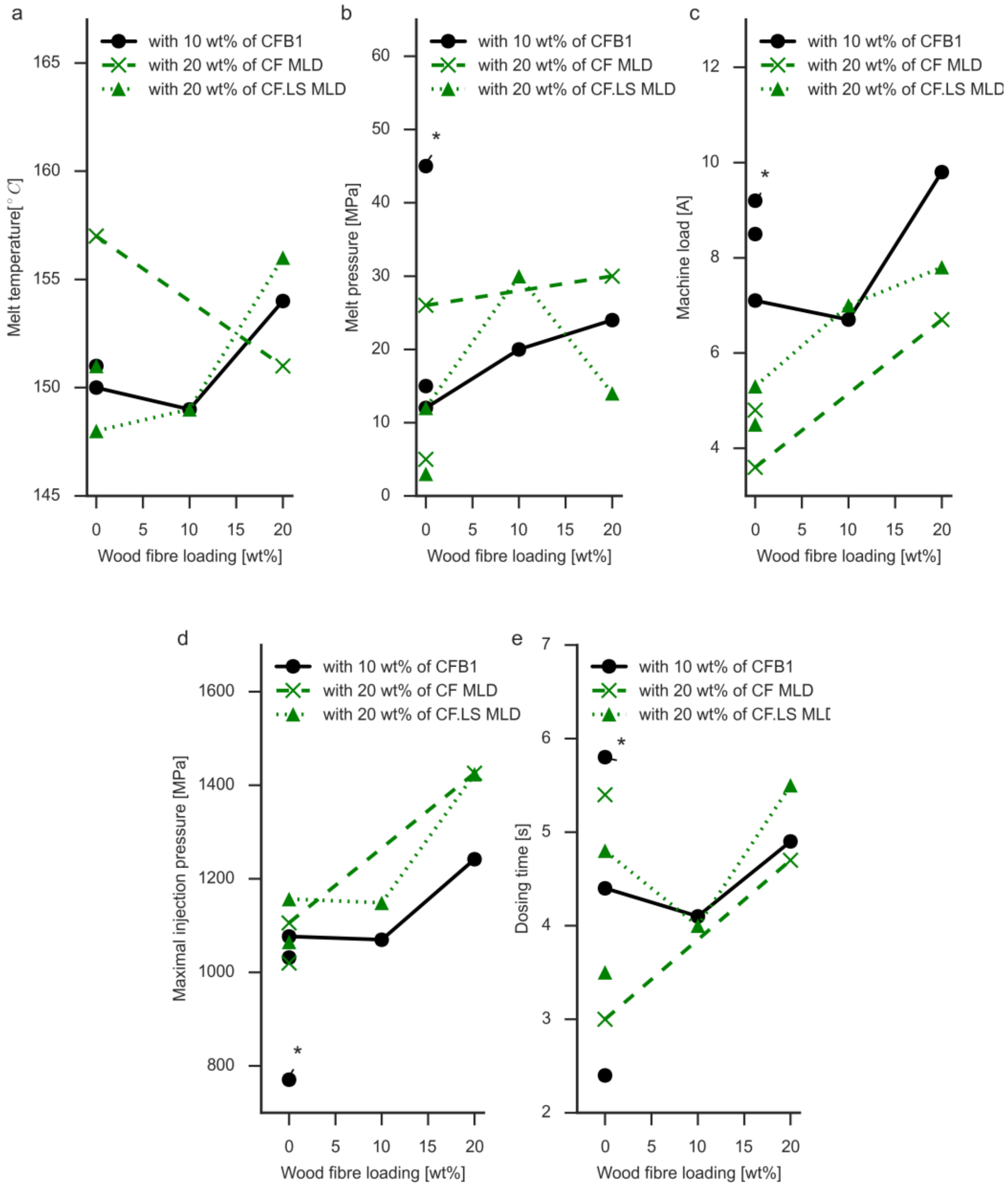

Figure 30: Melt pressure (a), melt temperature (b) and machine load (c) values during extrusion, injection pressure (d) and dosing time (e) during injection moulding of the composites filled with different wood fibre loading and with 10 wt% CFB1 (BFX32; 41;46-47; 59), with 20 wt% of CF MLD (BFX 45;57;60) or with CF. LS MLD (BFX 43; 48-49; 58) in PLA 3251D. The output data corresponding to the first production of PLA 3251D filled with 10 wt% CFB1 (BFX32) are annotated with *.

During the production of masterbatches the temperature measured was higher than the temperature selected for the heating zones with both polymer types. The difference was increasing when considering the zone closer to the die and was higher for Bio-PE-based productions than for PLA 3251D (up to 50 °C vs. 10 °C of variation). For the dilution step, the extrusion of the samples with MWCNTs in PLA 3251D and Bio-PE were done in two sets. Output data are presented in Figure 32. For the first production set with PLA 3251D the melt pressure increased linearly with the amount of MWCNT (from 0 to 5 wt%), while melt temperature was constant. For the productions with 7.5 and 10 wt% MWCNTs, higher melt temperatures were measured (corresponding to higher temperatures for zone 4) and melt pressure and machine load were found to be lower than the one of the production with 5 wt% MWCNTs. For the second production with MWCNTs in PLA 3251D, done at globally lower temperature than the first production set, melt pressure and machine load increased only between 5 and 10 wt% MWCNT loading. For the first production set with MWCNT-filled Bio-PE, melt pressure increased linearly from 0 to 10 wt% MWCNT loading. Machine load increased only between 2.5 and 5 wt% MWCNTs, and was then decreased at 7.5 and 10 wt% MWCNT loading. For the second production set with MWCNT-filled Bio-PE, extruded at lower temperatures than the first production set, a slight decrease in melt pressure and increase in machine load was observed while these composites were extruded under constant parameters. This was related to an increase in melt viscosity with the increase in MWCNT loading in Bio-PE and was not observed for MWCNT-filled PLA 3251D. In addition, higher increases in melt pressure and machine load were found for MWCNT-filled PLA 3251D than with Bio-PE. As this could not be explained from the production parameters, it was suggested that it is due to differences in the filler-polymer interaction, suggesting a better filler-polymer interaction for Bio-PE.

Concerning injection moulding, three production sets were executed. The injection pressure decreased from 0 to 2.5 wt% MWCNT loading, while it increased from 2.5 wt% to 10 wt% in PLA 3251D.In Bio-PE, injection pressure increased with MWCNT loading. No clear tendency was detected for the dosing time.

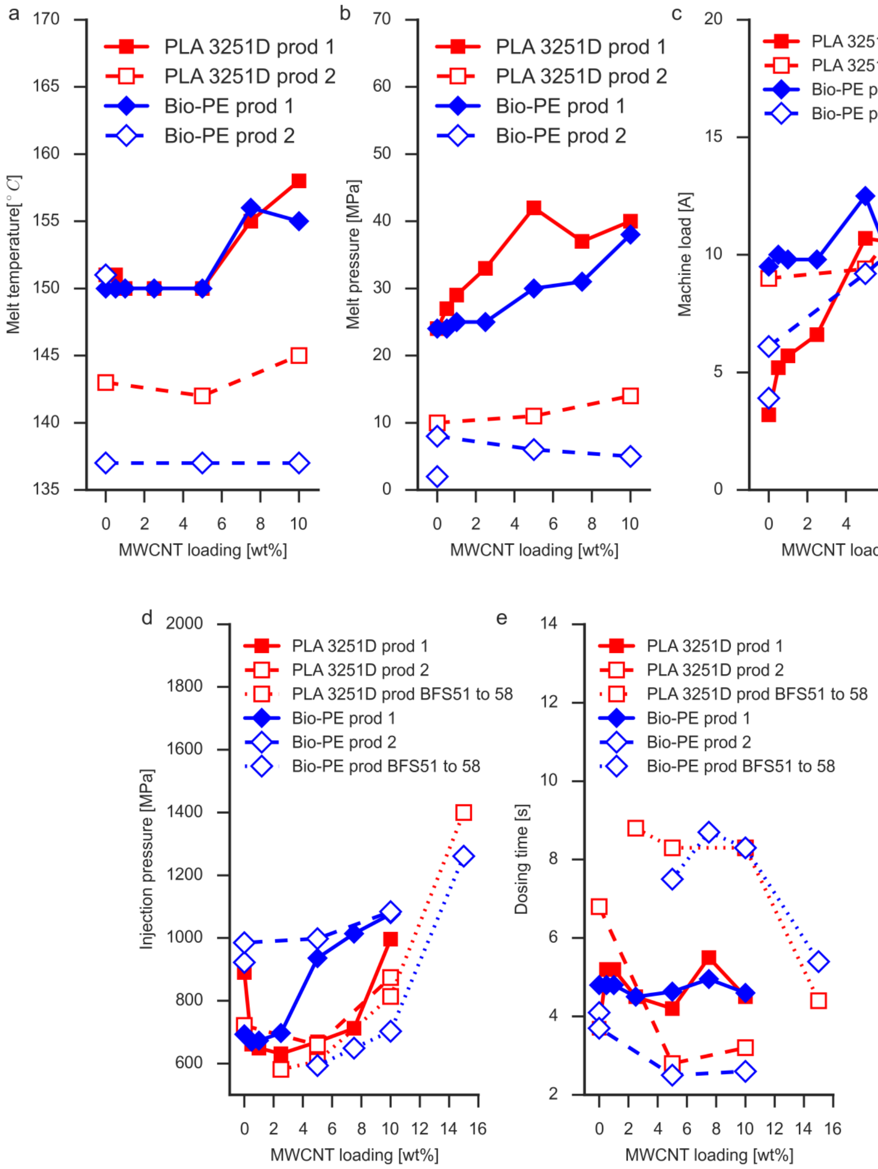

Figure 31: Melt pressure (a), melt temperature (b) and machine load (c) during extrusion, injection pressure (d), and dosing time (e) of the injection moulding step of the three production sets of PLA 3251D (BFX16-20;28-29;51;54;56) and Bio-PE filled with MWCNTs (BFX21-27;50;52-53;55) composites and the productions directly mixed during injection moulding (BFS51-58).

In general melt temperatures always reflected the temperature selected in the zone 4. For most of the composite types, an increase in melt pressure was found with the increasing filler contents, and simultaneously the machine load increased. This indicated an increase in melt viscosity. However, this was not the case for some composite produced at lower screw rotation speed (polyester sized CF and two replicates with 10 wt% polyurethane sized CF in PLA 3051D). This suggests that the effect of carbon fibres in PLA 3051D on the melt viscosity depends either on the screw rotation speed range, or on the type of carbon fibres used. Injection pressures were found to increase with the amount of fillers with most of the filler types tested. However, two composite types gave initially an increase when the carbon fibre loading was between 0 and 5 wt%, while a decrease was observed from 5 to 10 wt% loading (PLA 3051D with CFB1 and PAHS 18 with CFB2). Dosing time increased with the amount of carbon fibres, and varied with the type of filler.

These output data already suggest that the various fillers alter the melt behaviour during mixing and injection processing, relative to the used polymer.

4.2 Electrical conductivity

As explained in the introduction, different methods exist to determine the electrical conductivity of thermoplastic composite. In the present work, two-point, four-point and ring electrode methods proposed by different laboratories were compared to find a reliable method with limited material needs (sample dimension, silver paint or conductive tape). When possible, maximum electric fields applied for the measurements were considered uniform and approximated from the electric differential potential (voltage) applied for the measurement divided by the distance between the electrodes.

4.2.1 Two-point methods

Two different two-point methods for the characterization of composite surface conductivity were tested. The first one used two metallic bars as electrodes and the second one used two conductive stripes.

From the sets of measurements taken with the two metallic bar systems after 10, 20 and 60 s of exposition to the current, it was observed that the resistivity values varied with the time up to 24% for PLA 3251D with 5 wt% MWCNTs and decreased with the addition of weight on the metallic bars. For the rest of the measurements, the resistances were systematically taken one minute after switching on the source and under constant load. The corresponding conductivities are plotted in Figure 33. The conductivity of neat polymers, which could not be measured with the present method, were approximated with electrical volume conductivities reported in literature, being around 10^{-14} S m^{-1} for PLA and HDPE [57,65,118]. The value 10^{14} S was used in the graphics as surface conductivity value for neat PLA and Bio-PE to suggest their electrical conductivity range (insulators). Even if the calculation of conductivity took into account the difference in the distance between the two electrodes, variations remained between the values obtained from the two set-ups. The value measured differed by 50% from one system to the other for some of the most conductive composite characterized. For example, PLA 3251D with 10 wt% MWCNTs showed a surface conductivity of 5.5 10^{-3} S with system A and of 2.32 10^{-3} S with system B. However, for PLA 3051D filled with 15 wt% of CFB1 higher conductivity was measured with the system B. This was attributed to the quality of the contact between the electrodes and the sample inducing high variability of the results. This measurement method indicated that the electrical percolation threshold was at least below 7.5 wt% loading in the case of MWCNT-filled PLA 3251D and at least below 10 wt% loading for MWCNT-filled Bio-PE. For CFB1-filled PLA 3051D conductance was detected from 10 wt% loading and quadrupled from 10 to 15 wt% loading. The maximal conductivity detected for MWCNT-filled composites was with 10 wt% MWCNTs in PLA 3251D at 5.5 10^{-3} S and with 15 wt% CFB1 loading in PLA 3051D at 4.1 10^{-2} S with the system B.

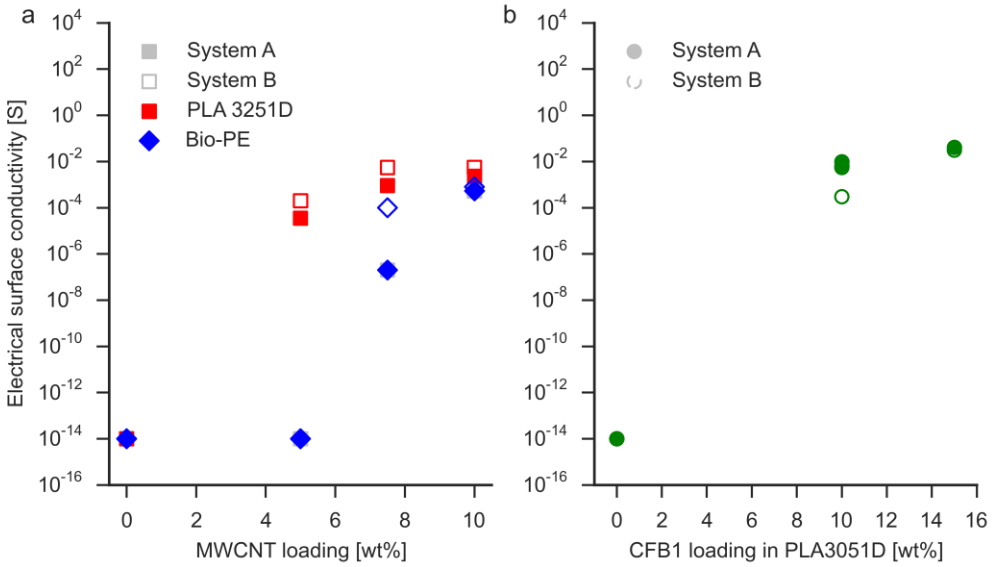

Figure 32: Electrical conductivity measured with the two different metallic bars measurement systems for MWCNT (a) and CFB1 (b) filled composites, with each point corresponding to one measurement. Maximum electric fields for the measurement were approximated at 225 N C^{-1} for system A and at 81 N C^{-1} for system B.

The tape stripe method, expected to give a continuous and reproducible contact with the sample was used only on samples with the lowest conductive filler loadings. The assessment was done on PLA 3251D-based composites with low amount of conductive filler (0 to 2.5 wt% for MWCNTs, 5 wt% for CFB1 and 10 wt% for CF.LS MLD. All the resistances measured at 23 °C and at 30% relative humidity were higher than 10^{11} Ω. The corresponding electrical surface conductivities were calculated considering the distance between the electrodes of 7.75 mm (*d* in Equation 2) and the length of the stripes of 70 mm (*p* in Equation 2). Results are presented in Table 10. It was concluded that all these composites were insulating in an electrostatic sense. Slight increases in the PLA 3251D-based composite conductivity with 2.5 wt% MWCNTs and 10 wt% of CF.LS MLD were detected when compared to neat PLA 3251D but this was measured on one sample and was therefore only used to suggest the percolation threshold.

Table 10: Electrical surface resistance measured with a megaohmmeter and two parallel conductive stripes on PLA 3251D-based samples.

Filler type	Filler loading [wt%]	BFS	Electrical surface conductivity [S]	
			Under 13 10^3 N C^{-1}	Under 65 10^3 N C^{-1}
No filler	0	16	5.8 10^{-16}	2.3 10^{-15}
MWCNT	1	18	6.2 10^{-16}	6.2 10^{-16}
MWCNT	2.5	19	8.5 10^{-15}	1.6 10^{-14}
CFB1	5	31	9.2 10^{-16}	2.3 10^{-15}
CF.LS MLD	10	42	1.8 10^{-14}	1.5 10^{-14}

Two different two-point methods for composite volume conductivity characterization were tested in the present work. The first method consisted in applying two clamped electrodes at the extremities of the samples and the second comprised two alligator clips.

The values obtained from the two-clamped electrodes are plotted in Table 11. For every characterized sample a linear relation was found between voltage potential and current intensity as observed in Figure A1. The corresponding electrical volume conductivities presented in Table 11 were approximated with A= 4 10^{-5} m^2 and d= 9.0 cm. The detection of conductivity already with 1 wt% MWCNTs in PLA 3251D (BFS18) indicated that the percolation threshold was already reached with 1 wt% MWCNTs when applying pressure on the electrode-sample contact areas. However, the pressure applied on the electrode-samples contact could not be determined and therefore this method was not reproducible. Furthermore, the variations in conductivity observed when increasing manually the pressure on the electrodes-sample contact surface showed that this method was not adapted for the characterization of our composite.

Table 11: Conductivity values measured with the two-clamped electrodes on PLA 3251D-based composites. The maximal electric field applied was between 6 and 311 N C^{-1}.

MWCNT loading [wt%]	BFS	Electrical volume conductivity [S m^{-1}]
1	18	2.3 10^{-4}
7.5	21	13.0
10	22	33.0

The alligator clip method was applied on the first productions of carbon fibre and MWCNT-filled composites based on PLA 3051D, PHBV, PLA 3251D and Bio-PE (BFS1 to 29). To assess the reproducibility of this method, ten measurements were done on one sample containing 5 wt% MWCNTs in PLA 3251D (BFS20), as this sample was expected to have an intermediate resistance when compared to other produced composites. A mean value of 338 kΩ with a standard deviation of 140 kΩ was found. The high standard deviation was explained by the high variability of the surface contact between the alligator clips and the sample surface. With this method, percolation threshold of MWCNT-filled composite was detected below 5 wt% MWCNT loading in PLA 3251D and below 7.5 wt% MWCNT loading in Bio-PE. The corresponding volume conductivities calculated from the data according to Equation 3 are presented in Table 12 and Figure 34. The conductivities reached with 10 wt% MWCNTs were significantly higher in the case of PLA 3251D (7.6 ± 2.3 S m^{-1}) when compared to Bio-PE (0.8 ± 0.2 S m^{-1}) and were in the same range as those reached with CFB1 when using 10 wt% of filler (4-10 ± 4 S m^{-1}).

The electrical volume conductivities reached with the PHBV-based composite were always higher than those obtained with the PLA 3051D-based composites for 10 wt% loading of the same carbon fibre types. The resistivity of the material varied with the tested carbon fibre type. Conductivity was detected from 10 wt% loading for all carbon fibre types except for the CFA1 (polyester sizing) in PLA 3051D for which no resistance value could be measured with the present equipment. By comparing the effect of the different carbon fibre types, it appeared that the polyurethane sized carbon fibres CFB1 and CFC1 induced a higher increase in the conductivity of PLA 3051D than the polyurethane sized carbon fibres CFA2 or polyamide sized carbon fibres CFB2. Concerning the PHBV-based samples, the conductivities reached with the polyurethane sized fibres (CFB1, CFC1 and CFA2) were significantly higher than those reached with polyamide sized fibres (CFB2) and the CFB1 type gave also significantly higher conductivities than CFA2 as indicated by Kruskal-Wallis test.

Table 12: Electrical resistance measured with two alligator clips, where”-“ means that the resistance was too high to be measured with this method. The maximal electric field applied was 8 10^2 N C^{-1}.

Polymer	Filler	Filler loading [wt%]	BFS	Electrical surface conductivity [S m^{-1}]
PHBV	CFB2	10	1	6.7 ± 3.6
	CFB1	10	6	61.2 ± 21.4
	CFC1	10	7	14.2 ± 5.5
	CFA2	10	8	26.7 ± 7.9
PLA 3051D	CFA1	5	14	-
		10	15	-
	CFB2	10	2	0.5 ± 0.3
	CFA2	10	4	0.2 ± 0.1
	CFC1	10	5	2.0 ± 0.7
	CFB1	1	9	-
		5	10	-
		10	3	4.3 ± 1.6
		10	11	9.9 ± 3.9
		10	13	4.4 ± 1.6
		15	12	42.7 ± 18.7
PLA 3251D	MWCNT	2.5	19	-
		5	20	0.1 ± 0.03
		7.5	21	2.7 ± 0.3
		10	22	7.6 ± 2.3
Bio-PE	MWCNT	5	27	-
		7.5	28	0.04 ± 0.01
		10	29	0.8 ± 0.2

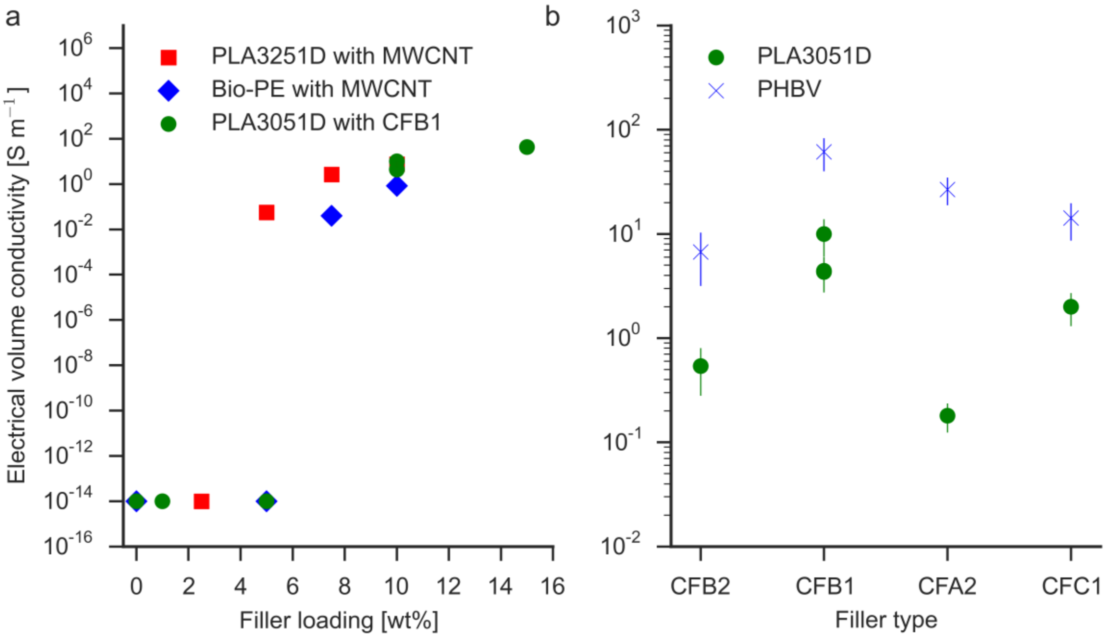

Figure 33: Electrical volume conductivity of various loadings of CFB1 and MWCNT in PLA 3051D, PLA 3251D and Bio-PE (a), and of different types of carbon fibres at 10 wt% loading in PLA 3051D and in PHBV (b). PLA 3051D with 10 wt% CFB1 (b) is the same as in (a) and was determined with the alligator clip two-point measurement method from minimum eight measurements.

All the two-point methods tested gave concordant classification of the composites regarding electrical conductivity level. Same estimation of percolation threshold was obtained from one method to the other however differences in maximal electrical conductivities and measurement reproducibility were found, regardless of considering volume or surface conductivity. The deviation within parallel measurements was reduced when applying the higher pressure on contact between the electrodes and the sample. It is explained by the increase in the surface of contact between the electrodes and the sample. As in the two-point measurement method, the contact resistance between the electrodes and the sample is added to the composite resistance, samples with lower resistance can only be detected when the contact resistance is lower than that of the sample [53]. This is challenging to assure with the two-point measurement methods without modifying irreversibly the sample surface. Therefore, four-point measurements without and with sample surface modification were tested for the composite with higher conductivities detected with the two-point methods.

4.2.2 Four-point methods

Four-point measurements were performed on selected samples to characterise higher conductivities. The tested measurement methods were used in two different configurations to approach both “surface” and “volume” conductivities.

The four-point measurement used for the determination of surface conductivity was realized with four pin electrodes and gave very disparate results. Corresponding electrical surface conductivity were approximated for *s*=1 cm and are presented in Table 13. A high variability was found for the samples having 10 wt% MWCNT loading in PLA 3251D. In Bio-PE, higher conductivity was detected with 7.5 wt% MWCNTs than with 10 wt% MWCNT loading. The pin electrodes in contact with the sample delivered non-constant data. These results suggested that the small contact areas between the pin electrodes and the composite surface were not adapted for the characterization of composites filled with conductive fibres and nanotubes. They were therefore not used for further material characterization.

Table 13: Electrical surface resistance determined with four aligned pin electrodes.

Polymer	Filler type	Filler loading	BFS	Electrical surface conductivity [S]
PLA 3051D	CFB2	10	2	4 10^{-5}
	CFB1	5	10	Overflow
		10	11	Overflow
		10	11 (replicate)	Overflow
		15	12	2 10^{-6}
		10	13	5 10^{-3}
PLA 3251D	-	0	16	Overflow
	MWCNT	5	20	2 - 3 10^{-7}
		10	22	3 10^{-4}
		10	22(replicate)	3 10^{-2}
Bio-PE	MWCNT	1	23	Overflow
		7.5	28	Overflow to 1 10^{-5}
		10	29	2 10^{-6}
PLA 3251D	CF MLD	10	33	Overflow

The volumic four-point measurement method indicated a conductivity of 7.8 ± 0.8 S m^{-1} with 5 wt% MWCNT loading in PLA 3251D as plotted in Figure 36. This shows that the sample is electrically conductive (e.g. $\sigma > 10^{-3}$ S m^{-1}). Conductivity further increased to 55 ± 16 S m^{-1} at 10 wt% MWCNT loading. Values were also obtained for the composites based on Bio-PE with 7.5 wt% loading of MWCNTs, delivering a conductivity of 0.43 ± 0.05 S m^{-1}. For Bio-PE based samples, the highest conductivity was measured with 2.2 ± 0.3 S m^{-1}, at 10 wt% MWCNT loading.

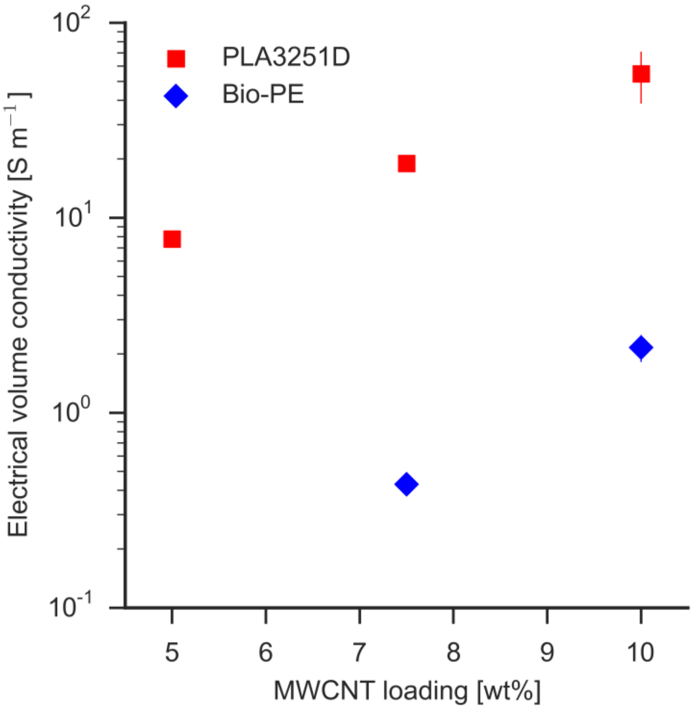

Figure 34: Electrical conductivity of MWCNT-filled composites measured by four-point method according to EN ISO 3915, measured under a maximal electric field around 9 10^2 N C^{-1}. The mean value and standard deviation were obtained from measurements on three samples for each composite type.

Additional characterization of the composite filled with MWCNTs using the same four-point method but by applying silver paint on the sample extremities and gold pads as sensor electrodes measured conductivity values in the same range as without the sample preparation. Results are depicted in Figure 37. The conductivity of the MWCNT-filled PLA 3251D was higher than that of MWCNT-filled Bio-PE. An increase from 5 S m^{-1} to 27 S m^{-1} between 5 wt% and 10 wt% loading was observed for MWCNT-filled PLA 3251D. This electrical percolation threshold was consistent with the existence of interconnected MWCNT networks observed by AFM imaging at 5 and 10 wt% MWCNTs (see Figure 27). The Bio-PE-based samples exhibited an increase in conductivity from 2 10^{-3} S m^{-1} to 0.7 S m^{-1} between 5 wt% and 10 wt% MWCNTs loading.

This four-point method with sample preparation was also used to characterize the annealed 10 wt% MWCNT-filled PLA 3251D, and Bio-PE composites. In both cases an increase in conductivity with filler loading was detected (Figure 37). However, these measurements were only done on one sample for each composite, meaning statistical significance could not be demonstrated.

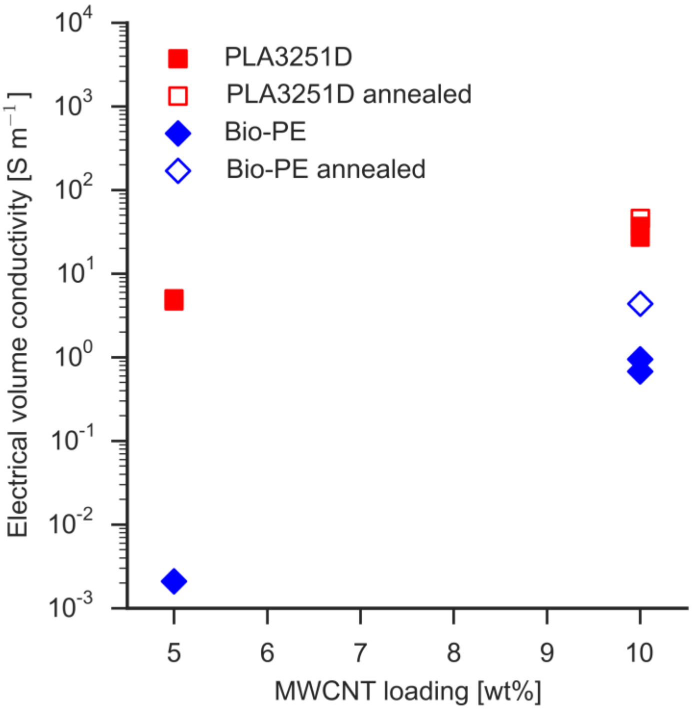

Figure 35: Electrical volume conductivity obtained with four-point measurements with silver paint and gold pads electrodes on un-annealed and annealed MWCNT reinforced biopolymers. The maximal electric field applied was of 18 10^3 N C^{-1}.

In general, the two “volumic” four-point methods tested gave higher conductivity values for MWCNT-filled PLA 3251D composites, compared to the metallic bars and alligator electrode methods and similar values to the clamped electrode method.

4.2.3 Ring electrode method

Ring electrode method presented the advantage that the two measurement configurations (surface and volume) were independently measured. The ring electrode method was used on the CFB1 and RCF-filled PLA 3251D and on some MWCNT-filled composites. The surface and volume conductivities are presented in Figure 38. In both configurations high variability was observed for the surface conductivities below 10^{-7} S and for the volume conductivities below 10^{-9} S m^{-1}. The differences observed between surface and volume conductivities trends were explained by the fact that the skin layer of the injection moulded parts acts as an insulating layer in volume conductivity, but gives higher conductivities in surface measurement (parallel to filler orientation) [27,29].

Concerning the PLA 3251D-based composites, the addition of 10 wt% CF MLD induced a significant increase in the surface conductivity; volume conductivity increased only from 20 wt% loading. With 20 wt% CF MLD, similar surface and volume conductivities as with 10 wt% CFB1 were obtained. CF MLD gave lower percolation threshold and higher conductivity properties at 20 wt% loading in PLA 3051D than CF.LS MLD. This was mainly attributed to the presence of sizing at CF MLD surface. However, differences in RCF dimensions could also have affected this result, as CF MLD were found to be longer than CF.LS MLD in the result part on filler characterization.

When adding wood fibres, (Figure 38b and d) in presence of 10 wt% CFB1 the surface conductivity was significantly increased with 10 wt% wood fibre loading but the higher wood fibre loading resulted in significantly lower conductivities. The same sample characterized in volume configuration showed only a significant decrease in the conductivity from 10 to 20 wt% wood fibre loading. For CF.LS MLD filled PLA 3251D samples, surface conductivity increased when adding from 10 to 20 wt% of wood fibres but the volume conductivity increased only when increasing the loading from 0 to 10 wt% of wood fibres.

For MWCNT-filled composites, lower percolation threshold and higher electrical conductivities for 10 wt% filler loading were found for PLA-based composites compared to Bio-PE-based composites. Surface and volume conductivities could be measured from 2.5 wt% MWCNT loading in PLA 3251D and from 5 wt% MWCNT loading in Bio-PE. This indicated that the percolation threshold was reached already at lower MWCNT loadings for PLA 3251D. The surface conductivities measured for PLA 3251D or Bio-PE with 10 wt% MWCNTs were in the same range of conductivity than PLA 3251D filled with 10 wt% of CFB1 (around 4 10^{-6} S). However, the volume conductivities of these same composite differed, the composites based on PLA 3251D and filled with 10 wt% MWCNTs gave conductivity in lower ranges 1 10^{-9} S m^{-1} vs. 3 10^{-8} S m^{-1} for Bio-PE filled with 10 wt% MWCNTs and 2 10^{-7} S m^{-1} with the 10 wt% CFB1 in PLA 3251D giving the highest conductivity.

The highest surface conductivity measured with this method was found for 10 wt% CFB1and 10 wt% wood fibres-filled PLA 3251D and was around 10^{-5} S. This was very low compared to the surface conductivities measured with the two metallic bar electrodes, which were around 10^{-2} S. Similarly, the upper limit of volume conductivity was found around 2 10^{-7} S m^{-1} for the composites based on PLA 3251D-filled with 10 wt% CFB1, whereas it was around 10 S m^{-1} when measured with alligator clips. Thus, ring electrode method measurements in the present work were limited by the resistance of the contact between the electrodes and the sample plate which was added in the measurement as it was observed for two-point measurement method.

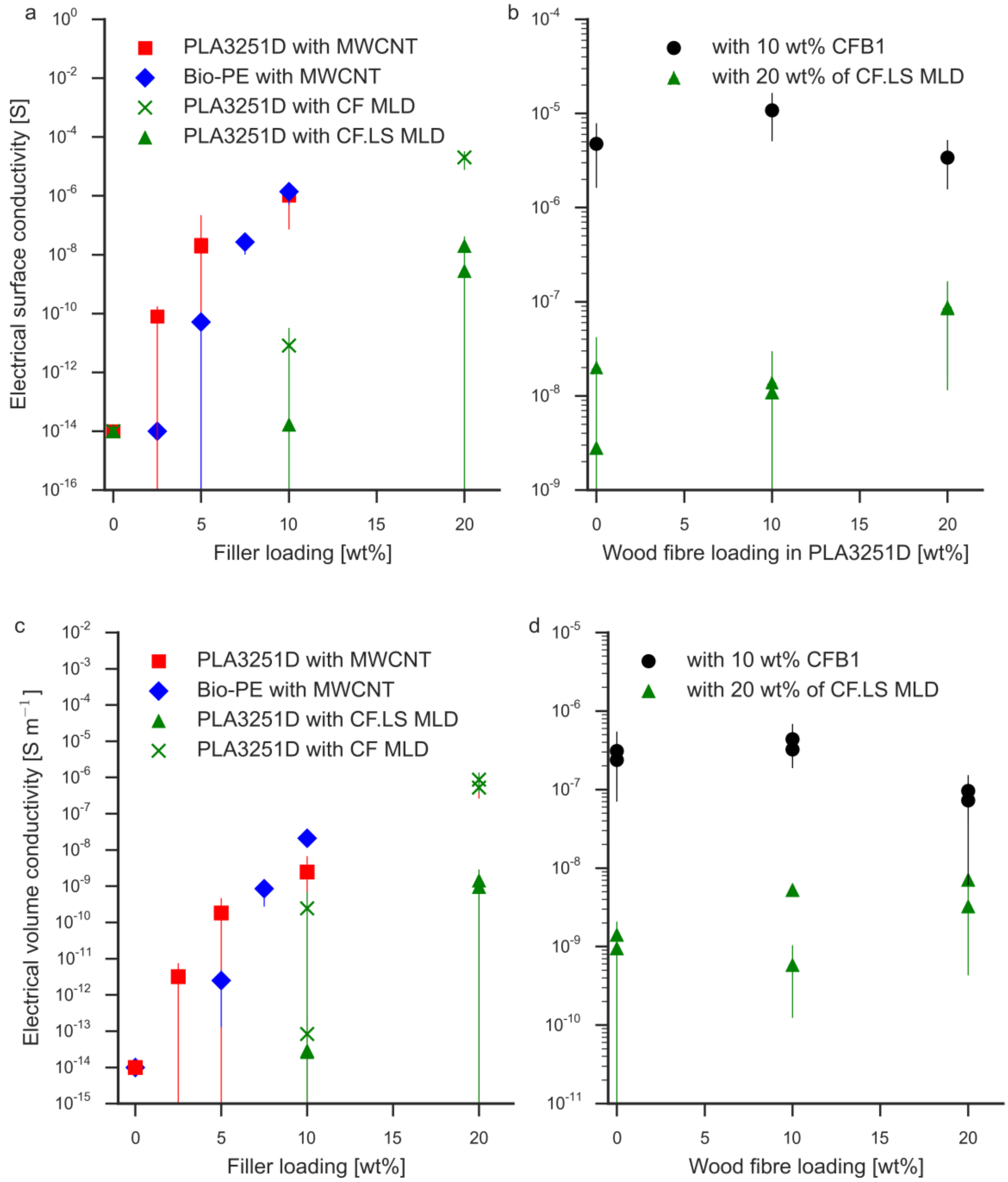

Figure 36: Surface (a,b) and volume (c,d) conductivities of PLA 3251D and Bio-PE based composites filled with MWCNTs, CFB1 and recycled carbon fibres without (a,c) and with wood fibres (b,d) determined with ring electrodes. The maximal electric field applied was of 1 10^{5} N C^{-1} for surface measurement and of 1 10^{4} N C^{-1} for volume measurement.

Concordant conductivity variation with filler loading was obtained with almost every method tested but the reproducibility of the measurement and the measured electrical conductivities differed from one method to the other. The two-point method tested which did not imply the use of silver tape did not give reliable results. The measurements obtained with the four-point method using pin electrodes and with the ring electrode method presented a high variability. In the ring electrode measurement, the conductivity varied when the filler sizing was altered. The difference between electrical conductivity of MWCNT and CF MLD filled samples was higher in the case of surface conductivity than in volume conductivity. This indicated that MWCNT were more involved in the surface conductivity in regards to volume conductivity than the recycled carbon fibres, suggesting some anisotropy in filler distribution. However, both surface and volume conductivity showed similar conductivity profile with filler loading increases. This suggested that the filler loading increased in the same way in the skin layer region than in the core region of the composite. In presence of wood the conductivity of the RCF types tested was increased by almost one order of magnitude; whereas the conductivity of CF-filled PLA 3251D decreased slightly. The four-point method built after EN ISO 3915, implying the use of a mechanical testing machine to control the load applied at the contact between sensor electrodes and the sample gave reliable results. These results were in agreement with the results obtained when using a four-point method in which the electrode-sample contact were ensured by the application of silver paint. Therefore the method built after EN ISO 3915 was selected over the others as the most reliable method which did not imply the use of silver paint or conductive tape. Its results were used for further electrical comparisons. Annealing induced very slight increase in the conductivity in the case of MWCNT-filled composite.

Percolation thresholds were not precisely determined with these measurements and therefore Nan's Law (Equation 8) was applied to the composites characterized with the four-point methods. In the case of the carbon fibres CFB1, percolation threshold was expected to be around 0.0035 vol% (0.05 wt% for PLA3251D density of 1.24 and CFB1 density of 1.8). The percolation thresholds predicted by Nan's Law for recycled carbon fibres were of 2.8 vol% (4.1 wt%) and of 5.8 vol% (8.4 wt%) respectively for CF MLD and CF.LS MLD (with density of 1.85 for recycled carbon fibres and PLA3251D density of 1.24). In the case of MWCNT filled PLA3251D composites, Nan's law predicted a percolation threshold around 0.24 vol% (0.33 wt%, considering for MWCNT a length of 10 µm, a diameter of 34 nm and a density of 1.7). In the case of Bio-PE filled with MWCNT, the percolation threshold was also expected to be around 0.24 vol% MWCNT, which corresponds to 0.42 wt% (with Bio-PE density equal to 0.96). The predictions appeared to fit better the experimental results in the case of recycled carbon fibres than in the cases of CFB1 and MWCNT filled composites.

4.3 Mechanical performances

Mechanical performance of the different composites was assessed through the characterization of tensile behaviour and resistance to impact.

4.3.1 Tensile properties and model

Tensile properties were characterised from the analyses of the traction test. Stress vs. strain curves were obtained from ten samples for each composite type (as presented in the case of MWCNTs in Figure 39). Tensile strength, tensile elongation and Young's modulus were determined from these curves and are presented in Figures 40 to 43. When increasing the loading of carbon-based fillers in PLA 3051D; PADS 18, PAHS 18, PLA3251D and Bio-PE increase in the composite tensile strength were detected with exception of MWCNT-filled PLA 3251D. At 10 wt% MWCNT loading in PLA 3251D the tensile strength was 26% lower than for neat PLA 3251D (Figure 41). The tensile elongation was globally reduced and Young's modulus was increased for all composites when adding carbon-based fillers.

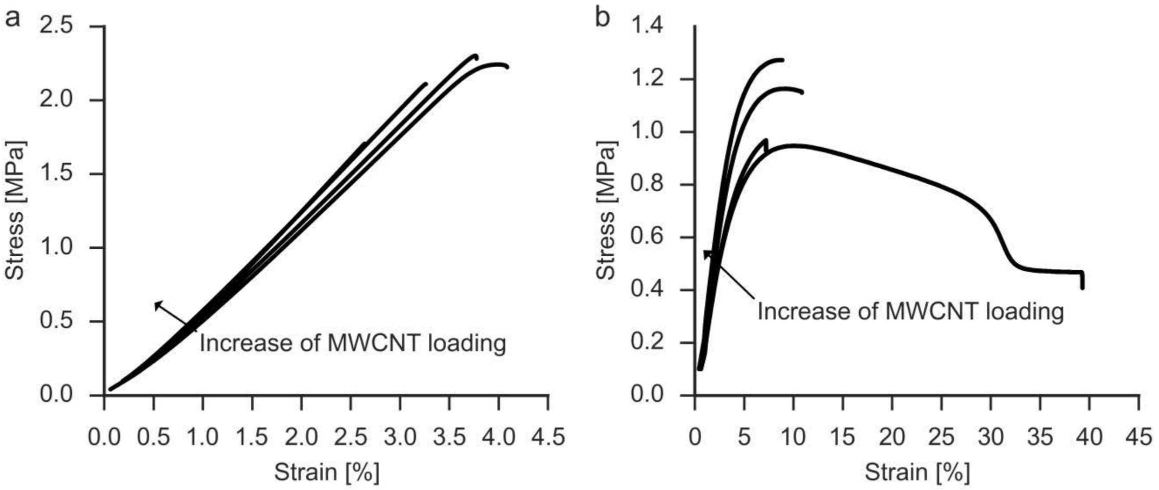

Figure 37: Stress vs strain behaviour of the PLA 3251D (a) and Bio-PE (b)-based composites with 0, 1, 5 and 10 wt% MWCNT loading, averaged from ten measurements.

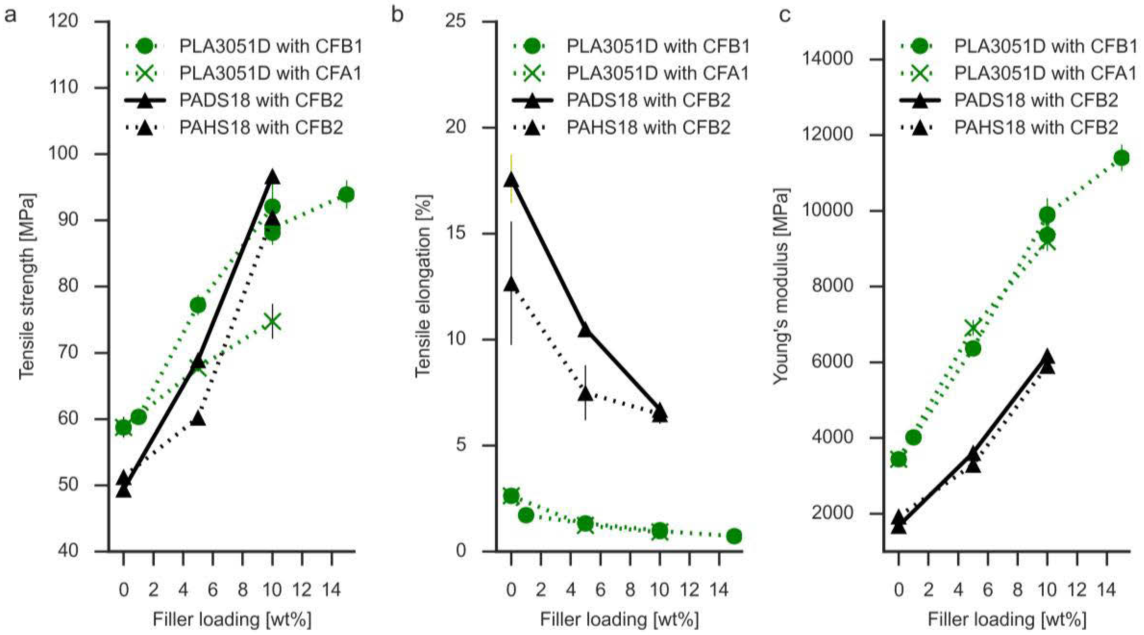

Figure 38: Tensile strength (a), tensile elongation (b) and Young's modulus (c) of PLA 3051D and polyamide based composites loaded with CFB1, CFA1 or CFB2. Mean values were calculated from ten tensile tests after standard ISO 527.

The higher increase in tensile strength obtained with CF MLD, compared to the increase found with CF.LS MLD, is explained by the remaining sizing present at CF MLD surface and removed from CF.LS MLD, which improved the interfacial affinity with the matrix polymer. Indeed, SEM imaging (Figures 22b and d) showed dust partially peeled off at the surface of CF.LS MLD assumed to correspond to carbonized sizing that shrank and lost partly their adherence to the fibres during the heat treatment. However, the slight variation in length between the two RCF types could also result in changes in tensile strength. On the SEM imaging of fractured surfaces of PLA 3251D-based composites (Figures 25b and c), the length of fibre parts protruding out of the broken surface was remarkably longer with CF MLD than with CF.LS MLD and was related to the original dimension of the RCF, as measured in the chapter on filler analysis in the results part (Figure 21 and Table 9). However, when comparing the improvement observed with CF MLD to the one observed with CFB1, comparable improvement was obtained with 10 wt% loading, while the difference in length was 100 times larger than the one between CF MLD and CF.LS MLD. The decrease of 26% in tensile strength detected from 10 wt% CF MLD-filled PLA 3251D and CF.LS MLD-filled PLA 3251D is therefore more likely to be due to variation in filler-polymer interaction.

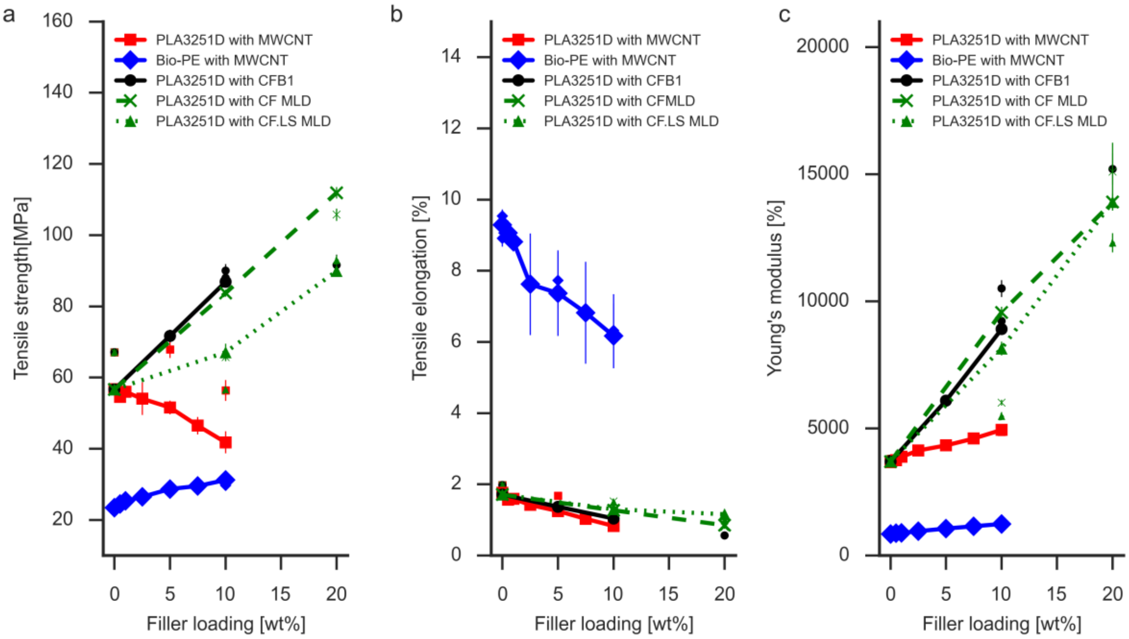

Figure 39: Tensile strength (a), tensile elongation (b) and Young's modulus (c) of PLA 3051D, PLA 3251D, and Bio-PE based composites loaded with CFB1, recycled carbon fibres and MWCNTs. Mean values were calculated from ten tensile tests according to standard ISO 527.

When comparing the effect of the CF types used in PLA 3051D or PHBV on mechanical behaviour, different tensile behaviours were detected. For PLA 3051D higher improvements were reached in presence of polyurethane sized and polyamide sized carbon fibres than with the polyester sized carbon fibres, except for the polyurethane sized carbon fibres from the third producer (i.e. CFC1) which induced similar tensile strength improvement as polyester sized CF (CFA1). For PHBV, the improvement was independent from the fibre sizing (Figure 40 and 42).

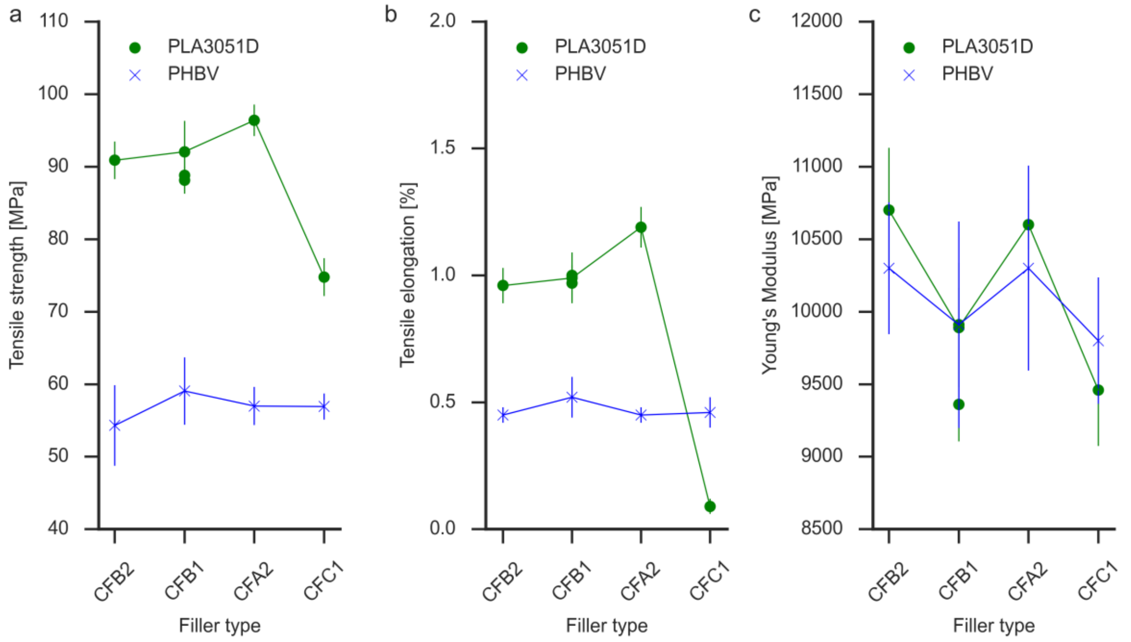

Figure 40: Tensile strength (a), tensile elongation (b) and Young's modulus (c) of PLA 3051D and PHBV composites loaded with 10 wt% of different carbon fibre types. The data for the CFB1 and CFA1-filled PLA 3051D and neat PLA 3051D polymers are the same as in the Figure 41.

The addition of wood fibres induced a decrease in tensile strength except when combined with 20 wt% of CF.LS MLD for which after a decrease with 10 wt% wood fibres loading, tensile strength equivalent to the one of the sample without wood fibre was reached with 20 wt% loading of wood fibres. The tensile elongation was decreased with increasing amount of wood fibres. No clear tendency was observed for the Young's modulus when adding the wood fibres.

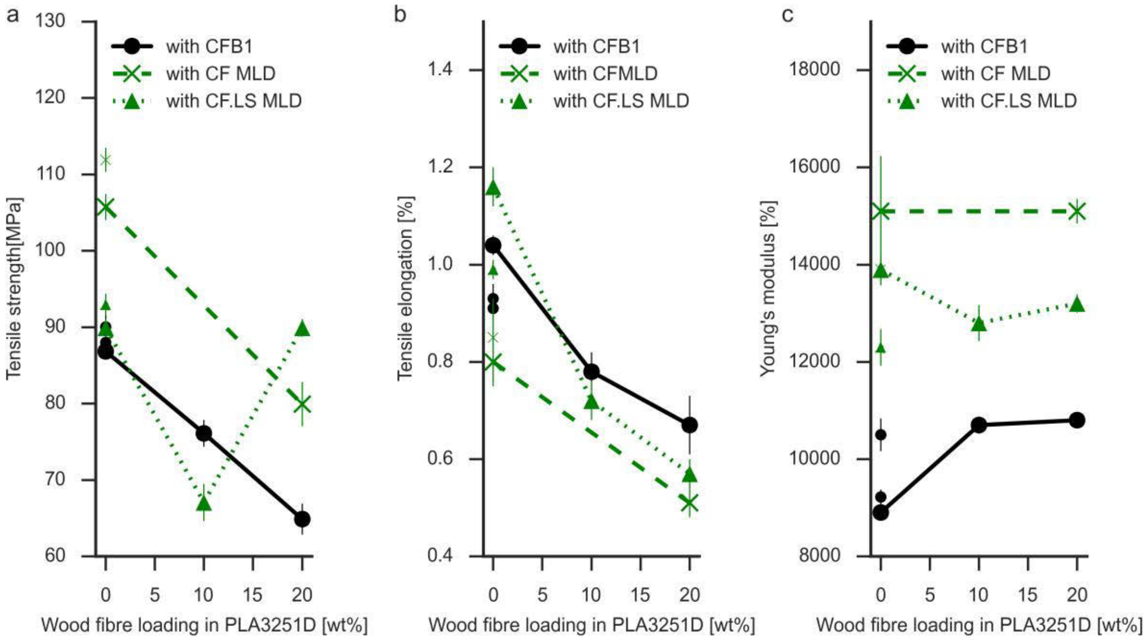

Figure 41: Tensile strength (a), tensile elongation (b) and Young's modulus (c) of wood fibre-filled samples, with the data for the CFB1 and CF.LS MLD and CF MLD without wood fibre being the same than in the Figure 41.

The Halpin-Tsai model was applied for the composite based on Bio-PE and filled with MWCNTs. Model and experimental values are presented in Figure 44. Halpin-Tsai model overestimated the Young's modulus when adding 10 wt% loading to the neat Bio-PE, it predicted an increase of almost +800%, which in the experiment only increased by 48%. When using shorter length for the MWCNT dimension in the model (0.5 µm), the predicted Young's modulus corresponded to the present experimental values. This suggests that the MWCNTs present in the Bio-PE had an equivalent effect as MWCNTs with shorter length having a good chemical interaction with Bio-PE. This could be explained by a reduction of the length of the MWCNTs due to the mixing process or to an entanglement of the MWCNTs giving a residual effective length of 0.5 µm.

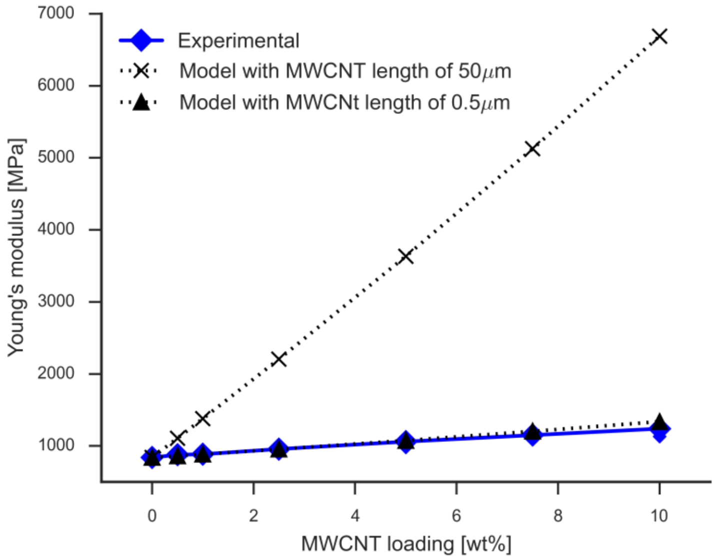

Figure 42: Application of the Halpin-Tsai model to the Bio-PE-based composites with two MWCNT lengths and comparison to experimental data.

4.3.2 Impact Strength

Unnotched Charpy impact strength results are presented in Figure 45. The samples combined with wood fibres were not characterised. When increasing the amount of CFB1 from 1 to 5 wt% loading in PLA 3051D, the impact strength was found to decrease significantly according to Kruskal Wallis test ($p<0.5$). In the case of the PLA 3251D-based composites filled with CFB1 or recycled carbon fibres, or MWCNTs no significant variation in the impact strength was found when increasing filler loading. In the case of Bio-PE-based composites at the lower loading (0.5 to 5 wt% MWCNT) impact strength was increased and at the higher loading (5 to 7.5 wt% MWCNT) it was decreased until it reached the value of neat Bio-PE. The addition of 5 and 10 wt% CFB2 in the two polyamide types induced a decrease in the impact strength.

When comparing the effect of the different tested fibre types at 10 wt% in PLA 3051D, it was found that CFA2 gave significantly higher impact strength than CFB1, CFA1 and CFB2, which gave impact strength in the same ranges as the neat PLA 3051D. All the different types of carbon fibres added to PHBV induced the same increases in impact strength compared to neat PHBV.

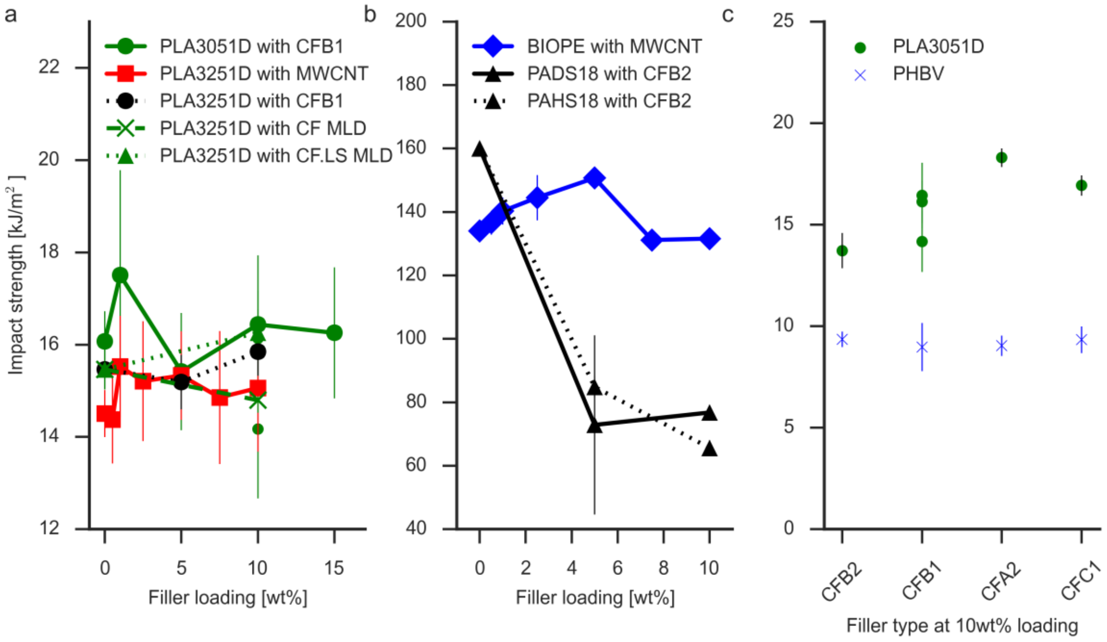

Figure 43: Impact strength with corresponding standard deviations of PLA 3051D and PA 3251D types combined with different loading of CFB1, recycled carbon fibres and MWCNTs (a) Bio-PE and PADS 18 and PAHS 18 types combined with MWCNTs and CFB2 respectively (b) and PLA 3051D and PHBV with different types of carbon fibres at 10 wt% loading (c) calculated from ten measurements by Charpy unnotched method.

Tensile strength improvements were found for carbon-based fillers with the highest aspect ratio. However, the addition of unmodified MWCNTs to PLA 3251D decreased the tensile strength (Figure 41a). This was related to the filler-polymer interaction. Impact strength was in general not changed by the addition of carbon-based filler. It only decreased for PA-based samples. This was explained by the relatively high impact strength of polyamide neat polymer. In the case of Bio-PE which had also very high neat polymer impact strength, an increase in impact strength was measured until 5 wt% loading and at higher content (up to 10 wt%) a decrease was observed. Thermal degradation stability was further tested only in the case of MWCNT-filled composites.

4.4 Thermal stability

Thermal degradation of the MWCNT-filled composites was characterised by TGA under air. Averaged thermograms from three measurements of the composites loaded with 0, 1, 5 and 10 wt% are presented along with their first derivatives in Figures 46 and 47. For the PLA 3251D-based composites, the start of the decrease in weight was slightly shifted to lower temperatures with the increasing MWCNT loading as shown in Figure 46 (from 322.3 °C to 301.3 °C for 0 to 10 wt% MWCNTs), while the thermal stability of the Bio-PE composites increased with the increasing MWCNT loading as shown in Figure 47 (from 356.4 °C to 428.2 °C for 0 to 10 wt% MWCNT). It was also noticed that there was almost no change in the temperature at which the completion of the degradation took place for PLA 3251D-based composites.

To characterise precisely the thermo-oxidative degradation of the samples, the temperatures at which 5 wt% of the sample was degraded (T_d) and the temperature at which the maximal degradation rate was reached (T_{dmax}) were recorded. They are plotted in Figure 48. For PLA 3251D-based composites, the addition of MWCNTs decreased the T_d and the T_{dmax} increased when adding up to 5 wt% of MWCNTs but then decreased with higher MWCNT loadings. However, for Bio-PE both T_d and T_{dmax} increased until reaching equilibrium at 2.5 wt% loading. In general, the effect of the increasing filler loading from 0 to 10 wt% loading was more pronounced for Bio-PE-based composites reaching an improvement of the T_d of approximately 60 °C, whereas for PLA 3251D-based composites the change was around 20 °C.

As catalyst residues were reported in the literature to possibly alter the composite thermal stability, the amount of catalyst in the MWCNTs was determined. Residual mass obtained from TGA measurement on MWCNTs showed a catalyst percentage of 3.4% with a standard deviation of 1%.

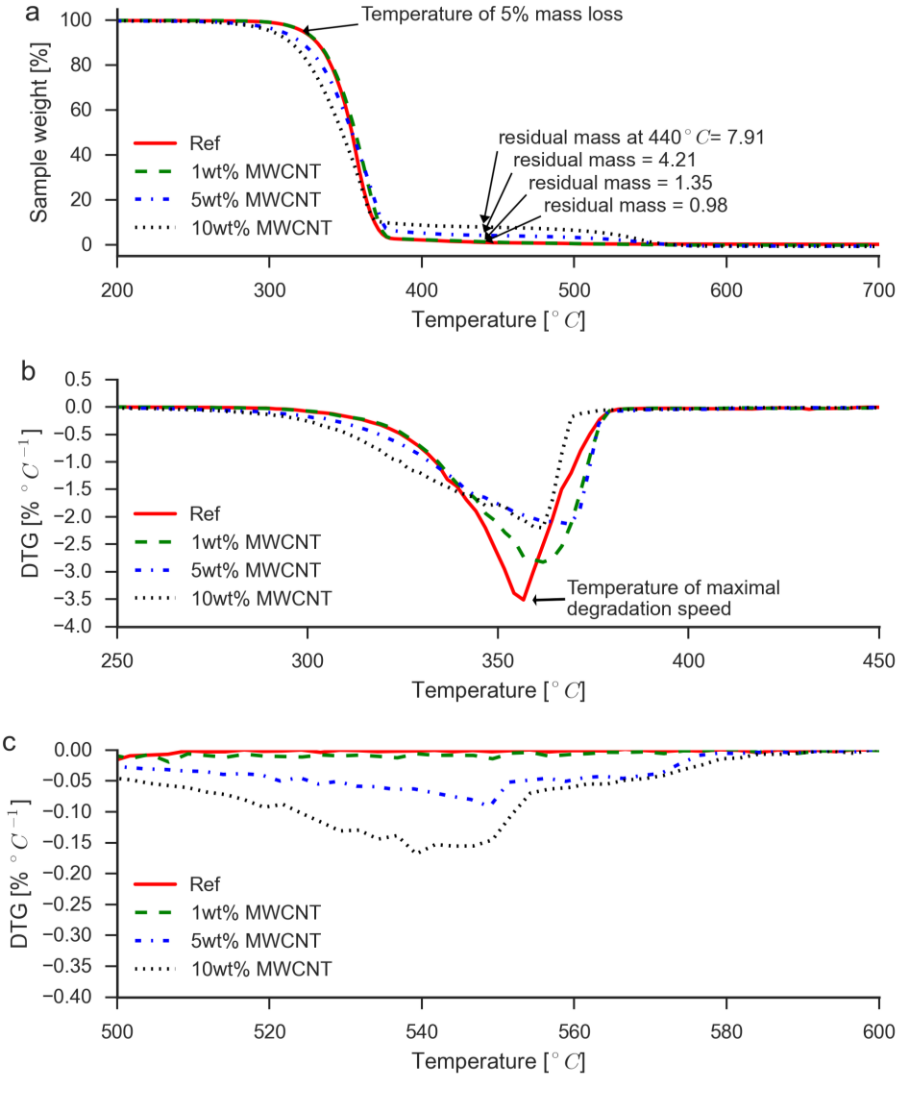

Figure 44: Thermal degradation in air (a) and corresponding first derivatives from 250 to 450 °C (b) and from 500 to 600 °C (c) of the PLA 3251D-based composites, averaged from three TGA measurements.

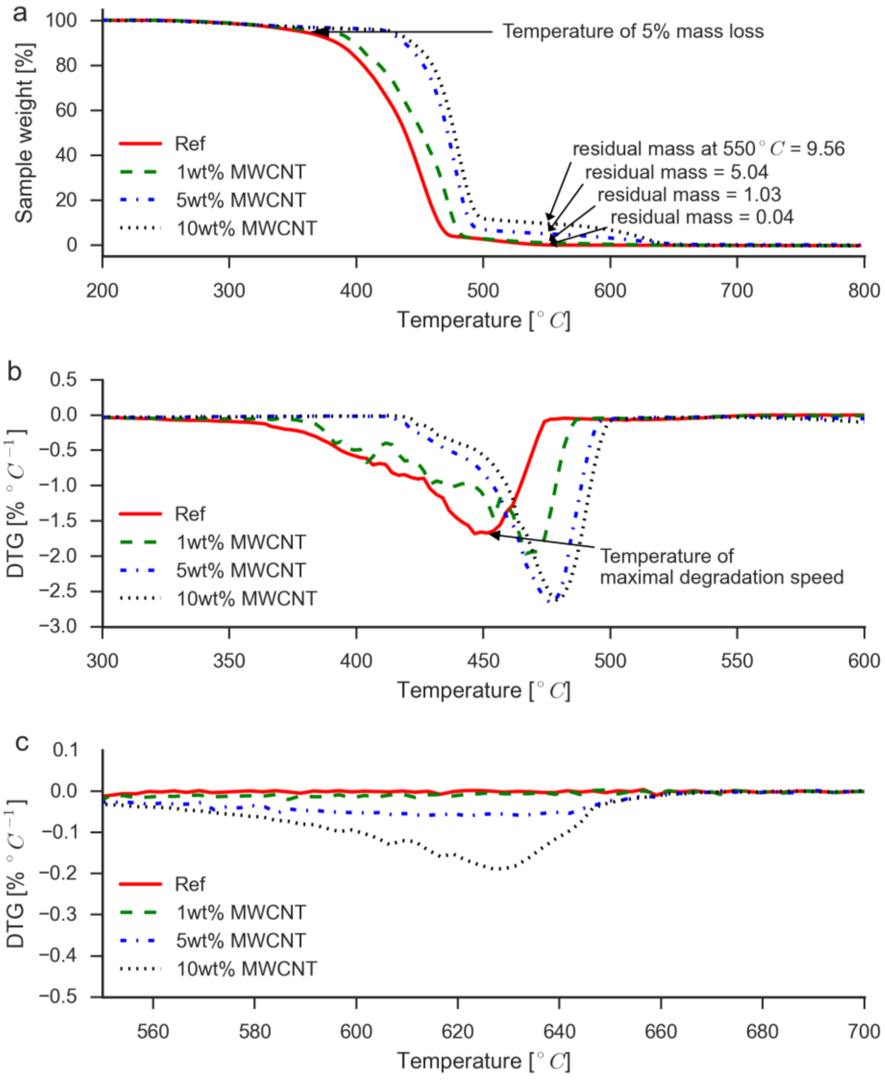

Figure 45: Thermal degradation in air (a) and corresponding first derivatives from 300 to 600 °C (b) and from 550 to 700 °C (c) of the Bio-PE-based composites, averaged from three TGA measurements.

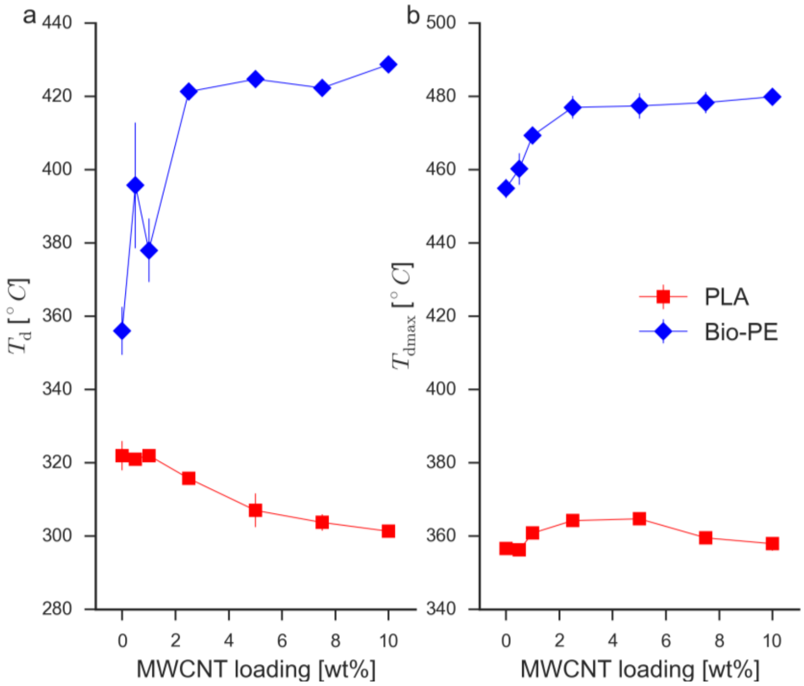

Figure 46: Temperature of 5% mass loss T_d (a) and of maximal degradation rate T_{dmax} (b) averaged from three TGA thermograms of the nanocomposites filled with 0, 0.5, 1, 2.5, 5, 7.5 and 10 wt% MWCNTs.

4.5 Crystallisation and thermal transitions of MWCNT-filled composites

As some of the composites studied were based on semi-crystalline polymers filled with nanofillers, the effect of the nanofillers on the polymer crystallinity and the thermal transition temperatures of these composites were further characterised. Variation in polymer crystallisation process is expected to change crystallinity and to modify the thermal behaviour of the composites. Therefore, the polymer crystallisation process as well as glass transition, melting and deflection behaviour of MWCNT-filled PLA 3251D and Bio-PE composites were further analysed.

4.5.1 Crystallisation process

Formation of crystalline regions in the nanocomposites exposed to slow and fast cooling was analysed by polarized light microscopy on films prepared from injection moulded composites. Figure 49 presents the images of the cuts prepared from neat polymer, and polymer mixed with 1 wt% MWCNTs. In the case of PLA 3251D no crystallisation was observed for the films when cooled quickly from 175 °C to 15 °C, which was classified as fast cooling. In contrast, the slow cooling rate of 1°C min^{-1} led to a higher degree of crystallisation. Comparing the slowly cooled samples containing neat PLA 3251D with those with 1 wt% of MWCNTs, it is apparent that in presence of nanotubes the spherulite sizes were strongly reduced (Figures 49a’ and b’). For neat Bio-PE no difference could be stated after slow and fast cooling. For Bio-PE filled with 1 wt% of MWCNT, no increase of the crystalline proportion over the amorphous part was observed between fast and slow cooling (Figure 50). However, for both polymer types, in the presence of 1 wt% MWCNTs, a slight change in the repartition of the black areas (corresponding to higher density in MWCNTs) was observed. The black areas were also more sharply distinguished from the transparent area than after fast cooling. This was more evident particularly for PLA 3251D-based composites.

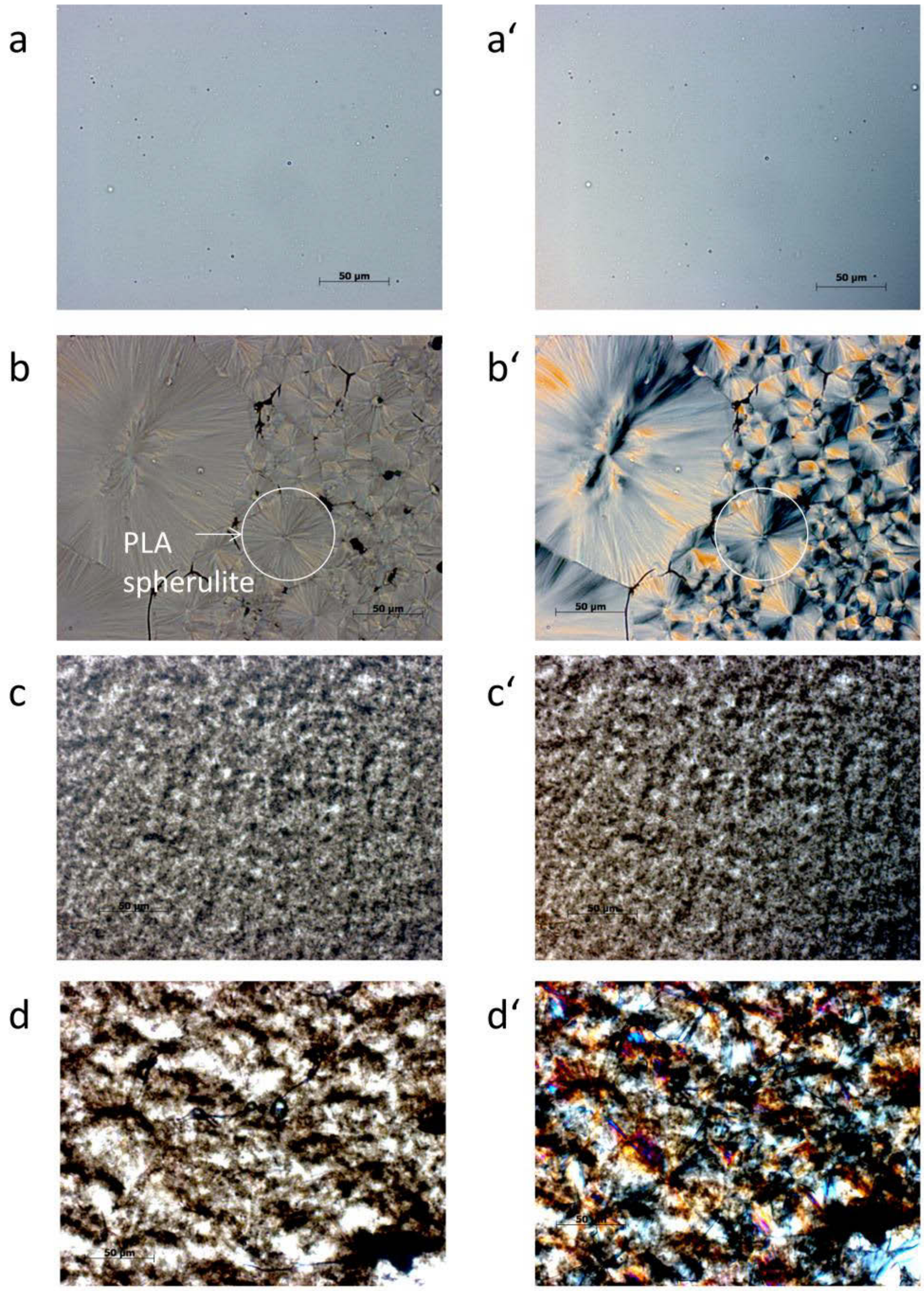

Figure 47: Microscopic analyses of crystalline structure of neat PLA 3251D films (a, a' and b, b') and PLA 3251D films with 1 wt% MWCNTs (c, c' and d, d'), exposed directly to a change in temperature from 175 °C to 15 °C (a, a' and c, c') and under cooling rate lower than 1 °C min^{-1}, (b, b' and d, d'). The image pairs correspond to observation under non-polarized light (x) and under polarized light (x'). One PLA 3251D spherulite was circled in white on b and b' pictures. All pictures were taken at the same magnification with the scale bar as shown in (a) corresponding to 50 µm.

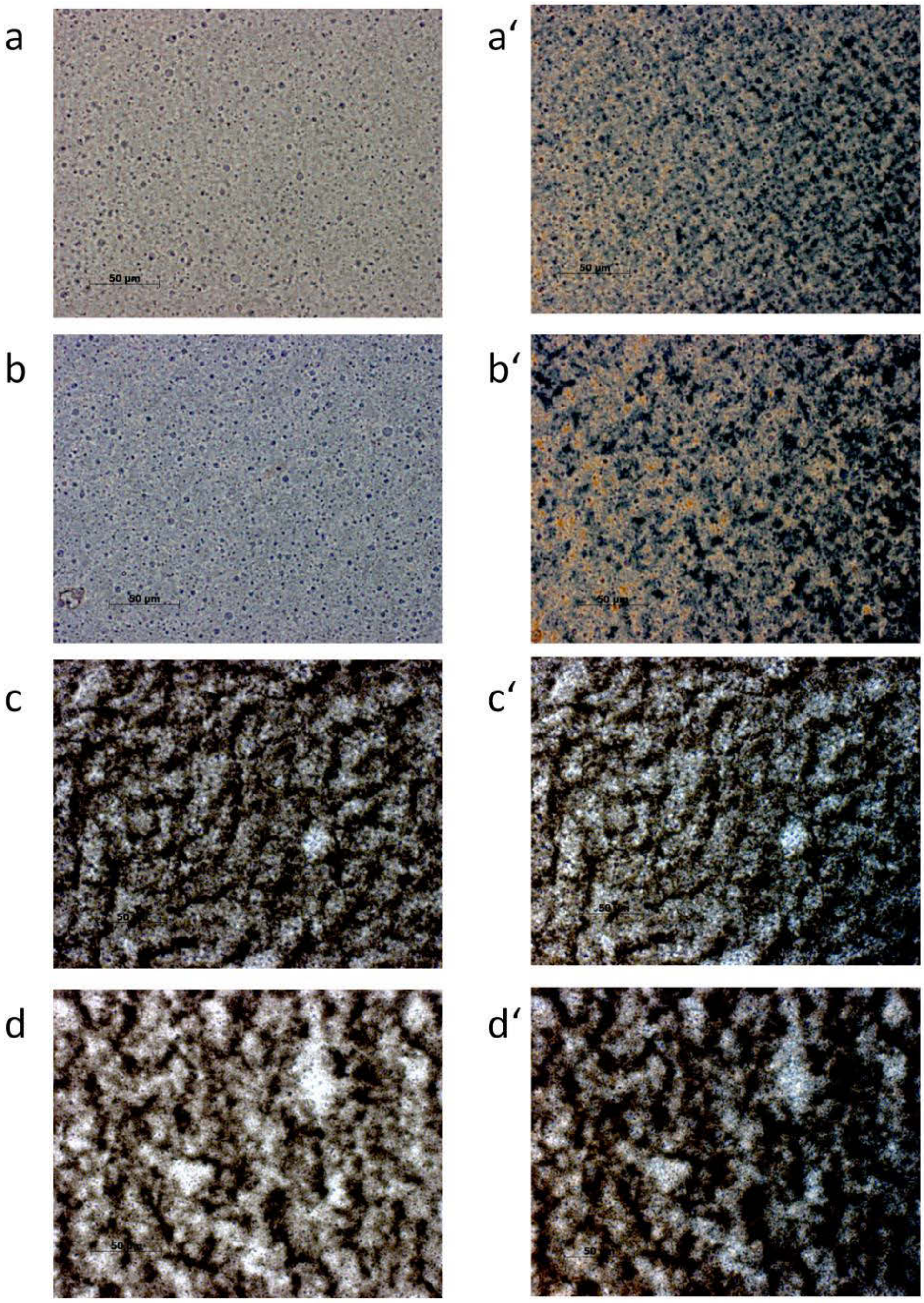

Figure 48: Microscopic analysis of crystalline structure of neat Bio-PE films (a, a’ and b, b’) and Bio-PE films with 1 wt% MWCNTs (c, c’ and d, d’), exposed directly from 175 °C to 15 °C (a, a’ and c, c’) and under cooling rate lower than 1 °C min^{-1}, (b, b’ and d, d’). The image pairs correspond to observation under non-polarized light (x) and under polarized light (x’). All pictures were taken at the same magnification with the scale bar as shown in (a) corresponding to 50 µm.

4.5.2 Crystallinity

DSC measurements were used to assess the effect of unmodified MWCNTs on the crystallinity of PLA 3251D and Bio-PE in the injection-moulded parts (Figure 51). It is generally accepted that the crystallinity derived from the first heating step observed in DSC analyses corresponds to the thermal state obtained after injection moulding, while the second heating step gives the crystallinity after a controlled cooling process [119,120].

The crystallinity measured during the first heating step for both polymer types was not significantly changed by the increased MWCNT loading (Kruskal-Wallis test, significance level of 0.05). On the contrary, the crystallinity of PLA 3251D-based composite measured during the second heating step was more than twice as high and was significantly increased with increasing MWCNT loading, reaching 57% with 10 wt% MWCNT loading. DSC curves suggested that for loadings higher than 2.5 wt% MWCNTs the onset of crystallisation shifted to increasingly higher temperatures during cooling step. Thus, it was concluded that directly after injection moulding any potential nucleation of the MWCNTs was hindered by the fast cooling of the melt in the mould, which was kept at 20 °C. In the case of Bio-PE-based composite, the neat polymer achieved 83% crystallinity after slow cooling (step 2) when compared to fast cooling (step 1, crystallinity of 71%). Regardless of cooling speed, the presence of MWCNTs at 1 wt% loading resulted in lower crystallinity but when further increasing MWCNT loadings (5 to 10 wt%) increase in crystallinity was detected. For slow cooling (step 2), the crystallinity reached with 10 wt% MWCNT loading was equal to that of the neat polymer (83%). At fast cooling (step 1), the crystallinity reached with 10 wt% MWCNT loading was slightly higher than the one with neat polymer (74% vs. 71%). The increase in crystallinity detected with 10 wt% MWCNTs at fast cooling speed (step 1), indicates that MWCNTs could nucleate the Bio-PE crystallisation, however they hinder the maximal crystallinity that can be reached with neat Bio-PE at slow cooling speed.

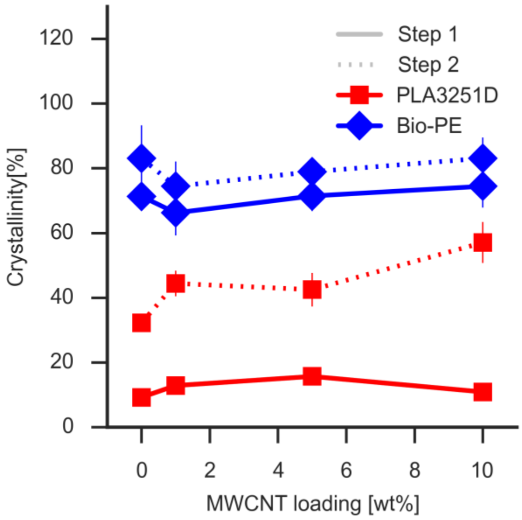

Figure 49: Crystallinity ratios of first and second heating steps (step 1 and step 2) for PLA 3251D and Bio-PE based nanocomposites.

As the crystallinity of the polymer matrix was shown to possibly affect the thermal transitions, glass transition, melting and deflection behaviours were characterised.

4.5.3 Glass transition and melting behaviours

Glass transition and melting behaviours were characterised by DSC by analysing glass transition temperature (for PLA 3251D-based samples, T_g), melting-onset ($T_{m\text{-onset}}$) and melting- peak ($T_{m\text{-peak}}$) temperatures and are presented with standard deviation values in Table 14. It appeared that the addition of MWCNTs did not induce significant modification in the glass transition temperature of PLA 3251D. A slight decrease in the $T_{m\text{-onset}}$ and $T_{m\text{-peak}}$ was detected for PLA 3251D when adding 10 wt% of MWCNT. No significant variation was observed in the Bio-PE composite melting behaviour.

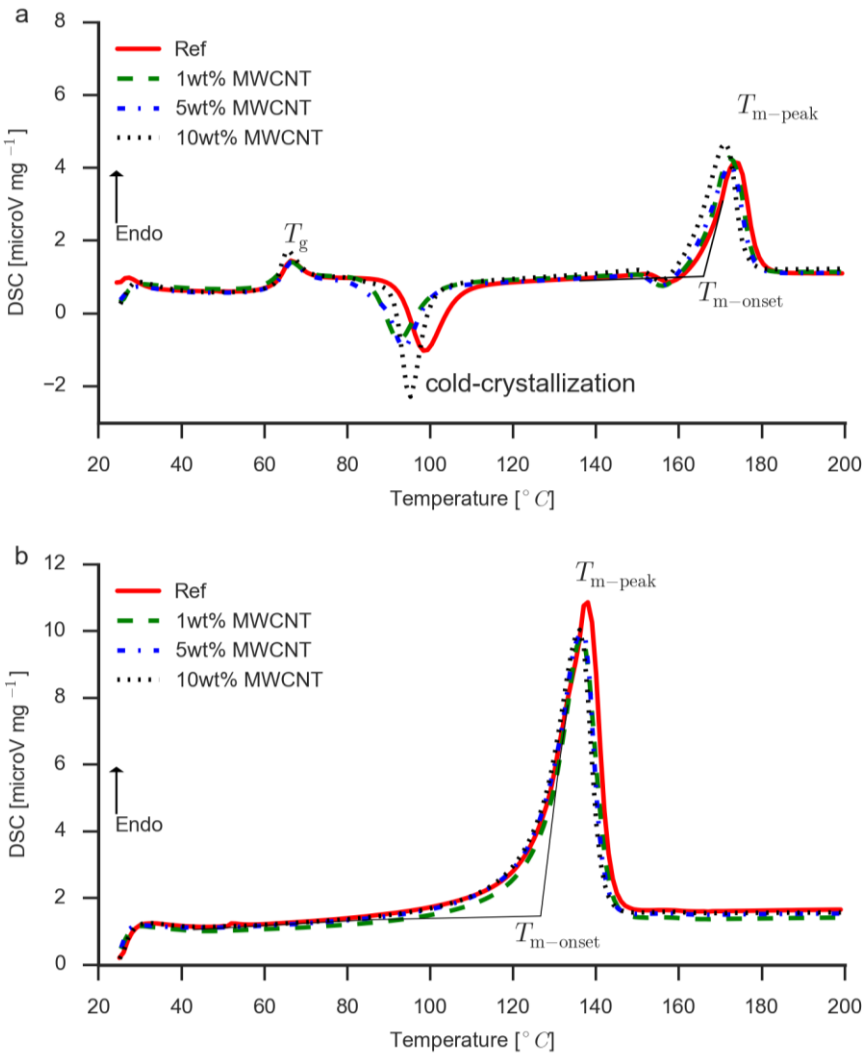

Figure 50: DSC thermograms of the PLA 3251D (a) and Bio-PE (b) based composites loaded with 1, 5 and 10 wt% of MWCNTs, averaged from three parallel measurements except for Bio-PE reference, which was based on two measurements.

Table 14: Characteristic temperatures measured by DSC on the bulk composites, where "n.m." denotes that the values were not measured.

Polymer	MWCNT loading [wt%]	Glass transition temperature [°C]	Onset melting temperature [°C]	Peak melting temperature [°C]
PLA 3251D	0	64.6 ± 0.5	165.8 ± 2.4	173.8 ± 0.8
	1	64.2 ± 0.4	165.2 ± 1.0	172.1 ± 0.8
	5	65.0 ± 0.5	164.1 ± 1.3	173.6 ± 1.0
	10	64.1 ± 0.3	162.0 ± 0.3	171.3 ± 0.6
Bio-PE	0[1]	n.m.	126.7 ± 0.6	137.7 ± 0.4
	1	n.m.	126.2 ± 3.1	137.2 ± 1.3
	5	n.m.	125.7 ± 2.7	136.6 ± 0.4
	10	n.m.	124.9 ± 1.8	136.2 ± 1.2

[1] The values were averaged from two measurements

4.5.4 Heat deflection behaviour

Heat deflection behaviour of MWCNT-filled thermoplastics was characterised through two methods: one bulk characterization method (HDT B) and one measurement method at sample surface in nanometric ranges (nanoTA). The purpose of the HDT characterization by HDT B method is to assess the temperature at which the composite will deform when exposed to a selected load. Therefore, the reasoning for increase in the HDT is expected to coincide with the reasons for deflection in the nanothermal ramping.

The heat deflection temperature of the PLA 3251D composites measured after HDT B method was not significantly changed with the addition of 0 to 10 wt% MWCNTs. On the contrary the Bio-PE-based samples experienced significant increases in the heat deflection temperature from 0 to 5 wt% and from 5 to 10 wt% MWCNT loading according to the Kruskal-Wallis statistical test with a significance level of 0.05 (Figure 53).

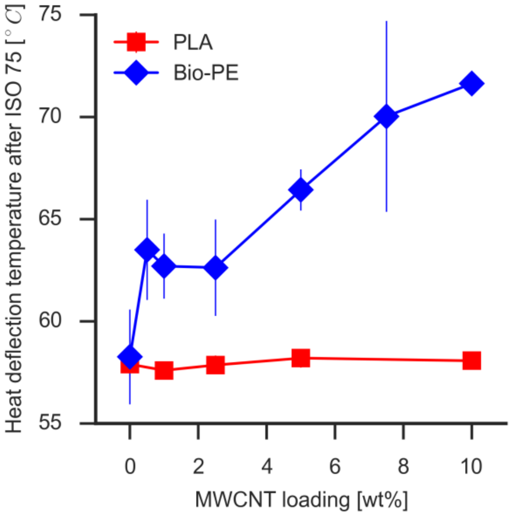

Figure 51: Heat deflection temperature determined after HDT B method from three samples.

Nanothermal measurements with AFM were first done at varying heating rates as presented in Figure 54. The indentation caused by the tip remaining after the measurement at the surface of the polymer can be seen on the topography images (as indicated by the blue arrow in Figure 54). The softening temperature obtained on neat PLA 3251D was found to be independent from the heating rate for the three heating rates tested. They all reflected a deflection temperature of 71 °C. The indentation size decreased when increasing the heating rate.

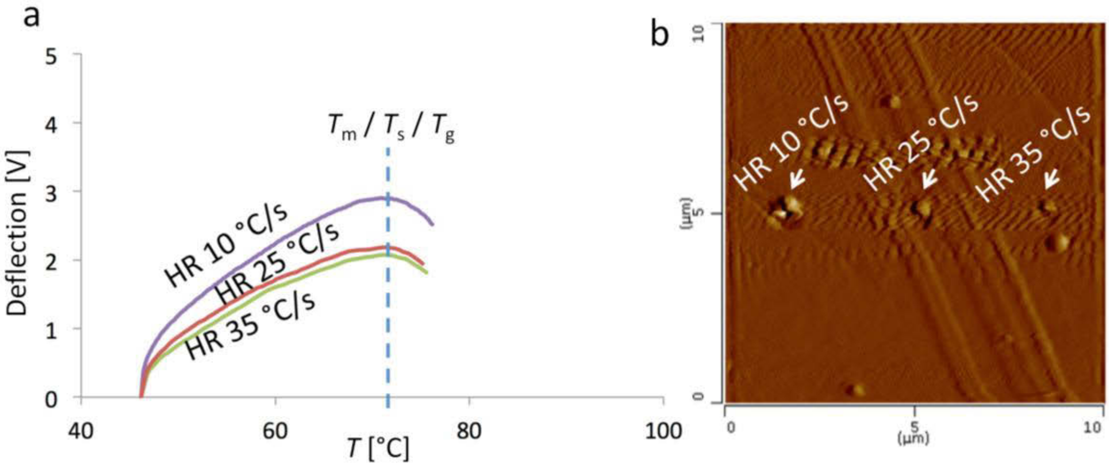

Figure 52: The effect of heating rate (HR) on the thermal ramp deflection vs. temperature (a) and the resulting indentation (b).

The nanothermal mappings performed along the imaging area were averaged for each of the composite and are presented in Figure 55 as the cantilever deflection versus temperature. The thermal ramps of neat PLA 3251D samples showed that the tip sinks to the composite around 71 °C (Figure 55a). As the filler loading increases to 1 wt% the melting temperature remains unchanged. However, the deflection of the cantilever, which can be measured from the initial slope of the curve, gets steeper. This indicates that prior to melting the composite undergoes thermal expansion. A further increase in the filler loading to 5 and 10 wt% resulted in a slightly decreasing thermal expansion compared to the 1 wt% loading. At the same time the melting temperature shifted to a higher temperature reaching ca. 83 °C with the 10 wt% loading.

The thermal ramping investigation for the Bio-PE composites is presented in Figure 55b. The softening temperature and thermal expansion of the neat polymer composite were considerably more pronounced than in the case of PLA 3251D. Inclusion of 1 wt% of the MWCNTs to the Bio-PE matrix caused a slight increase in the thermal expansion, similarly to the one observed for the PLA 3251D composite. This effect diminished with increasing loading to 5 and 10 wt%, whereas the melting point shifted towards higher temperatures. An increase of + 33.4 °C for Bio-PE and + 11.8 °C for PLA 3251D in the softening temperature was observed by addition of 10 wt% MWCNTs.

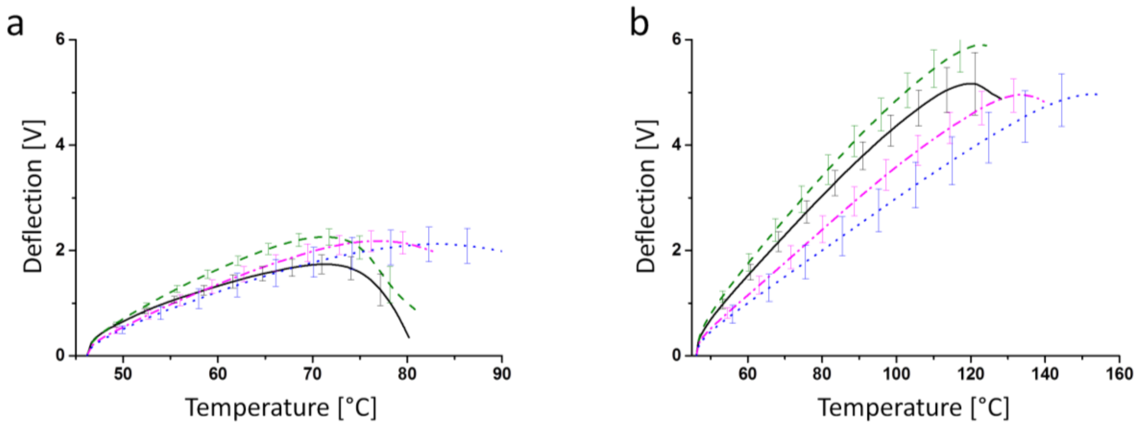

Figure 53: Nanothermal ramping of PLA 3251D (left) and Bio-PE (right) composites containing 0 (solid black line), 1 wt% (dashed green line), 5 wt% (dash-dotted purple line) and 10 wt% (dotted blue line) of MWCNTs.

In addition to the thermal ramping, the analysed surfaces were recorded with AFM before (Figures 56 and 57, left columns) and after (Figures 56 and 57, right columns) the thermal ramping. Prior to thermal ramping, the composite surfaces appeared smooth. Inclusion of 1 wt% loading of MWCNTs in PLA 3251D resulted in less distorted images. As the filler content was increased to 5 wt% and 10 wt% in PLA 3251D (Figures 56c and d, respectively) small features appeared that were deemed to be due to inclusion of the filler. After the thermal ramping, the indentations on all of the composites were observed (Figure 56, right column). Interestingly, the indentations with the 1 wt% addition appeared larger compared to the ones appearing with the higher filler loadings. It was suggested that this maximum is related to the maximum observed for thermal expansion at 1 wt% loading (Figure 55a).

Corresponding contact mode images of Bio-PE-based composites with 0 to 10 wt% MWCNT loading are presented in Figure 57. The filler incorporation is not as clearly detectable as in PLA 3251D. The increasing filler content did not cause apparent changes in the shape of the indentations with 1, 5 and 10 wt% filler loadings (Figure 57b and c, respectively). The width and depth of the indentation are reported in the annexe (A2).

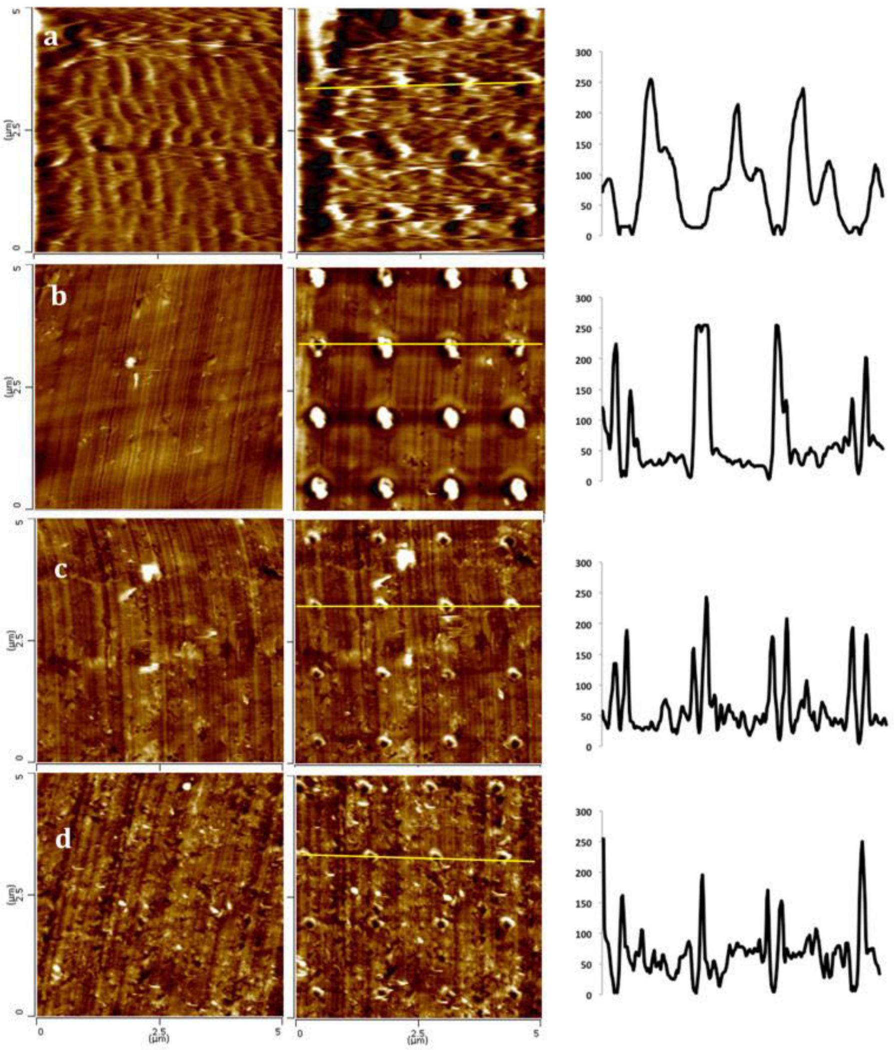

Figure 54: AFM contact mode imaging of the cross section of PLA 3251D-based composites with a) 0, b) 1, c) 5 and d) 10 wt% MWCNTs before (images in the left column) and after (images in the column in the middle) ten nanothermal measurements with the yellow line indicating the location of the profile that is presented in the graphs on the right column.

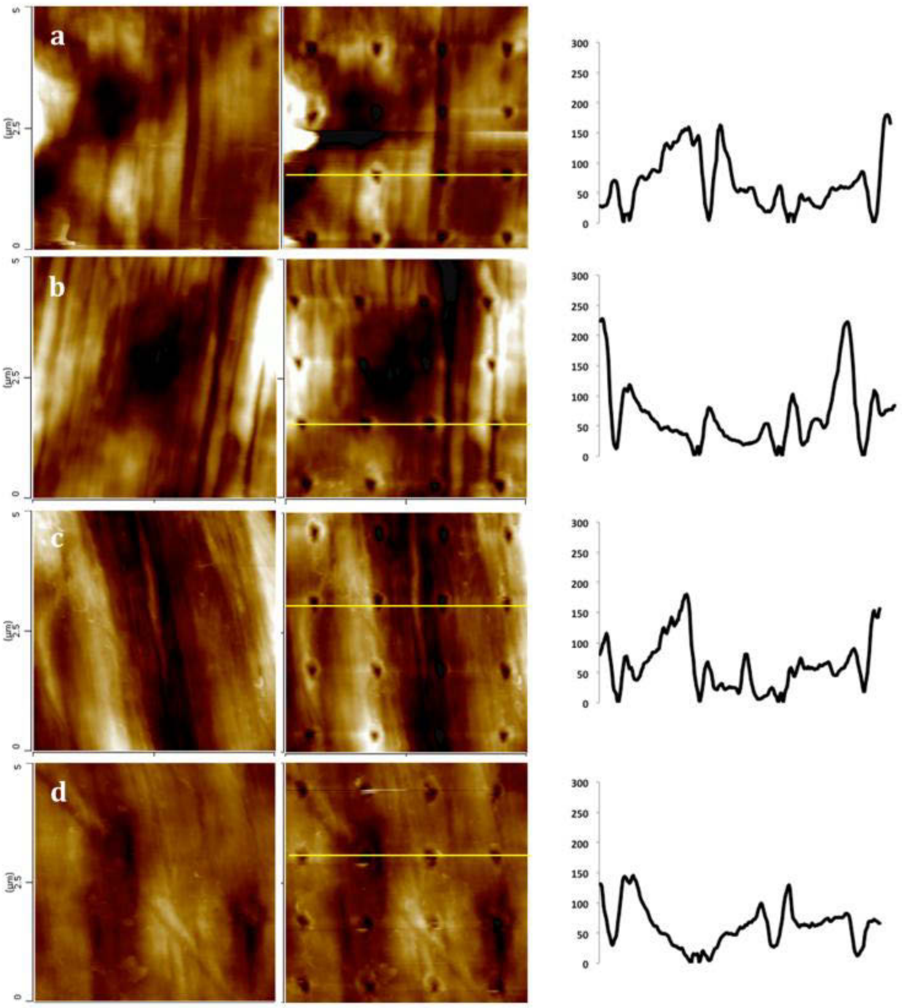

Figure 55: AFM contact mode imaging of the cross section of Bio-PE-based composites with a) 0, b) 1, c) 5 and d) 10 wt% MWCNTs before (images in the left column) and after (images in the column in the middle) 16 nanothermal measurements, with the yellow line indicating the location of the profile that is presented in the graphs in the right column.

Softening temperature determined by nanoTA increased with the increasing filler loading in both polymer types. The variation in softening temperature of the Bio-PE was observed to be higher than the one of PLA 3251D. NanoTA softening temperatures were graphed together with the glass transition and melting temperature derived from DSC measurements (Figure 59). Comparing all characteristic temperatures, it was concluded that the molecule movement probed by nanoTA was caused by glass transition for PLA 3251D, while for Bio-PE the melting of the material was probed.

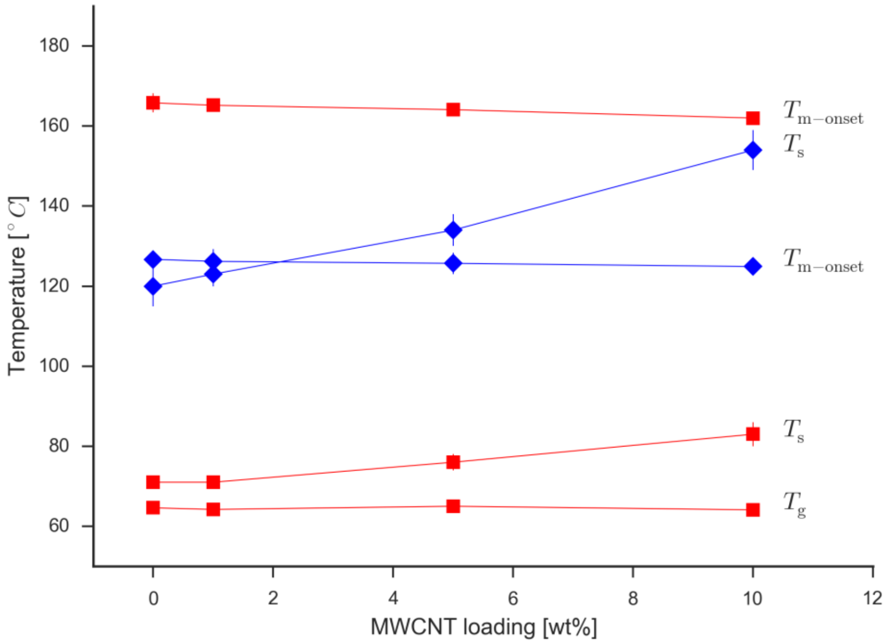

Figure 56: Softening, glass transition and melting temperatures of the composites loaded with 0, 1, 5 and 10 wt% MWCNTs (b), calculated from three measurements for each composite except for the softening temperatures, which were averaged from ten measurements with the nanothermal mode of AFM.

Nanothermal analyses gave thermal transition temperature for PLA 3251D and Bio-PE-based composites, which both increased with the MWCNT loading. This was different from the results found by HDT B. The higher slope in softening temperature detected by nanothermal ramping for Bio-PE than for PLA 3251D-based composites corresponded to the variation observed from HDT B measurements but in higher temperature ranges. A slight increase in softening temperature was detected for PLA 3251D-based composite but not with HDT B analysis. This can be explained by the fact that the nanoTA is done under much lower mechanical loading and the sample is heated only at the extremity of the probe by electrical current, whereas for HDT B, the entire composite is submerged in a heated oil bath. Thus, increase in temperature in one point of the sample can dissipate through the composite to the surrounding and retard deflection for nanoTA, which will not happen in HDT B characterization. In addition, for nanoTA, the deflection can be retarded due to the MWCNT electrical networking. Moreover, nanoTA indentation after thermal ramping varied dependent on the amount of MWCNTs present but also on the type of polymer used as basis. This will be further discussed in the discussion.

5 Discussion

Properties of thermoplastics filled with electrically-conductive solid fillers were found to strongly depend on the filler and polymer types and filler-polymer interaction but also on the composite structure. The filler distribution and dispersion obtained from extrusion followed by injection moulding as well as the effect of composite composition on the production process will be discussed in the first part of the discussion. In a second part, the effect of filler loading, type and of its interaction with the polymer in injection moulded composites on the composite electrical conductivity, mechanical behaviour, and thermal stability will be considered. In a last part, the effect of unmodified MWCNTs as nanofillers on the crystallisation of two semi-crystalline polymers (PLA 3251D and Bio-PE) after injection moulding will be discussed as well as their effect on composite thermal transitions and heat deflection behaviour as obtained from macro and nanometric scale analyses.

5.1 Filler distribution and dispersion in injection moulded composites

5.1.1 Composite structure and filler type

Homogeneous distribution and good-dispersion of the fillers in the composite are essential for the homogeneity and the optimization of the effect of the fillers on composite properties. Melt mixing by extrusion before injection moulding gave homogenous filler distribution for all composite type. Filler distribution anisotropy could have been further described by combining electrical conductivity local characterization with TEM imaging of samples slices, as done by Villmow et al.[26]. In their study they detected higher conductivity near the injection sprue and in the central area of the sample. More recently another conductivity measurement method giving information on filler distribution was reported by Planes et al.[121,122]. By measuring the local conductivity with four-point aligned probes (needles) in the two orthogonal directions, they described the anisotropy of compressed sheets filled with a mixture of carbonaceous fillers [121]. In the present work, electrical conductivity characterization by ring electrodes suggested anisotropy in the filler distribution; however the anisotropy could not be precisely described.

CF and RCF were found to be well dispersed in the composites, while MWCNT dispersion level and orientation varied with the MWCNT loading in PLA 3251D. The alignment observed for low MWCNT loading in PLA 3251D was similar to the one reported by Ajayan et al.[123]. It could be explained by a dragging of the MWCNTs by the microtome blade during cutting. However, it could also be due to the high shearing forces applied during extrusion, as reported by Bauhofer and Kovacs [87]. As no alignment was detected by AFM at higher loading (5 and 10 wt% MWCNTs), it suggested that to some degree an entanglement of the MWCNTs within the samples, prevented eventual alignment of mobile MWCNTs on cut surfaces, as assumed with the 1 wt% samples. In their study Pegel et al.[24] suggested that MWCNTs reformed agglomerates during processing. They called this phenomenon: “a secondary agglomeration”. As microscopic analyses were done only after injection moulding, no conclusion could be stated considering potential second agglomeration during injection moulding.

No difference in filler-polymer interaction was detected by microscopy between the composites filled with carbon fibres and with recycled carbon fibres having surface sizing (CF MLD). CF MLD filled PLA 3251D samples, presented less pullouts than CF.LS MLD-filled PLA 3251D composites (Figure 25). Concerning the MWCNTs-filled composites, the nanotubes appeared distinct from the polymer matrix for PLA 3251D but not for Bio-PE on AFM imaging (Figures 27 and 28). This was related to differentiating filler-polymer interaction. Yoon et al.[77] described that the boundary between the PLA-grafted

MWCNTs and the PLA matrix was less discernible on the scanning electron microscopy of fractured surface, compared to unmodified MWCNTs. They explained this by improved wrapping of the modified MWCNTs by the polymer matrix [77]. The clear delimitation of the MWCNTs in the current study suggests a restricted interaction between the unmodified MWCNTs and the PLA matrix, resulting from the difference in their surface energies. This interaction specificity of the nanotubes was already considered in the studies of Wu et al.[91] and Wang et al.[124] to create connections between two immiscible polymer types in a blend. The effect of changing the filler dimensions or the polymer type under constant processing parameters on the production process was further studied through the analysis of melt behaviour during processing.

5.1.2 Effect of the filler type on the melt behaviour

In general melt behaviour analyses reflected increases in melt viscosity with increasing filler loading (Figures 29; 31 and 32). However, variations were found in melt behaviour between the composites independent of the selected processing parameters.

Increase in the melt temperature independently from the heating system was detected in presence of one type of polyurethane sized CF (CFC1) and also in the production of the MWCNT masterbatches. This was explained by an increase in the friction forces due to the filler as reported by Sykacek et al.[18]. As thermoplastics become less viscous when the temperature is increased in the melting ranges, it explains the simultaneous decrease in melt pressure. On the contrary, the melt temperature decreased when adding wood fibres to polymer filled with carbon-based fillers. This is explained by the low thermal conductivity of wood fibres and their lack of interaction with the polymer matrix. It explains as well the simultaneous increase in melt pressure and in machine load. Variations in melt pressure and machine load detected during extrusion between the productions with 10 wt% of CF having different surface sizing in PLA 3051D were associated to the carbon fibre sizing. It suggested that better interaction decreased the melt viscosity. Injection pressure generally increased with the filler loading as well showing increase in melt viscosity. Moreover, the dosing time, expected to predict filler packing in the matrix in case of good polymer-filler interaction, did not give information in agreement with the conclusion obtained during extrusion on melt viscosity. Therefore, no indication was obtained on CF sizing giving better compatibility with PLA or PHBV.

From the observations made on the microscopic images combined with melt behaviour observations, better filler-polymer interactions were expected for PLA-based composites filled with sized recycled carbon fibres compared to recycled carbon fibres from which the sizing had been removed (CF MLD vs. CF LS MLD). Composite with better filler-polymer interactions are expected to induce higher increases in mechanical properties and thermal stability. However, the relation between filler-polymer interaction quality and composite electrical conductivities is not so evident.

5.2 Composite main electrical, mechanical and thermal properties

In this second part the effect of filler loading, type and interaction with the polymer on the composite main properties, in particular electrical conductivity, tensile behaviour, impact strength property, and thermal stability is discussed.

5.2.1 Effect of filler loading

The electrical conductivity observed with all tested carbon-based filler types increased with the filler loading following a typical conductivity increase profile (Figure 38). Electrical conductivities obtained from four-point and ring electrode methods were used as reference for comparison of the present results with literature data. Variations between MWCNT-filled composites were more particularly detailed here since MWCNT dispersion is generally more problematic than the one of CF and RCF. Table 15 lists data from studies dealing with unmodified and probably entangled MWCNTs in thermoplastics [9,28,38,46,55–57,87,125–130]. The present results are within the range with the studies presenting unmodified MWCNT-filled thermoplastic polymers, all presenting high conductivities compared to MWCNT-filled nanocomposites (Figure 59) [24,30,57,125–128,131,132].

Table 15: Variation in electrical conductivity properties of thermoplastic polymers filled with electrically conductive fillers from the literature.

Formulation			Methods		Results			Ref.
Polymer		Filler type	Production of the samples	Measurement method	Percolation threshold [wt%]	Maximal content tested [wt%]	Maximal conductivity [S m^{-1}]	
Type	Conductivity [S/m]							
PLA	10^{-14}	MWCNT	Bars after melt mixing and injection moulding	Ring electrode and four-point DIN EN ISO 3915(10N) Parallel to the injection flow	<2.5	10	51.7	Current work
Bio-PE	10^{-14}	MWCNT	Bars after melt mixing and injection moulding	Ring electrodes and four-point DIN EN ISO 3915(10N) Parallel to the injection flow	<5	10	2.16	Current work
PLA	10^{-14}	MWCNT	**Sheets after ultrasonication in chloroforme and evaporation**	**Surface** four-point method	0-2.5	10	40	[9]
PLA	10^{-14}	MWCNT	Plates after melt mixing and **compression moulding**	Volume conductivity **two-point** method	0.5	3	1	[57]
PLA	10^{-14}	**PLA-grafted MWCNT**	Plates after melt mixing and **compression moulding**	Volume conductivity **two-point** method	0.5	3	ca. 0.032	[57]
PC	**10^{-17}**	MWCNT	Bars from melt mixing and injection moulding	-	1	5	3	[28]
PC	**10^{-17}**	MWCNT	**Strands extruded** after melt mixing	-	1	5	71	[28]

PC	**~10^{-16}**	**SWCNT**	Plates from melt mixing and **compression** moulding	DIN EN ISO 3915 **Perpendicular to pressing**	0.5 -2 (ring electrodes IEC 93:1980)	10	10^{-1} (to 10 if precoagulation)	[55]
PC	**~10^{-15}**	MWCNT	Sheets after melt mixing and **compression** moulding	Volumetric **two-point** method **In the compression direction**	1	12.5	5 (at 3 wt% loading)	[125]
PC	**10^{-14}**	MWCNT	Sheets after melt mixing and **compression** moulding	Volumetric **two-point** method **In the compression direction**	1.44	5	2	[126]
PC	**10^{-11}**	MWCNT	Bars after melt mixing and **compression** moulding	Volumetric **two-point** method **Perpendicular to the compression direction**	2	15	10	[127]
PP	**10^{-15}**	**CB and acetylene CB (aCB)**	Bars cut from plates after melt mixing and **compression** moulding	Volumetric **two-point** method **In the compression direction**	CB: 5 (2.6 vol%) aCB: 9,8 (5.3 vol%)	49.5 (30 vol%)	CB: 8 aCB: 11	[38]
PP	**10^{-9}**	MWCNT	Melt mixing	-	0.02 (0.01 vol%)	0.3 (0.15 vol%)	10^{-1}	[129]
PP	**10^{-8}**	MWCNT	Plates after melt mixing and **compression** moulding	Volumetric **two-point** method **in the compression direction**	0.44 (0.22 vol%)	9 (4.5 vol%)	2	[128]
PA 6	**~10^{-13}**	MWCNT	Bars after melt mixing and injection moulding	Volumetric **two-point** method **perpendicular** to the injection direction	3-7	16	10	[132]
PA 6	**~10^{-12}**	MWCNT	Sheets after melt mixing followed by **compression** moulding	-	2.5	4	10^{-1}	[130]
PA 6	**10^{-14}**	**Lamellar copper powder**	Bars from plates after extrusion and Injection moulding	Four-point DIN EN ISO 3915 parallel to the injection flow	77-81 (30-40 vol%)	81 (40 vol%)	730	[56]

PLA: polylactic acid, PC: polycarbonate, PP: polypropylene and PA6: polyamide

wt% were calculated when necessary from vol% using polypropylene density of 0.9, polyamide density of 1.1, CB and aCB densities of 1.8, MWCNT density of 1.7 and lamellar copper powder (type Cubrotec 5000 from Schlenk AG) density of 1.

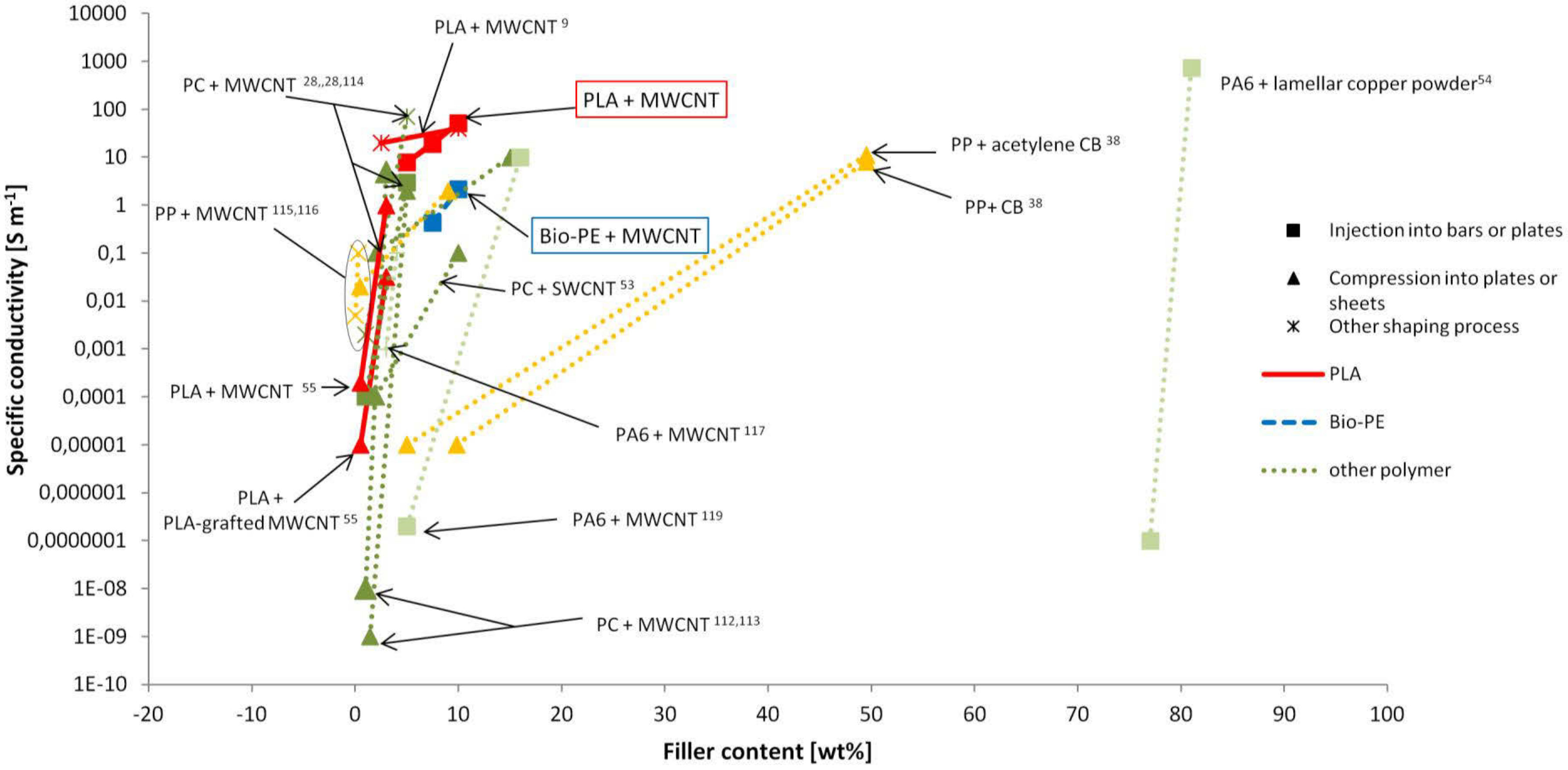

Figure 57: Comparison of the present conductivity results (boxed legends) with conductivities of composites reported in the literature.

Variations in tensile strength were proportional to the filler loading (Figures 40 and 41). It increased with most of the carbon-based filler types tested. Carbon-based filler loading did not alter composite impact strength except when the neat polymer matrix used had a very high impact strength (Figure 45).

As the thermal stability was characterised only for MWCNT-filled composites, the discussion concerning thermal stability properties is limited to this group of composites. Two different variation tendencies were found depending on the polymer type considered. The thermal degradation started at lower temperatures with the increasing MWCNT loading in PLA, whereas it increased in Bio-PE. Thus, it was suggested that the filler type and the filler-polymer interaction were strongly altering the composite thermal stability. Therefore, the effect of MWCNTs on composite thermal stability is further detailed in the discussion part on filler-polymer interaction.

5.2.2 Effect of composite structure

The conductivity of the samples produced in the present work was found to be 30% higher than the conductivity measured on PLA films filled with 10 wt% MWCNTs prepared by ultrasonication; by Moon et al.[9] This mixing method is usually described as a very good method to disperse MWCNTs, and obtain random orientation of the filler after solvent evaporation [25]. Similarly, another study on PLA-filled with unmodified MWCNTs processed by compression moulding presented by Novais et al.[57] reported conductivities significantly lower than the results of the current work. However, these lower values might also be due to the fact that they used a two-point measurement method to characterise electrical conductivity. Hornbostel et al.[55] reported comparable percolation threshold but lower conductivity than the current results when analysing single-wall carbon nanotube (SWCNT)-filled polycarbonate (PC) films. This may be due to the notorious difficulty of dispersing SWCNTs due to their high degree of entanglement as compared to MWCNTs. In addition to MWCNT dispersion, MWCNT orientation was found to affect the electrical conductivity. Indeed, Bauhofer and Kovacs [87] reported that lower electrical conductivity found for extruded materials in comparison to other dispersion method were probably due to the high shearing forces applied during the process inducing an excessive alignment of the nanotubes at low MWCNT loadings [87]. In their study, Mack et al.[28] compared the electrical conductivity of extruded strands to the one of injection moulded samples made of the same material (PC filled with MWCNTs). They found much lower conductivities for the injection moulded parts and explained this difference by the flow alignment of the filler and the absence of skin layer in the extruded samples. As the MWCNTs were aligned in the direction of the current flow applied during conductivity measurement, higher conductivity was obtained. In a study from Villmow et al.[26] on injection moulded MWCNT-filled PC plates, the composites produced at lower injection velocity and higher melt temperature, presented worse MWCNT dispersion and less preferential orientation in the skin layer as detected by TEM and gave better volume conductivities. This was in agreement with the observations reported by Pegel et al.[24], Alig et al.[108] and Combessis et al.[61] showing that the presence of MWCNT agglomerates in the composite induced an increase in electrical conductivity and a decrease in percolation threshold for filler loadings near the percolation threshold. In the present study conductivity was measured in the direction parallel to the flow during injection and directly on injection moulded bars. No MWCNT agglomerates were detected by SEM and by AFM for PLA 3251D-based composites.

These comparisons indicate that electrical conductivity values can vary depending on filler entanglement, polymer type but also on processing and measurement methods. Based on a comparison of 150 types of polymer-CNT composites, Bauhofer and Kovacs [87] suggested that the electrical percolation and the maximum conductivities are more influenced by the polymer type and the dispersion method than by the CNT type and the production method.

5.2.3 Effect of filler aspect ratio

Increase in filler aspect ratio was found to decrease electrical conductivity percolation threshold but no variation in the maximal conductivity values was obtained. Electrical conductivities of MWCNT-filled composites from the present work were compared with the results on conductive filler with lower aspect ratio and characterised by four-point method [38,56]. Both reported conductivities far away from the ranges presented by the CNT-filled composites (Figure 58). The carbon black-filled PP composites prepared by compression moulding presented percolation threshold around 5 and 10 wt% [38]. This was higher than in presence of CNTs but lower than with CF or copper powder (77 wt%) [56]. The copper powder-filled PA6 composites prepared by injection moulding reached higher conductivity than the one presented as upper limit for studies on CNT-filled polymer. This was explained by the better electrical conductivity properties of metallic fillers as copper regarding carbon-based fillers (as CNTs and CB but also CF).

Electrical percolation threshold obtained from Nan's law predicted low percolation thresholds when compared to the experimental results presented in the literature. They also suggested that in the present study, carbon fibres of CFB1 type should give lower percolation threshold than MWCNT filled composites. This was not fitting with experimental results and suggested that the aspect ratio used in the calculation for the carbon fibres and the MWCNT do not correspond to the dimensions of the fillers in the material after processing or that other parameters such as processing conditions and filler orientation need to be considered in percolation threshold prediction as indicated by Combessis et al.[61].

As expected, increasing filler aspect ratio gave increasing improvement in tensile strength, and Young's modulus (Figure 41). Filler aspect ratio was found to emphasize the importance of the variations obtained when increasing filler loading. No change in maximal electrical conductivity and in impact strength was found with changing the filler dimensions in PLA.

5.2.4 Effect of filler-polymer interaction

Electrical conductivity changed depending on the filler-polymer combination. These results show that the better filler-polymer interaction expected from melt behaviour analyses or from chemical miscibility rules did not always result in higher electrical conductivity. In general, when comparing the conductivity of unmodified MWCNT-filled polycarbonate presented in Table 15, lower values were obtained than with unmodified MWCNT-filled PLA. This was explained by the higher affinity and thereby efficient embedment of MWCNTs in polycarbonate, which has a lower electrical conductivity than PLA. Both effects would increase the tube/tube contact resistance. Novais et al.[57] observed similar percolation threshold but much lower conductivities for PLA-grafted MWCNTs compared to unmodified MWCNTs in PLA. These results suggested that for MWCNTs, better filler wetting by the polymer reduced the quality of the tube/tube contacts and therefore the conductivity of the network.

Adhesion between the two components can induce dramatic tensile strength improvements [77]. This is typically obtained using polymers giving a low filler-polymer interfacial tension and/or by geometrical entanglement [37]. In the present study, composite tensile strengths were improved when using any kind of sizing on CF or RCF. Even if no clear difference in pullout level was observed by microscopy between the different sizing, tensile strength varied depending on the sizing. Similarly, the decrease in tensile strength observed when adding wood fibres to PLA 3251D in presence of CF MLD or CFB1 was explained by the lack of interaction between the cubic wood fibres and the polymer matrix. No explanation was found for the variation in mechanical behaviour when adding wood fibres to CF.LS MLD-filled PLA 3251D. Results obtained for CF-filled composites showed better filler-polymer interaction for polyamide and polyurethane CF and were related to better electrical conductivity compared to polyester sized CF. In the case of RCF, filler polymer interaction was enhanced for the sized fibres and was as well related to improved electrical conductivity.

However, for MWCNTs, opposite relation was observed, better electrical conductivities were obtained for the worst filler polymer interaction tested. In the literature, non-polar polymers such as polypropylene (PP) have been reported to wet more efficiently the unmodified MWCNTs, which have low polarity and surface tension, than polar polymers as polyethylene glycol (PEG) [34]. As no modification of the MWCNT surface was performed, the interaction between MWCNTs and the polymer matrix was supposed to be weak [77,99]. The strong decrease in tensile strength observed when adding MWCNTs to PLA 3251D reflected the poor interaction between MWCNTs and PLA 3251D as already observed by e.g. Yoon et al.[77]. Novais et al.[57] found an increase in tensile strength of hot-pressed panels when adding 0.5 wt% of unmodified MWCNTs to PLA, but a decrease in tensile strength occurred with 1 wt%, compared to the neat polymer. Andrews et al.[47] studied the effect of unmodified MWCNTs on polystyrene films and observed a tensile strength decrease up to 55%, when 5 vol% (approximately 7.5 wt% for polystyrene density of 1.04 and MWCNT density of 1.7) of MWCNTs were added. They explained the initial decrease by the poor interaction between the MWCNTs and the polymer and the presence of defects in MWCNT structure. However, between 5 to 15 vol% (7 to 22 wt%) MWCNTs, the tensile strength increased until it reached the value of neat polystyrene. This was explained by a bridging effect of clustered MWCNTs, which retarded the opening of cracks. Such behaviour was not observed for PLA in the present study.

On the contrary, the addition of MWCNTs to Bio-PE increased the tensile strength (Figures 39 and 41). For 5 wt% MWCNTs in Bio-PE, the tensile strength increased by 17% and Young's modulus by 26% which is comparable to respectively increases 12% and 26% for a study made on HDPE films reinforced with unmodified MWCNTs produced by melt extrusion [99,133]. This demonstrates the importance of filler-polymer interaction on composite mechanical properties. This is also in agreement with the observation on the AFM topographic images, in which the MWCNTs are clearly distinct from the PLA 3251D polymer matrix opposed to Bio-PE in which they are hardly apparent (Figures 27 and 28). Additionally, the less distorted images observed by AFM when adding 1 wt% MWCNT loading in PLA 3251D was probably due to improved rigidity of the composite and concords with the increase in Young's modulus observed for MWCNT-filled PLA 3251D composites. The relatively low improvement observed by comparing experimental data to Halpin-Tsai model suggests that MWCNT-Bio-PE interaction was not perfect or MWCNTs were curved and not ideally involved in reinforcing composite mechanical properties.

When considering the impact strength of MWCNT-filled composite, MWCNTs were reported to modify the impact strength of the composites in various ways: Prashanta et al.[134] observed a decrease in unnotched Charpy impact strength and a slight increase in the notched Charpy impact strength when adding MWCNTs. They concluded that MWCNTs limit crack propagation in polypropylene by bridging, while the aggregates support crack initiation. Contrarily, Mack et al.[28] measured a decrease in notched impact strength when the loading of unmodified MWCNTs added to polycarbonate was increased [28]. From these studies it seems likely that the increased impact strength observed between 0 and 5 wt% MWCNT loadings in Bio-PE results from the bridging effect.

Different variations in T_{d} and T_{dmax} were detected for the PLA 3251D and the Bio-PE composites when adding MWCNTs. In the literature, many studies reported an improved thermal stability (+10 to +30 °C) when adding MWCNTs to PLA compared to the neat polymer [9,10,135]. However, such improvement depended on the amount of MWCNTs added and concerned different phases of the degradation. In the case of PLA, thermal stability change was reported when unmodified MWCNT loading varied (Table 16). Moon et al.[9] used unmodified MWCNTs with poly(L-lactic acid) (PLLA) and observed increases of 10°C to 20°C when comparing the temperature of 10 wt% mass loss of composites filled with 3-10 wt% MWCNTs to the neat polymer. Krul et al.[10] reported an increased thermo-oxidative stability when adding MWCNTs into poly(D,L-lactic acid) through solution casting for loadings between 0.02 and 0.4 wt%. Maximum stabilization was found at a loading of 0.2 wt% MWCNTs. Kim et al.[135] observed a T_d increase of 29°C when adding 2 wt% of unmodified MWCNTs to PLLA and of 11 °C for the temperature of 50% mass loss ($T_{50\%}$). Thus, in PLA 3251D-based composites, the maximum in T_{dmax} observed for the loadings from 1 to 5 wt% MWCNTs was related to a possible increase in composite thermal conductivity from 2.5 wt% MWCNT loading due to the formation of an electrical conductive network. It is suggested that below the electrical percolation threshold, the MWCNTs present at the periphery of the sample can protect the underlying material from degradation and dissipate the heat to the surrounding air. Above the percolation threshold, i.e. between 2.5 and 5 wt% MWCNTs in PLA 3251D, this effect is balanced by the increased conduction of the heat through the entire sample. With 10 wt% MWCNTs, the T_{dmax} is equivalent to the T_{dmax} of the neat polymer.

Table 16: Variation in the temperatures characteristic of thermal degradation for MWCNT-filled PLA composites, as presented in the literature.

Polymer	MWCNT type	Loading [wt%]	Variation in thermal degradation	Ref.
Poly(L-lactic acid)	Unmodified	0 to 10	Temperature at 10 wt% mass loss +10 to +20 °C (for 3.5 and 10 wt% MWCNT) No precision concerning the peak of degradation	[9]
Poly(D,L-lactic acid)	Unmodified	0.02 to 0.4	+20 °C from neat polymer to 0.02 wt% MWCNT and decrease at higher loading	[10]
Poly(L-lactic acid)	PLA-grafted	2	+25 °C for T_d and +18.6 °C for temperature at 50 wt% mass loss	[135]
Poly(L-lactic acid)	Unmodified	2	+28.7 °C for T_d and +11.2 °C for temperature at 50 wt% mass loss	[135]
PLA	Unmodified	0.5 to 7	No variation in the T_d and +10 °C for T_{dmax} at 5 wt%	[91]
PLA	Modified (carboxyled or hydroxyled)	0.5 to 7	No variation in the T_d +10 °C for T_{dmax} with 5 wt% of carboxyled MWCNT and around -5 °C for $Tdmax$ with 5 wt% of hydroxyled MWCNT.	[91]

The thermal analysis was measured under air and was therefore for PLA 3251D directly compared to the thermal analysis made under N_2 where no oxidation takes place. However, this is not the case for polyethylene. Kodjie et al.[116] showed in their study the progressive oxidation of the polyethylene under air. By adding up to 1 wt% of unmodified single wall carbon nanotube (SWCNT), they found increases in the T_d and T_{dmax} and explained these enhancements by the formation of radical scavenging SWCNT network. Kanagaraj et al.[42] reported that adding between 0.11 and 0.44 vol% (respectively 0.19 and 0.8 wt% for HDPE density of 0.95 and MWCNT density of 1.7) of modified MWCNTs in HDPE induced a decrease in T_d but no significant variation in T_{dmax}. This was explained by the early degradation of carbonaceous residues on the MWCNTs or impurities.

Bocchini et al.[136] and Barus et al.[137] studied the effect of unmodified MWCNTs on the thermo-oxidative degradation of low density polyethylene. Bocchini et al.[136] stated that the degradation took place in two-steps. The start of degradation was not changed but the completion of the first step of degradation was shifted to temperatures higher than the temperature of neat polymer volatilization. Bocchini et al.[136] and Barus et al.[137], both, reported an increase in T_{dmax}, and suggested to be due to the activation of polyaromatic carbon char formation from the polyethylene decomposition by MWCNTs (probably by oxidative dehydrogenation). The char layer prevented the passage of oxygen to the underlying material and the release of polymer volatiles. This could explain as well the thermal stability behaviour of the Bio-PE-based composites presented in Figure 48.

To further understand the importance of filler-polymer interaction on this property, a comparison with literature data on modified and unmodified MWCNT-filled composites was done. In their study Schartel et al.[93] suggested that unmodified MWCNTs are acting as an inert material in polycarbonate because they observed a decrease in both the temperature of degradation start, taken at 5 wt% loss (T_{d}) and in T_{dmax} with increasing the MWCNT loading. The authors suggested that this could be due to a decrease in polycarbonate molecular weight, and due to crosslinking or impurities in the MWCNTs. The low filler-polymer interaction and the possible presence of impurities in the MWCNTs could also explain the decrease of the onset degradation temperature observed for the PLA 3251D-based composites in the current study. In a comparable study on EVA-based nanocomposite prepared by solution casting, George et al.[138] reported an increase of 13 °C in temperature showing the maximal degradation speed (T_{dmax}), when the unmodified MWCNTs loading was raised from 1 to 4 wt%. This increase was the same as obtained when using 1 wt% of silane modified MWCNTs instead of unmodified MWCNTs. They compared it to the thermal conductivity of the composites and observed that the thermal conductivity increase obtained with 1 wt% of silane modified MWCNTs was much lower than the one obtained with 4 wt% unmodified MWCNTs [138]. This shows that the effect of MWCNT addition on T_{dmax} was not proportionally related to the effect on thermal conductivity of the sample.

In the light of the aforementioned studies, it appears that the MWCNTs dispersed in the Bio-PE composites improve thermal stability due to (1) delay in the release of degradation gases, (2) to the polymer interacting chemically with the filler at the interface, and (3) increased thermal conductivity that dissipates heat. In the case of MWCNT, an improvement in the polymer crystallisation process is also expected as it has been reported in the literature that MWCNTs could act as a nucleator during the cooling of the composite. Meaning that MWCNTs presence can help the crystallisation of the polymer to start at higher temperatures and induce the formation of smaller spherulites in the polymer matrix than with neat polymer This can change the composite crystalline structure and crystallinity, which will affect composite mechanical and thermal transitions properties. Therefore, the effect of MWCNTs on composite crystallinity, thermal transitions and deflection behaviour were further discussed.

5.3 Effect of MWCNTs on polymer crystallisation and on composite deflection behaviour

Both PLA 3251D and Bio-PE-based composites filled with MWCNTs were considered here. In a first part, the effect of MWCNTs on polymer crystallisation process and crystallinity is discussed to describe the composite structure and is completed by the analyses of the glass transition and melting transition behaviours. In a second part, effects of MWCNTs on the composite deflection behaviour detected by bulk and surface analyses are discussed.

5.3.1 Crystallisation

MWCNTs were found to induce heterogeneous nucleation in PLA 3251D as observed by Zhang et al.[102]. Observation by polarized light microscopy of annealed samples suggests that the crystallisation process induces a migration of the MWCNTs out of the crystalline regions as suggested by Leute [43] for CB-filled semi-crystalline polymers. Moreover, the electrical conductivity of composites filled with 10 wt% MWCNTs measured by four-point method was found to increase after annealing. This supports the hypotheses that annealing altered MWCNT distribution [43] and increases the electrical conductivity as suggested by Alig et al.[108]. This is not in agreement with the decrease in conductivity observed by Kuan et al.[82] when comparing the electrical conductivity of HC(high crystalline) PLA and LC(low crystalline)-PLA filled with unmodified MWCNTs. However, it can be explained by the fact that Kuan et al.[82] were considering two polymers with different maximal crystallinity, whereas in the present study one polymer type at different crystallinity level was analyzed. The dimension of polymer spherulite and the covering of MWCNT surface with crystalline polymer in the injection moulded composite as well as the inclusion of MWCNTs in the spherulites, or their migration to the spherulite periphery could not be stated here.

The decrease in crystallinity observed for low MWCNT loading in Bio-PE can be compared to the one reported by Kodjie et al.[116]. In their study, they added SWCNTs and unmodified MWCNTs to HDPE and they observed a slight decrease in crystallinity. They explained it as the nanotubes block the growth of the spherulites during crystallisation and therefore uniform lamellae cannot be formed and there are more grain boundaries and defects, which results in lower crystallinity. Thus, if the crystallinity ratio increases, it indicates a nucleation effect of the filler. However, if no increase in the crystallinity ratio is detected, it does not directly mean that no nucleation takes place. Indeed spherulites formation can be activated but the MWCNTs can simultaneously hinder polymer mobility, and a high percentage of amorphous polymer will remain between the spherulites [27]. This decreases the crystallinity ratio. However, if the crystalline structure of the composite was changed due to the presence of MWCNTs but no increase of the crystallinity is measured, effect on the glass transition and melting temperatures can still be detected by DSC.

Simultaneous increase in crystallinity and temperature of crystallisation start during composite cooling is typical for heterogeneous nucleation induced by a filler [77,100]. Thermal transition of MWCNT-filled PLA composites were compared to the thermograms presented by Moon et al.[9]. They measured the T_g and $T_{m\text{-peak}}$ of unmodified MWCNT-filled PLA composites during the first heating scan after production. On their thermograms it can be observed that the T_g and $T_{m\text{-onset}}$ were shifted to lower temperatures for the MWCNT loading of 2 and 5 wt% and slightly increased for the loading 10 wt%. Similarly to the present results, the $T_{m\text{-peak}}$ was not changed by the amount of MWCNT added. Moon et al. [9]. suggested that the variations in T_g were related to the nucleation effect of MWCNTs and their interaction with PLA. Therefore, the absence of change in the T_g found for the injection moulded composites when increasing the MWCNT loading was related to the absence of variation in crystallinity. Similarly, the slight decrease in $T_{m\text{-onset}}$ was related to the lack of interaction between MWCNTs and PLA 3251D.

In the case of MWCNT-filled Bio-PE composites, the $T_{m\text{-onset}}$ and $T_{m\text{-peak}}$ seemed to decrease slightly but not significantly. In the literature Kanagaraj et al.[42] reported that the addition of modified MWCNTs to polyethylene did not modify the $T_{m\text{-peak}}$ temperature but gave an increase in melting enthalpy. Kodjie et al.[116]; who added unmodified SWCNTs and MWCNTs to HDPE observed no significant modification of the $T_{m\text{-peak}}$ simultaneously to a slight decrease in crystallinity. This was in agreement with the present results.

In summary, MWCNTs can indeed nucleate spherulites formation in PLA 3251D and Bio-PE. However, in the injection moulded PLA-based composites the cooling was too fast for nucleation to impact crystallinity level and glass and melting transitions significantly (Figures 51, 52 and Table 14). For Bio-PE the presence of MWCNTs hindered polymer mobility and thereby the polymer crystallisation. To further understand the effect of MWCNTs on polymer mobility, composite deflection behaviour was studied as well.

5.3.2 Deflection behaviour

The information obtained from both, macro- and nanoscale methods on composite deflection behaviour properties are compared and discussed. Bao et Tjong [83] reported that adding MWCNTs at loading between 0.1 and 1 wt% to polypropylene induced an important increase in the HDT measured on the bulk composite and in the Young's modulus. This was also the case in the present study for the Bio-PE-based composites. However, the HDT of PLA 3251D was not improved by the addition of MWCNTs. Commonly, the HDT of composite can be improved by three factors: the increase in glass transition temperature (related to a decrease in polymer mobility), the increase in crystallinity, or an effective reinforcing effect [139]. It was suggested that the absence of variation in HDT observed for PLA 3251D was related to the very limited variation in composite T_g and to the lower filler polymer interaction when compared to Bio-PE. Indeed, an increase in HDT was detected in presence of MWCNTs for Bio-PE from 2.5 wt% MWCNT loading which suggested that when good filler polymer interaction is in place the resistance to the load/heat applied during HDT B measurement is supported by the filler network.

If assuming a simple addition law, the thermal expansion of the composites determined by nanoTA should decrease along with the increasing filler loading assuming that the MWCNTs have a lower thermal expansion coefficient than the biopolymers [139]. Clearly the thermal expansion first increased and then decreased when filler-loading increased, for both Bio-PE and PLA 3251D. The slight increase in thermal expansion from 0 to 1 wt% loading for both polymers cannot be explained by the lower thermal expansion coefficient of MWCNT but could be related to the presence of MWCNTs, limiting polymer mobility. It is suggested that at higher loading the transfer of heat through filler network to the surroundings balanced this effect. No thermal expansion was detected in HDT B measurements.

The size and appearance of the indentations obtained from nanoTA measurements can be used as a tool to identify the effect of heating and cooling on transformation of the material depending on its thermal properties [140,141]. Variations in the indentation width and depth with the MWCNT loading were detected for PLA 3251D-based composite but not for Bio-PE based composites. Since it is now evident that for PLA 3251D the glass transition behaviour was probed, the indentation patterns presented in Figures 56 and 57 can be used to derive information regarding the effect of the filler on the glass transition. It was observed that with the loading of 1 wt% the indentations were larger and had a halo around them, whereas above this loading the indentation decreased and the materials mobility around the indentations was reduced. Therefore, it seems that incorporation of the filler above the percolation network makes it possible to render the structure more rigid and restrict molecular movement. This can be related to the limitation in polymer mobility due to the presence of MWCNTs but also to the ability of the MWCNTs to dissipate the heat.

According to the nanoTA analysis imaging it seemed clear that with the 5 wt% loading in PLA as well as in Bio-PE, the filler started to contribute to the resistance of the PLA-based composite towards deflection. This was most probably due to the filler enabling stiffening of the structure and more rigid composite as reported in many studies [90,133,139]. This was in agreement with the fact that the addition of MWCNTs induced an increase of the

Young's modulus as shown in Figure 41 and more particularly for PLA 3251D. NanoTA showed variations in thermal expansion and in deflection temperatures, which were not detected in bulk thermal analyses.

6 Conclusions and outlook

Extrusion followed by injection moulding was found to give homogeneous filler distribution for all types of carbon-based fillers as shown by SEM characterization. The skin layer expected in injection moulded composites was not clearly detected. All types of carbon fibres and recycled carbon fibres were well-dispersed in the polymer matrices. AFM images showed well-dispersed MWCNTs in PLA 3251D, with a particular alignment of the MWCNTs at low filler loading. However, MWCNTs could not be clearly detected in Bio-PE-based composites. In parallel, it was observed that the filler type had variable effects on melt behaviours dependent on used polymer type. It was concluded that filler aspect ratio, thermal conductivity and surface treatment induced variations in the mixing and moulding processes. Therefore, when processing new composites, I would suggest to perform first processing tests using a factorial experimental design to prevent uncontrolled variation in melt temperature or machine load.

Three composite properties were particularly studied in this work: electrical, mechanical and thermal stability properties. For electrical conductivity characterization, different methods were used: two-point; four-point and ring electrode methods. Two-point methods without sample surface modification were tested in surface or volume configurations. Conductivity values and standard deviation differed from one method to the other depending on the pressure applied on the composite and the electrode-sample contact surface. It indicated that these methods were not adapted to characterize such composites. The four-point method in volume configuration allowed a reliable characterization of the maximal volume conductivity of the tested composites. The ring electrode method was simpler to use and surface and volume conductivity were clearly distinguished and presented lower standard variations than the other two-point methods. However, the maximal conductivities measured were lower than the highest one obtained with the four-point methods. Increase in electrical conductivity was detected with the addition of most of the CF types at 10 wt% loading, with the addition of CF MLD and CF.LS MLD at 20 wt% and from minimum 5 wt% loading with MWCNTs. Variations in percolation threshold and conductivity level were detected when changing the filler and/or the polymer types. For example, no conductivity was found when adding polyester sized CF in PLA 3051D, whereas conductivity was detected with 10 wt% polyurethane or polyamide sized CF.

Lower percolation threshold and higher conductivities were detected in presence of unmodified MWCNTs in PLA 3251D than in Bio-PE. Moreover, the percolation threshold and conductivity values obtained in this study were in the same range as those reported for other nanocomposites filled with unmodified carbon nanotubes in the literature when compared to composites filled with modified CNTs or with conductive filler having lower aspect ratio (CB, copper plates). The slight differences observed between the composites filled with unmodified CNTs were explained by the variations in the measurement method and in the used production process. Thus, percolation threshold varied between the composites mainly because of variations in filler aspect ratio, polymer type, filler surface modification, composite production method, preparation and orientation during measurement. All composites filled with carbon-based fillers tend towards maximal conductivity level between 10 and 100 S m^{-1} with the exception of modified nanotubes for which the maximal conductivities observed were lower. It was suggested that due to the surface modification, MWCNT surface is covered by a polymer layer and the carbon structure is degraded, which hinders the quality of the conductive network. It would be interesting to clarify this point by measuring the electrical conductivity at low temperature to determine which conduction mechanisms are involved as reported in the study of Celzard et al.[142]. If polymer layer is present on CNT surface and prevents direct contact between the nanotubes, a localized modification at CNT extremities could give higher maximal electrical conductivity. When considering the addition of volumic non-conductive filler, the difference observed for the CF and RCF filled composites with increasing wood fibres loading suggested that the wood fibres could modify the network formation and induce lower percolation threshold. However, the reason why this did not happened with all fibre types tested was not clear. Therefore, further microscopic observations on this type of composite would be of interest.

Composite tensile and impact resistance were analysed as well. Improvements in tensile strength were interpreted as good filler-polymer interactions. In the case of CF, it was observed that CFA1 gave lower tensile strength improvement than polyamide and polyurethane sized fibres except for the type CFC1, which was also at 75 MPa. No difference was detected between the tensile strength obtained with the polyurethane and polyamide sized CF in PHBV. Thus, no relation between the tensile strength and electrical conductivity due to the type of CF used could be stated. In the case of RCF electrical conductivity was higher when filler-polymer interaction was better. For MWCNT-filled polymer, decrease in tensile strength was observed when adding unmodified MWCNTs to PLA 3251D, whereas a strong increase was observed for Bio-PE-based composites. Tensile strength measurement indicated that unmodified MWCNTs did not interact with the PLA 3251D. The application of the Halpin-Tsai model to MWCNT-filled Bio-PE suggested that the unmodified MWCNTs in Bio-PE were not used at their maximal potential. Thus, for MWCNT-filled composites, better filler-polymer interaction gave worse electrical conductivity. This was the opposite effect to the one observed with RCF. It was suggested that in the case of the nanotubes, better filler-polymer interaction would hinder the formation of little nanotube agglomerates. This was supported by the higher increase in electrical conductivity observed after annealing in the case of Bio-PE in comparison to PLA at high filler loading.

Decrease in tensile elongation simultaneously to increase in Young's modulus with increasing carbon-based filler loading was related to the higher stiffness of the conductive fibres in comparison to the polymer matrix. One type of CF with polyurethane sizing (CFC1) gave particularly lower tensile elongation than all other tested CF types. This was not explained here. The addition of wood fibres resulted in a decrease in tensile strength and in elongation, which were explained by the lower strength of wood fibres when compared to carbon fibres. An exception was the composite filled with 20 wt% CF.LS MLD, for which tensile strength with 20 wt% wood fibres was equal to the one of the composite without wood fibres. The lowest tensile strength obtained in presence of wood fibres and carbon fibres or recycled carbon fibres were all superior to the one of neat PLA 3251D (lower than 60 MPa). This indicates that the wood fibres were interacting to a certain extent with the PLA. This could be verified by measuring the wettability of the wood fibres with the method of the contact angle presented in the introduction.

Concerning the impact strength, no clear variation was detected for polymer types with the lower impact strength (14 and 20 kJ m^{-2}). However, for PA and Bio-PE-based composites, change in impact strength was detected. The decrease in impact strength observed for PA-based composites when adding polyamide sized CF was related to the rigidity of the CF, well-embedded in the polymer matrix, increasing the brittleness of PA. In the case of Bio-PE based composite, the increase in impact strength observed when adding between 0 and 5 wt% MWCNT loading before decreasing at higher loadings was explained by the bridging effect of MWCNTs.

Effect of MWCNTs on composite thermal stability was found to depend on the used polymer type. In the case of PLA 3251D-based composites, it was suggested that the lack of interaction between MWCNTs and PLA 3251D induced a start of degradation at lower temperature, whereas an increase of this temperature was detected for Bio-PE. Increase found for both polymers for maximum degradation speed temperature was attributed to the formation of a char layer made of MWCNTs at the periphery of the tested composite granules. It was suggested that the decrease observed from 5 wt% loading in PLA 3251D was explained by the easier heat transfer through the MWCNT conductive network to the inside material of the granule, and supported by the lack of polymer-filler interaction.

The effect of MWCNTs on polymer crystallisation was found to depend on the cooling speed but also on the used polymer type. MWCNTs are able to nucleate PLA 3251D and Bio-PE crystallisation at low cooling speed. However, after injection moulding, nucleation is limited by the high cooling speed for PLA 3251D and is balanced by the limitation of polymer mobility in Bio-PE. This was supported by the fact that no significant variation in glass transition temperature and melting temperatures for PLA 3251D-based composite and in melting temperature for Bio-PE-based composites were detected after injection moulding when adding MWCNTs. Moreover, LPM observations and electrical conductivity measurements on annealed composites suggested that MWCNT distribution was modified during crystallisation, which resulted in improved electrical conductivity. The location of the MWCNTs inside the crystalline or amorphous polymer regions was not determined here. This could be determined using AFM on composites at varying crystallisation time.

Bulk measurement on thermal deflection behaviour (HDT B) and surface measurement at nanoscale (nanoTA) gave different trends depending on the polymer type. It was suggested that the deflection temperature characterized by nanoTA was increased due to heat dissipation through the conductive filler network in PLA 3251D, whereas the absence of variation observed by HDT B was explained by the homogeneous heating of the entire composite. NanoTA measurement gave also supplementary information concerning the polymer matrix expansion which first increased in presence of MWCNTs at low loading and then decreased at loading higher than 1 wt%. This was related to the limitation of polymer mobility or increase in stiffness, balanced by the formation of the conductive network around 5 wt% loading. The analysis of the shape of the indentation, and the polymer surface after measurement suggested variations in composite mechanical stiffness and polymer mobility. NanoTA measurement demonstrated the advantage in the characterization of nanocomposites filled with conductive fillers.

In complement to this work, first experiments were made to characterize the effect of the addition of carbon-based fillers to biodegradable polymers on their biodegradability in compost. More work is needed to assure reliable results and therefore further experiments are recommended to obtain detailed information. Another idea to improve the amount of bio-based components in this type of composite would be to use CF based on lignin or natural fibres after pyrolysis [143,144].

7 References

1. Peelman N, Ragaert P, De Meulenaer B, Adons D, Peeters R, Cardon L, et al. Application of bioplastics for food packaging. Trends Food Sci. Technol. Elsevier Ltd; 2013;32:128–41.

2. Ge JJ, Hou H, Li Q, Graham MJ, Greiner A, Reneker DH, et al. Assembly of well-aligned multiwalled carbon nanotubes in confined polyacrylonitrile environments: electrospun composite nanofiber sheets. J. Am. Chem. Soc. 2004;126:15754–61.

3. Shen L, Worrell E, Patel M. Present and future development in plastics from biomass. Biofuels, Bioprod. Biorefining. 2009;4:25–40.

4. Biocomposites EB and I for B and. Bioplastics market grows above average between 2012 and 2017 [Internet]. european-bioplastics.org. 2013 [cited 2014 Jun 24]. Available from: bioplastics.org/wp-content/uploads/2013/12/EuBP_market_data_2012.pdf

5. Liu J. Reactive Extrusion of biodegradable Poly (lactic acid) and Polyester blends: Effects of PLA/EB062 ratio, Miscibility and Thermal Behavior. University of Toledo; 2011.

6. Palacio J, Orozco VH, López BL. Effect of the Molecular Weight on the Physicochemical Properties of Poly(lactic acid) Nanoparticles and on the Amount of Ovalbumin Adsorption. J. Braz. Chem. Soc. 2011;22:2304–11.

7. Rodriguez-Contreras A, Koller M, Miranda-de Sousa Dias, M. Calafell-Monfort M, Braunegg, G. M.S.Marques-Calvo MS. High production of poly(3-hydroxybutyrate) from a wild Bacillus megaterium Bolivian strain. J. Appl. Microbiol. 2013;

8. Kim H-S, Hyun Park B, Yoon J-S, Jin H-J. Thermal and electrical properties of poly(l-lactide)-graft-multiwalled carbon nanotube composites. Eur. Polym. J. 2007;43:1729–35.

9. Moon S-I, Jin F, Lee C, Tsutsumi S, Hyon S-H. Novel Carbon Nanotube/Poly(L-lactic acid) Nanocomposites; Their Modulus, Thermal Stability, and Electrical Conductivity. Macromol. Symp. 2005;224:287–96.

10. Krul LP, Volozhyn AI, Belov DA, Poloiko NA, Artushkevich AS, Zhdanok SA, et al. Nanocomposites based on poly-D,L-lactide and multiwall carbon nanotubes. Biomol. Eng. 2007;24:93–5.

11. Avella M, Buzarovska A, Errico ME, Gentile G, Grozdanov A. Eco-Challenges of Bio-Based Polymer Composites. 2009;911–25.

12. Lagaron J, Lopez-Rubio A. Nanotechnology for bioplastics: opportunities, challenges and strategies. Trends Food Sci. Technol. 2011;22:611–7.

13. Tábi T, Sajó IE, Szabó F, Luyt AS, Kovács JG. Crystalline structure of annealed polylactic acid and its relation to processing. Express Polym. Lett. 2010;4:659–68.

14. Ambrosio-Martın J, Gorrasi G, Lopez-Rubio A, Fabra MJ, Mas LC, López-Manchado MA, et al. On the use of ball milling to develop PHBV–graphene nanocomposites (I)—Morphology, thermal properties, and thermal stability. J. Appl. Polym. Sci. 2015;

15. Chandra R, Rustgi R. Biodegradable polymers. Prog. Polym. Sci. 1998;23:1273–335.

16. Morschbacker A. Bio-Ethanol Based Ethylene. Polym. Rev. 2009;49:79–84.

17. Wroblewska A, Zych A, Thiyagarajan S, Dudenko D, van Es D, Hansen MR, et al. Towards sugar-derived polyamides as environmentally friendly materials. Polym. Chem. Royal Society of Chemistry; 2015;6:4133–43.

18. Sykacek E, Hrabalova M, Frech H, Mundigler N. Extrusion of five biopolymers reinforced with increasing wood flour concentration on a production machine, injection moulding and mechanical performance. Compos. Part A Appl. Sci. Manuf. Elsevier Ltd;

2009;40:1272–82.

19. Valente M, Sarasini F, Marra F, Tirillo J, Pulci G. Hybrid recycled glass fiber/wood flour thermoplastic composites: Manufacturing and mechanical characterization. Compos. Part A Appl. Sci. Manuf. Elsevier Ltd; 2011;42:649–57.

20. Nanda MR, Misra M, Mohanty AK. Performance Evaluation of Biofibers and Their Hybrids as Reinforcements in Bioplastic Composites. Macromol. Mater. Eng. 2013;298:779–88.

21. Sykacek E, Schlager W, Mundigler N. Compatibility of Softwood Flour and Commercial Biopolymers in Injection Molding. Polym. Compos. 2009;

22. Fu SY, Lauke B, Mäder E, Yue CY, Hu X. Tensile properties of short-glass-fiber- and short-carbon-fiber-reinforced polypropylene composites. Compos. Part A Appl. Sci. Manuf. 2000;31:1117–25.

23. Villmow T, Pötschke P, Pegel S, Häussler L, Kretzschmar B. Influence of twin-screw extrusion conditions on the dispersion of multi-walled carbon nanotubes in a poly(lactic acid) matrix. Polymer. 2008;49:3500–9.

24. Pegel S, Pötschke P, Petzold G, Alig I, Dudkin SM, Lellinger D. Dispersion, agglomeration, and network formation of multiwalled carbon nanotubes in polycarbonate melts. Polymer. 2008;49:974–84.

25. Byrne MT, Gun'ko YK. Recent Advances in Research on Carbon Nanotube-Polymer Composites. Adv. Mater. 2010;22:1672–88.

26. Villmow T, Pegel S, Pötschke P, Wagenknecht U. Influence of injection molding parameters on the electrical resistivity of polycarbonate filled with multi-walled carbon nanotubes. Compos. Sci. Technol. 2008;68:777–89.

27. Nobile MR, Simon GP, Valentino O, Morcom M. Rheological and Structure Investigation of Melt Mixed Multi-Walled Carbon Nanotube/PE Composites. Macromol. Symp. 2007;247:78–87.

28. Mack C, Sathyanarayana S, Weiss P, Mikonsaari I, Hübner C, Henning F, et al. Twin-screw extrusion of multi walled carbon nanotubes reinforced polycarbonate composites: Investigation of electrical and mechanical properties. IOP Conf. Ser. Mater. Sci. Eng. 2012;40:12020.

29. Thomas S, Joseph K, Malhotra SK, Goda K, Sreekala MS. Polymer Composites, volume 1: Macro/and Microcomposites. Thomas S, Joseph K, Malhotra SK, Goda K, Sreekala MS, editors. Weinheim, Germany: John Wiley & Sons; 2012.

30. Valentino O, Sarno M, Rainone NG, Nobile MR, Ciambelli P, Neitzert HC, et al. Influence of the polymer structure and nanotube concentration on the conductivity and rheological properties of polyethylene/CNT composites. Phys. E Low-dimensional Syst. Nanostructures. 2008;40:2440–5.

31. Taipalus R, Harmia T, Zhang M., Friedrich K. The electrical conductivity of carbon-fibre-reinforced polypropylene/polyaniline complex-blends: experimental characterisation and modelling. Compos. Sci. Technol. 2001;61:801–14.

32. Wan YZ, Wang YL, Li QY, Dong XH. Influence of surface treatment of carbon fibers on interfacial adhesion strength and mechanical properties of PLA-based composites. J. Appl. Polym. Sci. 2001;80:367–76.

33. Du F, Scogna RC, Zhou W, Brand S, Fischer JE, Winey KI. Nanotube Networks in Polymer Nanocomposites:Rheology and Electrical Conductivity. Macromolecules. 2004;37:9048–55.

34. Nuriel S, Liu L, Barber AH, Wagner HD. Direct measurement of multiwall nanotube

surface tension. Chem. Phys. Lett. 2005;404:263–6.

35. Nypelö T. Surface-modified nanoparticles for ultrathin coatings. Aalto University, School of Chemical Technology; 2012.

36. Zisman WA. surface chemistry of plastics reinforced by strong fibers. I &EC Prod. Res. Dev. 1969;8:98–111.

37. Al-Saleh MH, Sundararaj U. A review of vapor grown carbon nanofiber/polymer conductive composites. Carbon N. Y. Elsevier Ltd; 2009;47:2–22.

38. Merzouki A, Haddaoui N. Electrical Conductivity Modeling of Polypropylene Composites Filled with Carbon Black and Acetylene Black. ISRN Polym. Sci. 2012;2012:1–7.

39. Kumar P, Sandeep KP, Alavi S, Truong VD. A Review of Experimental and Modeling Techniques to Determine Properties of Biopolymer-Based Nanocomposites. J. Food Sci. 2011;76:E2–14.

40. Mallick PK. Fiber- Reinforced Composites. Mech. Eng. 2007.

41. J. C. Halpin, Kardos JL. The Halpin-Tsai equations: A review. Polym. Eng. Sci. 1976;16:344–52.

42. Kanagaraj S, Varanda F, Zhil'tsova T, Oliveira M, Simões J. Mechanical properties of high density polyethylene/carbon nanotube composites. Compos. Sci. Technol. 2007;67:3071–7.

43. Leute U. Kunststoffe und EMV Elektromagnetische Verträglichkeit mit leitfähigen Kunststoffen. 8 expertve. Bartz J, Mesenholl H-J, Wippler E, editors. Renningen, Germany,: Kontakt and Studium Band 67; 2014.

44. Ramuz M, Vosgueritchian M, Wei P, Wang C, Gao Y, Wu Y. Evaluation of solution-processable carbon based Electrodes for all carbon solar cells. ACS Nano. 2012;6:10384–95.

45. SHIH Y, Wang Y, Hsieh C. Preparation and properties of PLA/long alkyl chain modified multi-walled carbon nanotubes naocomposites. J. Polym. Eng. 2011;31:13–9.

46. Paradise M, Goswami T. Carbon nanotubes – Production and industrial applications. Mater. Des. 2007;28:1477–89.

47. Andrews R, Jaqques D, Qian D, Rantell T. Multiwall carbon nanotubes: Synthesis and application. J. Acc. Chem. Res. 2002;35:1008–17.

48. Combessis A, Charvin N, Allais A, Fournier J, Flandin L. Understanding dynamic percolation mechanisms in carbonaceous polymer nanocomposites through impedance spectroscopy: Experiments and modeling. J. Appl. Phys. 2014;116.

49. Celzard A. Contribution à l'étude du phénomène de percolation dans des matériaux composites à propriétés anisotropes. 1995.

50. Chiu F. A Review on Conduction Mechanisms in Dielectric Films. Adv. Mater. Sci. Eng. 2014;2014:18.

51. Domininghaus H, Elsner P, Eyerer P, Hirth T. Kunststoffe Eigenschaften und Anwendungen. Springer. Domininghaus H, editor. 2008.

52. Aguilar JO. Influence of carbon nanotube clustering on the electrical conductivity of polymer composite films. eXPRESS Polym. Lett. 2010;4:292–9.

53. Guoquan W. Electrical resistance measurement of conductive network in short carbon fibre-polymer composites. Polym. Test. 1997;16:277–86.

54. Bigg DM. An Investigation of the Effect of Carbon Black Structure, Polymer

Morphology and Processing History on the Electrical Conductivity of Carbon-Black-Filled Thermoplastics. J. Rheol. (N. Y. N. Y). 1984;28:501–16.

55. Hornbostel B, Pötschke P, Kotz J, Roth S. Single-walled carbon nanotubes/polycarbonate composites: Basic electrical and mechanical properties. Phys. Status Solidi Basic Res. 2006;243:3445–51.

56. Markov A V, Bock H-J, Mauser A, Müller T, Vyshnepolskiy B. Spritzgegossene kupfergefüllte Thermoplaste für die Erzeugnisentwicklung. Materwiss. Werksttech. 2007;38:836–41.

57. Novais RM, Simon F, Pötschke P, Villmow T, Covas JA, Paiva MC. Poly(lactic acid) Composites with Poly(lactic acid)-Modified Carbon Nanotubes. J. Polym. Sci. PART A Polym. Chem. 2013;51:3740–50.

58. McLachlan DS. A new interpretation of percolation conductivity results with large critical regimes. Solid State Commun. 1986;60:821–5.

59. McLachlan DS, Blaszkiewicz M, Newnham RE. Electrical Resistivity of Composites. J. Am. Ceram. Soc. 1990;73:2187–203.

60. Celzard A, MsRae E. Critical concentration in percolating systems containing a high-aspect ratio filler. Phys. Rev. B. 1996;53:6209–14.

61. Combessis A, Bayon L, Flandin L. Effect of filler auto-assembly on percolation transition in carbon nanotube/polymer composites. Appl. Phys. Lett. 2013;102.

62. Badard M, Combessis A, Allais A, Flandin L. CNT aggregation mechanisms probed by electrical and dielectric measurements. J. Mater. Chem. C. 2015;3:5769–74.

63. McLachlan DS. Complex ac conductivity of a carbon black composite as a function of frequency, compositioin, and temperature. Phys. Rev. B. 1999;60:12746–51.

64. McLachlan DS, Chiteme C, Park C, Wise KE, Lowther SE, Lillehei P, et al. AC and DC Percolative Conductivity of Single Wall Carbon Nanotube Polymer Composites. J. Polym. Sci. Part B Polym. Phys. 2005;43:3273–87.

65. Lisunova MO, Mamunya YP, Lebovka NI, Melezhyk A V. Percolation behaviour of ultrahigh molecular weight polyethylene/multi-walled carbon nanotubes composites. Eur. Polym. J. 2007;43:949–58.

66. Philipse AP, Wierenga AM. On the Density and Structure Formation in Gels and Clusters of Colloidal Rods and Fibers. Langmuir. 1998;14:49–54.

67. Flandin L, Bidan G, Brechet Y, Cavaillé JY. New Nanocomposite Materials Made of an Insulating Matrix and Conducting Fillers: Processing and Properties. Polym. Compos. 2000;21:165–74.

68. Pimenta S, Pinho ST. Recycling carbon fibre reinforced polymers for structural applications: Technology review and market outlook. Waste Manag. 2011;31:378–92.

69. Kuilla T, Bhadra S, Yao DH, Kim NH, Bose S, Lee JH. Recent advances in graphene based polymer composites. Prog. Polym. Sci. Elsevier Ltd; 2010;35:1350–75.

70. Roy N, Sengupta R, Bhowmick AK. Modifications of carbon for polymer composites and nanocomposites. Prog. Polym. Sci. Elsevier Ltd; 2012;37:781–819.

71. Costa P, Silva J, Ansón-Casaos A, Martinez MT, Abad MJ, Viana J, et al. Effect of carbon nanotube type and functionalization on the electrical, thermal, mechanical and electromechanical properties of carbon nanotube/styrene-butadiene-styrene composites for large strain sensor applications. Compos. Part B Eng. Elsevier Ltd; 2014;61:136–46.

72. Velasco-Santos C, Martinez-Hernandez AL, Castano VM. Carbon nanotube-polymer nanocomposites: The role of interfaces. Compos. Interfaces. 2005;11:567–86.

73. Iijima S. Helical microtubules of graphitic carbon. Nature. 1991;354:56–8.

74. Sathyanarayana S, Hübner C. Structural Nanocomposites. 2013.

75. Than XT. Croissance catalytique et étude de nanotubes de carbone multi-feuillets produits en masse et de nanotubes de carbone ultra-long individuels à quelques feuillets. University of Montpellier II, France; 2011.

76. Jeong HJ, Jeong SY, Shin YM, Han JH, Lim SC, Eum SJ, et al. Dual-catalyst growth of vertically aligned carbon nanotubes at low temperature in thermal chemical vapor deposition. Chem. Phys. Lett. 2002;361:189–95.

77. Yoon J, Jeong Y, Lee S, Min B. Influences of poly (lactic acid)- grafted carbon nanotube on thermal, mechanical, and electrical properties of poly (lactic acid). Polym. Adv. Technol. 2009;20:631–8.

78. Shieh Y-T, Liu G-L, Twu Y-K, Wang T-L, Yang C-H. Effects of Carbon Nanotubes on Dynamic Mechanical Property, Thermal Property, and Crystal Structure of Poly(L-lactic acid). J. Polym. Sci. PART B Polym. Phys. 2009;

79. Kordkheili HY, Farsi M, Rezazadeh Z. Physical, mechanical and morphological properties of polymer composites manufactured from carbon nanotubes and wood flour. Compos. Part B Eng. Elsevier Ltd; 2013;44:750–5.

80. Dujardin E, Ebbesen TW, Krishnan A, Treacy MMJ. Wetting of Single Shell Carbon Nanotubes. Communications. 1998;10:1472–5.

81. Barber AH, Cohen SR, Daniel Wagner H. Static and dynamic wetting measurements of single carbon nanotubes. Phys. Rev. Lett. 2004;92:186103–1.

82. Kuan C-F, Kuan H-C, Ma C-CM, Chen C-H. Mechanical and electrical properties of multi-wall carbon nanotube/poly(lactic acid) composites. J. Phys. Chem. Solids. 2008;69:1395–8.

83. Bao SP, Tjong SC. Mechanical behaviors of polypropylene/carbon nanotube nanocomposites: The effects of loading rate and temperature. Mater. Sci. Eng. A. 2008;485:508–16.

84. Corcione C, Frigione M. Characterization of Nanocomposites by Thermal Analysis. Materials (Basel). 2012;5:2960–80.

85. Beyer G. Short Communication: Carbon Nanotubes as Flame Retardants for Polymers. Fire Mater. 2002;26:291–3.

86. Moniruzzaman M, Winey K. Polymer nanocomposites containing carbon nanotubes. Macromolecules. 2006;39:5194–205.

87. Bauhofer W, Kovacs JZ, Swan T, Swan T, Swan T. A review and analysis of electrical percolation in carbon nanotube polymer composites. Compos. Sci. Technol. Elsevier Ltd; 2009;69:1486–98.

. Rimska Z, K ues l ek V, Spacek J. AC conductivity of carbon fiber–polymer matrix composites at the percolation threshold. Polym. Compos. 2002;23:95–103.

89. Király A, Ronkay F. Temperature dependence of electrical properties in conductive polymer composites. Polym. Test. 2015;43:154–62.

90. Alam MK, Islam MT, Mina MF, Gafur MA. Structural, mechanical, thermal, and electrical properties of carbon black reinforced polyester resin composites. J. Appl. Polym. Sci. 2014;131:1–11.

91. Wu D, Wu L, Zhang M, Zhao Y. Viscoelasticity and thermal stability of polylactide composites with various functionalized carbon nanotubes. Polym. Degrad. Stab. 2008;93:1577–84.

92. Schartel B, Pötschke P, Knoll U, Abdel-Goad M. Fire behaviour of polyamide 6/multiwall carbon nanotube nanocomposites. Eur. Polym. J. 2005;41:1061–70.

93. Schartel B, Braun U, Knoll U, Bartholmai M, Goering H, Neubert D, et al. Mechanical, thermal, and fire behavior of bisphenol a polycarbonate/multiwall carbon nanotube nanocomposites. Polym. Eng. Sci. 2008;

94. Feller JF, Roth S, Bourmaud A. Conductive polymer composites: Electrical, thermal, and rheological study of injected isotactic poly(propylene)/long stainless-steel fibers for electromagnetic interferences shielding. J. Appl. Polym. Sci. 2006;100:3280–7.

95. Xu Z, Niu Y, Yang L, Xie W, Li H, Gan Z, et al. Morphology, rheology and crystallization behavior of polylactide composites prepared through addition of five-armed star polylactide grafted multiwalled carbon nanotubes. Polymer. 2010;51:730–7.

96. Zhao Y, Qiu Z, Yan S, Yang W. Crystallization behavior of biodegradable poly (L-lactide)/multiwalled carbon nanotubes nanocomposites from the amorphous state. Polym. Eng. Sci. 2011;51:1564–73.

97. Li H, Huneault MA. Effect of nucleation and plasticization on the crystallization of poly(lactic acid). Polymer. 2007;48:6855–66.

98. Papageorgiou GZ, Achilias DS, Nanaki S, Beslikas T, Bikiaris D. PLA nanocomposites: Effect of filler type on non-isothermal crystallization. Thermochim. Acta. Elsevier B.V.; 2010;511:129–39.

99. Spitalsky Z, Tasis D, Papagelis K, Galiotis C. Carbon nanotube–polymer composites: Chemistry, processing, mechanical and electrical properties. Prog. Polym. Sci. Elsevier Ltd; 2010;35:357–401.

100. Tsuji H, Kawashima Y, Takikawa H, Tanaka S. Poly(l-lactide)/nano-structured carbon composites: Conductivity, thermal properties, crystallization, and biodegradation. Polymer. 2007;48:4213–25.

101. Yang J, Wang K, Deng H, Chen F, Fu Q. Hierarchical structure of injection-molded bars of HDPE/MWCNTs composites with novel nanohybrid shish-kebab. Polymer. Elsevier Ltd; 2010;51:774–82.

102. Zhang H, Zhang Z. Impact behaviour of polypropylene filled with multi-walled carbon nanotubes. Eur. Polym. J. 2007;43:3197–207.

103. Fitaroni LB, Lima JA De, Cruz SA, Waldman WR. Thermal stability of polypropylene e montmorillonite clay nanocomposites : Limitation of the thermogravimetric analysis. Polym. Degrad. Stab. Elsevier Ltd; 2015;111:102–8.

104. Eggedi O, Valiyaneerilakkal U, Darla MR, Varghese S. Nanoindentation and thermal characterization of poly (vinylidenefluoride)/MWCNT nanocomposites. AIP Adv. 2014;4:47102.

105. Velasco-Santos C, Martinez-Hernandez AL, Fisher F, Ruoff R, Castano VM. Dynamical – mechanical and thermal analysis of carbon nanotube – methyl-ethyl methacrylate nanocomposites R Ruoff and V M Castano. J. Phys. D. Appl. Phys. 2003;36:1423–8.

106. Kim J, Park H, Kim S. Multiwall-carbon-nanotube-reinforced poly (ethylene terephthalate) nanocomposites by melt compounding. J. Appl. Polym. Sci. 2007;103:1450–7.

107. Cadek M, Coleman JN, Ryan KP, Nicolosi V, Bister G, Fonseca a., et al. Reinforcement of Polymers with Carbon Nanotubes: The Role of Nanotube Surface Area. Nano Lett. 2004;4:353–6.

108. Alig I, Lellinger D, Dudkin SM, Pötschke P. Conductivity spectroscopy on melt

processed polypropylene–multiwalled carbon nanotube composites: Recovery after shear and crystallization. Polymer. 2007;48:1020–9.

109. Song M, Hourston DJ, Grandy DB, Reading M. An Application of Micro-Thermal Analysis. 2001;2136–41.

110. Souier T, Samad YA, Lalia BS, Hashaikeh R, Chiesa M. Nanoscale thermal analysis of multiphase polymer nanocomposites. J. Phys. Chem. C. 2012;116:8849–56.

111. Gotzen NA, Van Assche G, Ghanem A, Van Ingelgem Y, Hubin A, Van Mele B. Micro- and nano-thermal analysis applied to multi-layered biaxially-oriented polypropylene films. J. Therm. Anal. Calorim. 2009;95:207–13.

112. Nikiforov MP, Gam S, Jesse S, Composto RJ, Kalinin SV. Morphology mapping of phase-separated polymer films using nanothermal analysis. Macromolecules. 2010;43:6724–30.

113. Ago M, Okajima K, Jakes JE, Park S, Rojas OJ. Lignin-based electrospun nanofibers reinforced with cellulose nanocrystals. Biomacromolecules. 2012;13:918–26.

114. Germinario LT, Shang PP. Advances in nano thermal analysis of coatings. J. Therm. Anal. Calorim. 2008;93:207–11.

115. Vähä-Nissi M, Kauppi E, Sahagian K, Johansson L-S, Peresin MS, Sievänen J, et al. Growth of thin Al2O3 films on biaxially oriented polymer films by atomic layer deposition. Thin Solid Films. 2012;522:50–7.

116. Kodjie S, Li L, Li B, Cai W, Li C, Keating M. Morphology and Crystallization Behavior of HDPE/CNT Nanocomposite. J. Macromol. Sci. Part bPhysics. 2006;45:231–45.

117. Duvigneau J, Schönherr H, Vancso GJ. Nanoscale thermal AFM of polymers: Transient heat flow effects. ACS Nano. 2010;4:6932–40.

118. Liu F, Zhang X, Li W, Cheng J, Tao X, Li Y, et al. Investigation of the electrical conductivity of HDPE composites filled with bundle-like MWNTs. Compos. Part A Appl. Sci. Manuf. Elsevier Ltd; 2009;40:1717–21.

119. Sichina W. DSC as problem solving tool: measurement of percent crystallinity of thermoplastics. Perkin Elmer Instruments, and PETech. 2000;

120. Gregorova A. Application of Differential Scanning Calorimetry to the Characterization of Biopolymers. Appl. Calorim. a Wide Context – 6 Differ. Scanning Calorimetry, Isothermal Titration Calorim. Microcalorim. 2013.

121. Planes E, Gloaguen F, Alberola N, Flandin L. Spatial distribution of the electrical conductivity in highly filled polymers: Experiment, modeling, and application to bipolar plates. J. Appl. Phys. 2013;114.

122. Planes E, Gloaguen F, Flandin L. Carbon-polymer composites with extreme electrical conductivity. J. Appl. Polym. Sci. 2015;132.

123. Ajayan PM, Stephan O, Colliex C, Trauth D. Aligned Carbon Nanotube Arrays Formed by Cutting a Polymer Resin-Nanotube Composite. Science (80-.). 1994;265:1212–4.

124. Wang Y, Ju S, Huang TJ, Wang H. Modeling of polyethylene , poly (l-lactide), and CNT composites : a dissipative particle dynamics study. Nanoscale Res. Lett. Springer Open Ltd; 2011;6:433.

125. Pötschke P, Abdel-Goad M, Alig I, Dudkin S, Lellinger D. Rheological and dielectrical characterization of melt mixed polycarbonate-multiwalled carbon nanotube composites. Polymer. 2004;45:8863–70.

126. Pötschke P, Dudkin SM, Alig I. Dielectric spectroscopy on melt processed

polycarbonate - multiwalled carbon nanotube composites. Polymer. 2003;44:5023–30.

127. Pötschke P, Fornes TD, Paul DR. Rheological behavior of multiwalled carbon nanotube / polycarbonate composites. Polymer. 2002;43:3247–55.

128. Tjong SC, Liang GD, Bao SP. Electrical behavior of polypropylene/multiwalled carbon nanotube nanocomposites with low percolation threshold. Scr. Mater. 2007;57:461–4.

129. Kharchenko SB, Douglas JF, Obrzut J, Grulke EA, Migler KB. Flow-induced properties of nanotube-filled polymer materials. Nat. Mater. 2004;3:564–8.

130. Kodgire P V., Bhattacharyya AR, Bose S, Gupta N, Kulkarni AR, Misra A. Control of multiwall carbon nanotubes dispersion in polyamide6 matrix: An assessment through electrical conductivity. Chem. Phys. Lett. 2006;432:480–5.

131. Mcnally T, Pötschke P, Halley P, Murphy M, Martin D, Bell SEJ, et al. Polyethylene multiwalled carbon nanotube composites. Polymer. 2005;46:8222–32.

132. Meincke O, Kaempfer D, Weickmann H, Friedrich C, Vathauer M, Warth H. Mechanical properties and electrical conductivity of carbon-nanotube filled polyamide-6 and its blends with acrylonitrile/butadiene/styrene. Polymer. 2004;45:739–48.

133. Tang W, Santare M, Advani S. Melt processing and mechanical property characterization of multi-walled carbon nanotube/high density polyethylene (MWNT/HDPE) composite films. Carbon N. Y. 2003;41:2779–85.

134. Prashantha K, Soulestin J, Lacrampe MF, Krawczak P, Dupin G, Claes M. Masterbatch-based multi-walled carbon nanotube filled polypropylene nanocomposites: Assessment of rheological and mechanical properties. Compos. Sci. Technol. Elsevier Ltd; 2009;69:1756–63.

135. Kim H-S, Chae YS, Kwon H Il, Yoon J-S. Thermal degradation behaviour of multi-walled carbon nanotube-reinforced poly(L-lactide) nanocomposites. Polym. Int. 2009;58:826–31.

136. Bocchini S, Frache A, Camino G, Claes M. Polyethylene thermal oxidative stabilisation in carbon nanotubes based nanocomposites. Eur. Polym. J. 2007;43:3222–35.

137. Barus S, Zanetti M, Bracco P, Musso S, Chiodoni A, Tagliaferro A. Influence of MWCNT morphology on dispersion and thermal properties of polyethylene nanocomposites. Polym. Degrad. Stab. Elsevier Ltd; 2010;95:756–62.

138. George JJ, Sengupta R, Bhowmick AK. Influence of functionalization of multi-walled carbon nanotubes on the properties of ethylene vinyl acetate nanocomposites. J. Nanosci. Nanotechnol. 2008;8:1913–21.

139. Díez-Pascual A, Naffakh M. Enhancing the thermomechanical behaviour of poly (phenylene sulphide) based composites via incorporation of covalently grafted carbon nanotubes. Compos. Part A Appl. Sci. Manuf. 2013;54:10–9.

140. Remmert J. Nano Thermal and Contact Potential Analysis with Heated Probe Tips. 2007.

141. Zhang J, Bunker M, Parker A, Madden-Smith C, Patel N, Roberts C. The stability of solid dispersions of felodipine in polyvinylpyrrolidone characterized by nanothermal analysis. Int. J. Pharm. 2011;414:210–7.

142. Celzard A, McRae E, Marêché JF, Furdin G, Sundqvist B. Conduction mechanism in some graphite-polymer composites: Effects of temperature and hydrostatic pressure. J. Appl. Phys. 1998;83:1410–9.

143. Gellerstedt G, Sjöholm E, Brodin I. The Wood-Based Biorefinery: A Source of

Carbon Fiber? Open Agric. J. 2010;3:119–24.

144. Celzard a., Marêché JF, Payot F, Furdin G. Electrical conductivity of carbonaceous powders. Carbon N. Y. 2002;40:2801–15.

8 Index of tables

9 Table of figures

10 Appendix

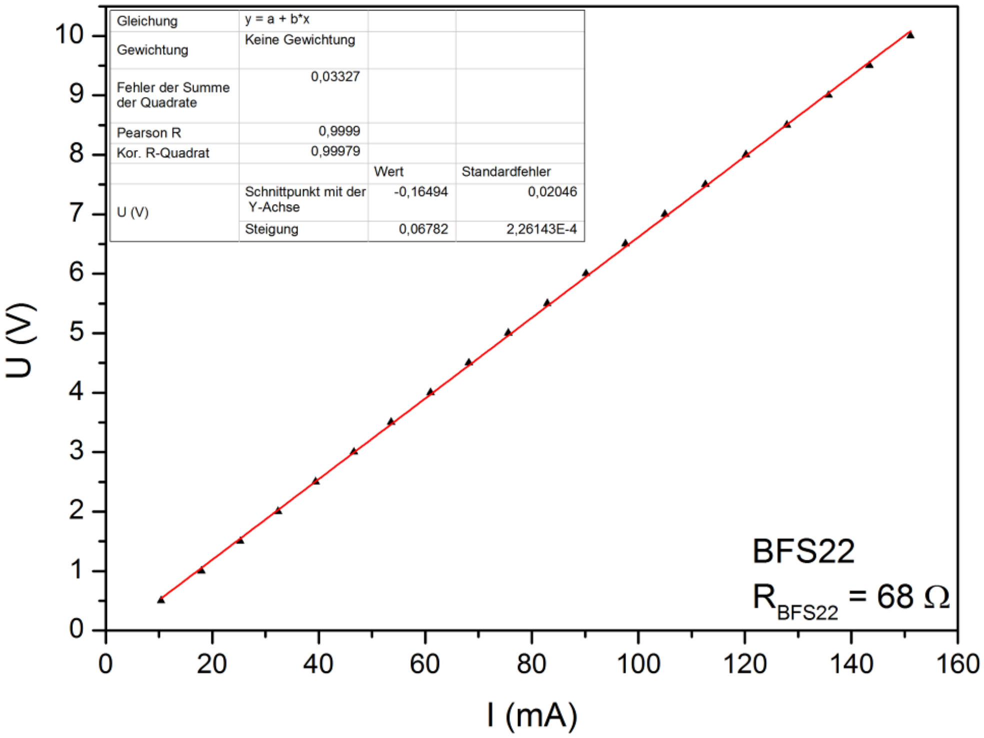

Gleichung	y = a + b*x		
Gewichtung	Keine Gewichtung		
Fehler der Summe der Quadrate	0,03327		
Pearson R	0,9999		
Kor. R-Quadrat	0,99979		
		Wert	Standardfehler
U (V)	Schnittpunkt mit der Y-Achse	-0,16494	0,02046
	Steigung	0,06782	2,26143E-4

Figure A1: Electrical resistance of BFS18 and BFS22 assessed by two-point method with clamped electrodes. With the clamped electrodes, linear increase of the voltage potential was measured when increasing the current applied to the MWCNT-filled samples. This indicated that the MWCNT-filled samples followed the Ohm's law equation and thereby behaved as ohmic resistor.

Table A2: Softening temperature of the Bio-PE and PLA 3251D composites derived from the nanothermal analysis and thermo-oxidative degradation temperatures and maximal speed of degradation derived from TGA.

Polymer	MWCNT loading [wt%]	Softening temperature [°C]	T_d [°C]	T_{dmax} [°C]	Speed rate [% min^{-1}]
PLA 3251D	0	71 ± 1	322 ± 4	357 ± 1	29 ± 1
	1	71 ± 1	322 ± 1	361 ± 1	28 ± 0
	5	76 ± 2	307 ± 5	365 ± 1	28 ± 0
	10	83 ± 3	301 ± 1	358 ± 2	23 ± 2
Bio-PE	0	120 ± 5	356 ± 7 [1]	455 ± 3 [1]	21 ± 2 [1]
	1	123 ± 3	378 ± 9	470 ± 1	18 ± 2
	5	134 ± 4	425 ± 2	477 ± 4	25 ± 0
	10	154 ± 5	429 ± 2	480 ± 2	24 ± 1

[1] The values were averaged from two measurements

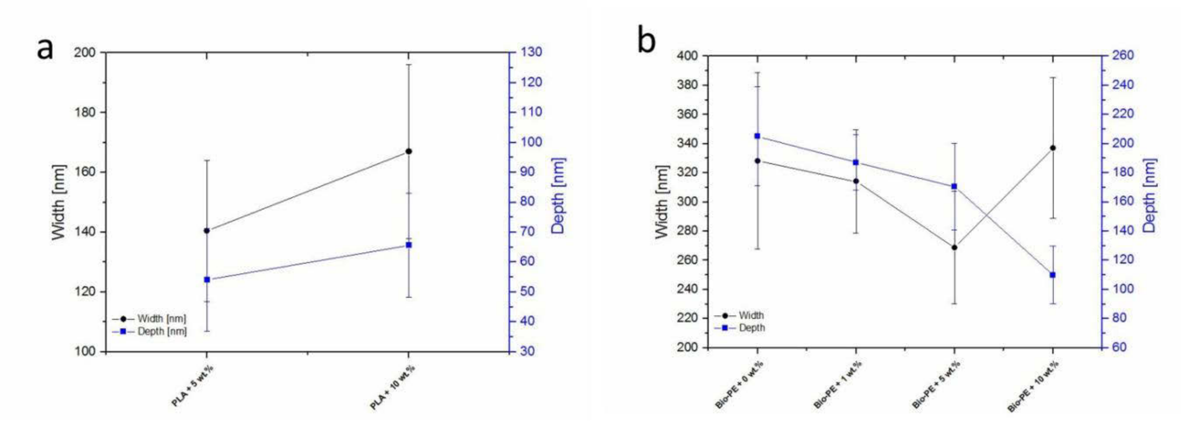

Figure A3: Width and depth of the indentation in PLA (a) and Bio-PE (b) composites induced by the nanothermal ramping (nanoTA measurements).

11 Table of abbreviations

AFM: Atomic force microscopy

BFS: Injection moulding production number (Biofunk Spritzguss)

BFX: Extrusion production number (Biofunk Extrusion)

Bio-PE: Bio-based polyethylene

BOKU: Universität für Bodenkultur

CB: Carbon black

CF: Carbon fibres

CF.LS MLD: Milled carbon fibres with low surface sizing

CF MLD: Milled carbon fibres

CNT: Carbon nanotube

DSC: Differential scanning calorimetry

HDPE: High density polyethylene

HDT: Heat deflection temperature

LPM: Polarized Light microscopy

MWCNT: Multi-walled carbon nanotube

PHBV: Poly(3-hydroxybutyrate-co-3-hydroxyvalerate)

PLA: Poly(lactic-acid)

RCF: Recycled carbon fibres

std dev.: Standard deviation

SWCNT: Single-walled carbon nanotube

Td: temperature of thermal degradation start (5 wt% loss)

Tdmax: Temperature of maximal degradation rate

TGA: Thermo-gravimetric analyses

Tm-onset: Temperature of melting onset

Tm-peak: Temperature of the melting peak

vol.%: Percent in volume

wt%: Percent in weight

AAA	Association of American Geographers
FAO	United Nations Food and Agriculture Organization
Sci.	Social Science, Beverly Hills

12 CV

Personal data

Name	Pauline Rivière
Date of Birth	19/12/1989
Place of Birth	LAVAL (53)
Country	France
Nationality	French
Marital status	Single
University	University of Natural Resources and Life Sciences

Work Experience

Oct. 2012-Feb. 2016	**Researcher**, IFA-Tulln, Austria Conducting a scientific project on electrical conductive thermoplastics at the Institute of Natural Materials Technology of the University of Natural Ressources and Life Sciences of Vienna, Austria. www.ifa-tulln.boku.ac.at/institut-fuer-naturstofftechnik

Education and Internship

2012-today	**Preparation of doctoral degree** at the University of Natural Resources and life Sciences of Vienna, Austria www.boku.ac.at On thermoplastic composites processed by injection moulding with the title: SEMI-CRYSTALLINE BIOPOLYMERS WITH CARBON-BASED FILLERS: ELECTRICAL, MECHANICAL AND THERMAL PROPERTIES (thesis currently under revision)
2009-2012	**Master of Engineering** in Wood Science and Timber Engineering at the University of Nancy, France www.enstib.uhp-nancy.fr Specialization in natural fibres, polymerization, design of composites, wood chemicals and wood modification
March-July 2012	**Engineer assistant in R&D** for the industrial group of Sonae Industriá in Le Creusot, France www.woodforce.com Technical development, communication and marketing of an innovative wood dice produced for plastic reinforcement in automotive and packaging industries
2007-2009	Undergraduate courses to prepare for entry exams to top universities at Lycée Chaptal, Paris

Paris — January 2017

Imprint of this document:

Elßlergasse 17, A-1130 Vienna
Phone. +43 (0)1 877 04 26, Fax: +43 (0)1 876 40 04
Dr.-Simoneit-Straße 36, D-45473 Mülheim a. d. Ruhr
E-Mail: verlag@guthmann-peterson.de
http://www.guthmann-peterson.de

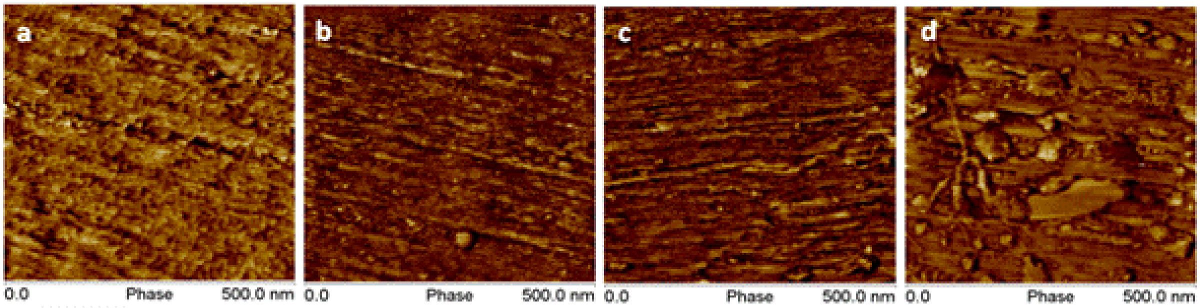

Figure 27: AFM phase images of the Bio-PE composites with (a) 0, (b) 1, (c) 5 and (d) 10 wt% of MWCNT.

From microscopic analyses it became clear that melt mixing by co-extrusion followed by injection moulding allowed a homogenous distribution of all filler types in thermoplastic polymers as expected. In the case of carbon fibre and recycled carbon fibre-filled samples, no difference in filler distribution and dispersion was detected from SEM imaging between the different used types of CF and RCF. Fillers appeared to be well-dispersed and randomly oriented at every loading except for MWCNT-filled composites as concluded from the AFM observations. Microscopic analyses were supplemented by the measurement of output data available from the extrusion and injection moulding processes to observe the effect of filler types on the process.

4.1.3 Melt behaviour during extrusion and injection moulding

The extrusion and injection output data are presented in Figures 29 to 32. The data of production set done at equal or close processing parameters are connected with segments on the Figures. For most of the productions, the melt temperature measured at the die of the extruder corresponded to the programmed temperature for zone 4. When the temperature programmed for zone 4 was increased, the melt temperature was also increased and polymer viscosity decreased at the die resulting in lower melt pressure. This was particularly detected when comparing the productions with 10 and 20 wt% of wood fibres in 20 wt% CF.LS MLD filled PLA 3251D (BFX48-49) and also for the first production set of MWCNT-filled PLA 3251D with 7.5 and 10 wt% loading (BFX28-29) when compared to PLA 3251D filled with 0 to 5 wt% MWCNTs (Figure 32a).

Melt pressure and machine load generally increased with the amount of carbon fibres added to PLA 3051D or PA, but decreased when the production was done at lower screw rotation speed; i.e. for PLA 3051D with 10 wt% CFB1 (BFX15, annotated with a * in Figure 29) and with CFA1 (BFX13-14). The injection pressures always increased with the carbon fibre loading, with exception of PLA 3251D and PAHS 18-based samples, for which the injection pressure reached the maximum at a loading of 5 wt%. This was not related to variation in the production parameters and could therefore not be explained here. The dosing time generally increased with the amount of filler.